UNIVERSIDADE ESTADUAL PAULISTA
"JÚLIO DE MESQUITA FILHO"
Campus de Ilha Solteira

PROGRAMA DE PÓS-GRADUAÇÃO EM ENGENHARIA MECÂNICA

PEDRO CHRISTIAN AYALA CASTILLO

AN INVESTIGATION INTO SOME SIGNAL PROCESSING TECHNIQUES FOR THE DEVELOPMENT OF A LOW-COST ACOUSTIC CORRELATOR TO DETECT AND LOCATE LEAKS IN BURIED WATER PIPES

UMA INVESTIGAÇÃO DE ALGUMAS TÉCNICAS DE PROCESSAMENTO DE SINAIS PARA O DESENVOLVIMENTO DE UM CORRELACIONADOR ACÚSTICO DE BAIXO CUSTO PARA DETECTAR E LOCALIZAR VAZAMENTOS DE AGUA EM TUBULAÇÕES DE AGUA

Ilha Solteira
2019

PROGRAMA DE PÓS-GRADUAÇÃO EM ENGENHARIA MECÂNICA

Pedro Christian Ayala Castillo

AN INVESTIGATION INTO SOME SIGNAL PROCESSING TECHNIQUES FOR THE DEVELOPMENT OF A LOW-COST ACOUSTIC CORRELATOR TO DETECT AND LOCATE LEAKS IN BURIED WATER PIPES

UMA INVESTIGAÇÃO DE ALGUMAS TÉCNICAS DE PROCESSAMENTO DE SINAIS PARA O DESENVOLVIMENTO DE UM CORRELACIONADOR ACÚSTICO DE BAIXO CUSTO PARA DETECTAR E LOCALIZAR VAZAMENTOS DE AGUA EM TUBULAÇÕES DE AGUA

Tese apresentada à Faculdade de Engenharia – UNESP – Campus de Ilha Solteira, para obtenção do título de Doutor em Engenharia Mecânica.

Área de Conhecimento: Mecânica dos Sólidos

Prof. Dr. Michael John Brennan

Orientador

Prof. Dr. Fabricio Almeida

Co-Orientador

Ilha Solteira
2019

FICHA CATALOGRÁFICA
Desenvolvido pelo Serviço Técnico de Biblioteca e Documentação

A973i

Ayala Castillo, Pedro Christian.
An investigation into some signal processing techniques for the development of a low-cost acoustic correlator to detect and locate leaks in buried water pipes / Pedro Christian Ayala Castillo. -- Ilha Solteira: [s.n.], 2019
146 f. : il.

Tese (doutorado) - Universidade Estadual Paulista. Faculdade de Engenharia de Ilha Solteira. Área de conhecimento: Mecânica de Sólidos , 2019

Orientador: Michael John Brennan
Co-orientador: Fabrício Almeida
Inclui bibliografia

1. Leak detection. 2. Plastic water pipes. 3. Quantization. 4. Clipping. 5. Acoustic correlator. 6. Quality index.

João Josué Barbosa ,
Serviço Técnico de Biblioteca e Documentação
Diretor Técnico
CRB 8-5642

UNIVERSIDADE ESTADUAL PAULISTA

Câmpus de Ilha Solteira

CERTIFICADO DE APROVAÇÃO

TÍTULO DA TESE: AN INVESTIGATION INTO SOME SIGNAL PROCESSING TECHNIQUES FOR THE DEVELOPMENT OF A LOW-COST ACOUSTIC CORRELATOR TO DETECT AND LOCATE LEAKS IN BURIED WATER PIPES

AUTOR: PEDRO CHRISTIAN AYALA CASTILLO
ORIENTADOR: MICHAEL JOHN BRENNAN
COORIENTADOR: FABRICIO CESAR LOBATO DE ALMEIDA

Aprovado como parte das exigências para obtenção do Título de Doutor em ENGENHARIA MECÂNICA, área: Mecânica dos Sólidos pela Comissão Examinadora:

Prof. Dr. MICHAEL JOHN BRENNAN
Departamento de Engenharia Mecânica / Faculdade de Engenharia de Ilha Solteira - UNESP

Prof. Dr. AMARILDO TABONE PASCHOALINI
Departamento de Engenharia Mecânica / Faculdade de Engenharia de Ilha Solteira - UNESP

Prof. Dr. RICARDO TOKIO HIGUTI
Departamento de Engenharia Elétrica / Faculdade de Engenharia de Ilha Solteira - UNESP

Prof. Dr. JOSÉ MARIA CAMPOS DOS SANTOS
Departamento de Mecânica Computacional / Universidade Estadual de Campinas - UNICAMP

Prof. Dr. ARCANJO LENZI
Departamento de Engenharia Mecânica / Universidade Federal de Santa Catarina - UFSC

Ilha Solteira, 13 de agosto de 2019

To Liesel and Margarita.

ACKNOWLEDGEMENTS

I would like to express my sincere gratitude to professor Mike Brennan for his valuable guidance, advice and patience during this project. Many thanks for all your smart supervisions and conversations. It is a pleasure working with you.

I would like to extend this acknowledgement to my co-supervisor professor Fabricio Lobato de Almeida, who helping me in some parts of this project with his experience and knowledge on leak detection.

I would like to thank my lovely wife Liesel and my family who have always stood by me in whatever I have ever done.

I would like to thank my beautiful daughter Margarita, I know that when she reads this, she will be an excellent person and professional, who with every smile she gives us makes our day at home happy and motivates us to keep moving forward more and more!

I would like also to thank Fabio Kroll, Camila Gonsalez, Douglas Bueno, Brenno Takiuti, Oscar Scussel, Mauricio Iwanaga, and Vinicius Clemente for your friendship and support all this time.

I would like to thank FAPESP (São Paulo Research Foundation) for the financial support. Grant 2015/26342-0.

RESUMO

O principal problema em companhias de água são os vazamentos em tubulações subterrâneas, devido a sua limitada fonte de recursos hídricos. Correlacionadores de ruídos de vazamentos são usados frequentemente para localizar vazamentos. A detecção de sinais de ruídos de vazamentos ocorre por meio da coleta de dados por sensores, aos quais estão inseridos em lugares extremos ao da localização de um suposto vazamento. Estes dados são correlacionados, obtendo o atraso do tempo entre estes sinais de vazamento. Para converter o atraso do tempo em distância, a velocidade de onda do ruído de vazamento necessita ser conhecida, frequentemente, este tempo é estimado por meio de dados históricos de velocidade ou por tabelas. Usualmente a velocidade não é medida diretamente pelo tempo, sendo uma potencial fonte de erro. Esta tese estuda os fatores que afetam a velocidade de propagação do ruído de vazamento em tubulações de água subterrâneas. Eles envolvem as caraterísticas do filtrado do sistema sensor-tubulação e a potencial faixa de frequência onde o ruído de vazamento possa estar presente, e o efeito da banda de frequência na estimação do atraso do tempo. Os efeitos de distorção na precisão da estimativa do atraso do tempo, são também estudados com foco na quantização e corte dos sinais de vazamento. O efeito de quantização é devido a um convertedor analógico digital. O corte dos sinais de vazamento acontece quando a amplitude do sinal excede os limites do intervalo dinâmico da instrumentação. A combinação de ambos os casos é também estudada, ao qual, pode acontecer quando o vazamento está perto de um ponto de medição, tal que o nível do sinal é grande e tem uma tendência a ser cortada, e no outro ponto de medição o nível do sinal pode ser pequeno tendo uma tendência a uma menor resolução. Este estudo mostra que, estes problemas tem um efeito negligenciável para a estimativa do atraso do tempo. Estudar a resposta destes efeitos poderiam ter como principal vantagem um hardware simples e, portanto, barato podendo ser usado em vez de sistemas complexos e caros, que estão geralmente em uso hoje. Uma tentativa é logo feita para esclarecer a qualidade da função de correlação cruzada e, em seguida, a estimativa do atraso de tempo. Cinco índices são propostos, cada um com características diferentes. Eles são então integrados em uma única quantidade chamada índice de qualidade. Finalmente, dois protótipos de correlacionadores são apresentados, no qual o autor contribuiu para o desenvolvimento. Para o primeiro protótipo, os dados são coletados usando cabos e os parâmetros são inseridos manualmente. Para o segundo protótipo, os dados são coletados usando um sistema sem fio. Também é necessário inserir dados do material, o tamanho do tubo, o tipo de solo, o local onde o tubo está instalado e o momento da aquisição. As interfaces foram projetadas para inserir os

parâmetros com facilidade e mostrar as informações necessárias, para uma melhor análise do comportamento do vazamento no sistema. A largura de banda é mostrada graficamente, podendo ajustá-lo manualmente. A localização do vazamento é mostrada de forma interativa.

Palavras Chave — Detecção de vazamento. Tubulações plásticas de distribuição de água. Correlacionador acústico. Quantização. Recorte de sinais. Índice de qualidade.

ABSTRACT

A major problem for water companies, are leaks in underground pipes because of a limited sources of water. Leak noise correlators are often used to locate leaks. Leak noise signals are correlated from sensors which are placed either side the location of a suspected leak. These data are correlated, obtaining a time delay between these signals. To convert the time delay into a distance, the wavespeed of the leak noise needs to be known. Often, this is estimated from historical wavespeed data or by tables. Usually it is not measured directly at the time and is therefore potentially a source of significant error. This thesis studies the factors that affect the wavespeed of the leak noise propagation in buried water pipes. They involve the filtering characteristics of the sensor-pipe system and the potential bandwidth where the leak noise can be present, and the effect of the bandwidth on the accuracy of the time delay estimate. The distortion effects on the accuracy of the time delay estimate are also studied, with focus on the quantization and clipping of the leak signals. The effect of the quantization is due to an analog/digital converter. Clipping of a leak signal occurs when the amplitude of the leak noise signal exceeds the limits of the dynamic range of the instrumentation. A combination of both cases is also studied, which can occur when the leak is near to one point of measurement, such that the level of the signal is very large and prone to clipping and at the other point of measurement the level of the signal can be small and is prone to low resolution. It is shown in this study that these issues have a negligible effect on the estimated time delay which could lead to simple and hence inexpensive hardware. An attempt is then made to clarify the quality of the cross-correlation function and hence the time delay estimate. Five indices are proposed, each one with different features. They are then integrated into a single quantity called the quality index. Finally, two correlator prototypes are presented in which the author contributed to the development. For the first prototype, the data is collected using cables and the parameters are entered manually. For the second prototype, data is collected using a wireless system. Also the material, the dimension of the pipe, the soil type where the pipe is installed and the time of the acquisition are entered. The interfaces were designed to enter the parameters easily and show necessary information for a better analysis of the behaviour of the leak in the system. The bandwidth is shown graphically, being able to adjust it manually. The location of the leak is shown interactively.

Keywords- Leak detection. Plastic water pipes. Quantization. Clipping. Acoustic correlator. Quality index.

LIST OF SYMBOLS

Symbol	Name	Units
Lower case		
a	Mean radius of the pipe	[m]
c	Wavespeed of leak noise	[m/s]
c_{m}	Estimated wavespeed	[m/s]
d	Distance between two measurement points	[m]
d_1	Distance minor relative to the leak position	[m]
d_2	Distance major relative to the leak position	[m]
$d_{2\mathrm{m}}$	Estimated measured distance major relative to the leak position	[m]
e	Quantization error	[V]
h	Thickness of the pipe-wall	[m]
k	Wavenumber	[m^{-1}]
k_{water}	free-field wavenumber of the water within the pipe	[m^{-1}]
k_{d}	Compressional wavenumber	[m^{-1}]
k_{t}	Shear wavenumber	[m^{-1}]
k_b	Bandwidth index	[-]
k_{co}	Coherence index	[-]
k_{ph}	Phase index	[-]
k_{pk}	Peak index	[-]
k_{sh}	Shape index	[-]
n	Modal order	[-]
n_1	Noise signal added to point 1	[V]
n_2	Noise signal added to point 2	[V]
p_{measured}	Internal pressure measured	[N/m^2]
p_{leak}	Internal pressure of the leak position	[N/m^2]

r_{ph}	ratio between the experimental phase to the best fit of it	[-]
s	Type of wave	[-]
s_1	Leak signal without noise added to point 1	[V]
s_2	Leak signal without noise added to point 2	[V]
t	Time	[s]
x	Discrete time signal	[V]
x_q	Quantized time signal	[V]
x_0	Distance from the measurement point to the leak noise	[m]
x_1	Leak signal simulated at point 1	[V]
x_2	Leak signal simulated at point 2	[V]

Upper case

A	Constant related to the properties of the pipes	[-]
B_{water}	Bulk modulus of the water	[N/m^2]
E_{pipe}	Young's Modulus of the pipe	[N/m^2]
G_{soil}	shear modulus of the soil	[N/m^2]
H	Frequency response function between the pressure measured at the sensor and the leak location	[-]
H_1	Frequency response function between leak and signal at d_1	[-]
H_2	Frequency response function between leak and signal at d_2	[-]
H	Frequency response function between the pressure measured at the sensor and the leak location	[-]
K	Quality index	[-]
K_{water}	Dynamic stiffness of the water in the pipe	[N/m^3]
K_{pipe}	Dynamic stiffness of the pipe-wall	[N/m^3]
K_{soil}	Dynamic stiffness of the surrounding soil	[N/m^3]
K	Quality index	[-]
N	Number of bits	[-]
$R_{x_1x_1}$	Auto-correlation function of leak signal x_1	[-]
$R_{x_2x_2}$	Auto-correlation function of leak signal x_2	[-]

$R_{x_1x_2}$	Cross-correlation function of two leak signals x_1 and x_2	[-]
$S_{x_1x_2}$	CPSD for two leak signals x_1 and x_2	[dB]
T_0	Time delay due to the leak	[s]
X	Amplitude of the sine wave	[V]
X_1	Fourier transform of x_1	[V]
X_2	Fourier transform of x_2	[V]

Greek symbols

β	Attenuation factor	[-]
ϕ_{f}	Fitted phase	[rad]
ϕ	Experimental phase	[rad]
ω	Circular frequency	[rad/s]
ω_{lower}	Lower frequency	[Hz]
ω_{higher}	Higher frequency	[Hz]
$\gamma^2_{x_1x_2}$	Coherence function	[-]
τ	Time lag	[s]
η	Loss factor	[-]
$\rho_{x_1x_2}$	Correlation coefficient between x_1 and x_2	[-]
ρ_{pipe}	pipe density	[kg/m^3]
ρ_{soil}	soil density	[kg/m^3]
Δ	Quantized step	[V]
σ_e^2	variance of the quantization error	[V^2]
σ_s^2	variance of the signal	[V^2]
ν_{pipe}	Poisson's ratio of the pipe	[-]

Superscripts

a	Denotes acceleration	[-]

LIST OF FIGURES

LIST OF TABLES

CONTENTS

1 INTRODUCTION

1.1 Background

The development of a low cost acoustic correlator implies a multidisciplinary team with different research topics. One of them, is the subject of this thesis which investigates some signal processing procedures to locate leaks in buried water pipes. Leaks are responsible for increasing energy by pumping more water, resulting in increased costs. There is also possible contamination of the water around the site where a leak is located. Furthermore, leakage damages roads and may endanger the foundations of buildings (PRICE; REED, 1989).

In 2014, 36.7% of water was wasted from the treatment to the final consumer in Brazil (SECRETARIA NACIONAL DE SANEAMENTO AMBIENTAL DO MINISTÉRIO DAS CIDADES - SNSA, 2016). In 2016, 19.8% of water was wasted due to leakage in water pipe networks and branches in São Paulo in comparison with 16% in the UK (SISTEMA DE ABASTECIMENTO DO ESTADO DE SÃO PAULO - SABESP, 2016).

Acoustic methods for leak detection and location have been applied to metallic pipes successfully for many years, being able to locate leaks in cast iron water pipes at large ranges (upwards of 1 km). However, this technique can be problematic in plastic pipes, due to a higher attenuation of the leak noise along them. Hence, information about the pipe system is necessary for the correct selection of appropriate instrumentation (sensors, data acquisition system, amplifiers, etc.) This information can help leak detection professionals in the measurement procedures and data processing to enable improved location estimates of leaks using such acoustic techniques. This limited information is of concern as there is a worldwide trend to change metal for plastic pipes for reasons of costs, maintenance, etc., (HUNAIDI; CHU, 1999).

Leak noise correlators are used to locate leaks. Leak noise signals are correlated from sensors which are placed either side the location of a suspected leak, obtaining a time delay between this signals. To convert the time delay into a distance, the wavespeed of the leak noise needs to be known. Often, this is estimated from historical wavespeed data or by tables. Usually it is not measured directly at the time and is therefore potentially a source of significant error. This thesis studies the factors that affect the wavespeed of the leak noise propagation in buried water pipes. Experimental data was collected in a test rig in São Paulo in which the position,

type and strength of leak, pressure and flow of the water, etc. can be controlled. The tests were carried out for different leaks with known distances, keeping the pressure of the system constant. The results show, the filtering characteristics of the sensor-pipe system and a potential bandwidth where the leak can be present. The effect of the bandwidth on the accuracy of the time delay and hence in the estimation of wavespeed is studied.

Two distortion effects in leak signals are also studied. First, the effect of quantization due to an analog/digital converter is studied. Second, the effect of clipping of a leak signal when the amplitude exceeds the limits of the dynamic range of the instrumentation is studied. A case where these two effects can appear is when the leak is near to one of the measurement positions so the level of the signal is very large and prone to clipping. At the other measurement position the level of the signal is small and is prone to low resolution (low number of bits). Detailed knowledge of these effects could have the major advantage that simple and hence inexpensive hardware could be used rather than the expensive complex systems generally in use nowadays. Theoretical simulations and experimental data are processed and analyzed in this thesis.

The output from an acoustic correlator is a cross-correlation function from which time delay and hence leak position is determined. An attempt is made to clarify the quality of the cross-correlation function and hence the time delay estimate. Five indices are proposed, each one with different features. They are then integrated into a single quantity called the quality index.

As part of the FAPESP project (process-2013/50412-3) to develop a national low cost acoustic correlator optimized to detect and locate leaks in buried plastic water pipes, some software and an interface for ease of operation is developed. This is described in this thesis.

1.2 Literature Review

In this section, previous work is reviewed and used as a base for the development of a low-cost device for leak detection in buried water pipes using the acoustical correlation technique.

1.2.1 Overview of the acoustical correlator

There are several types of acoustic equipment to detect leaks in buried water pipes, for example the stethoscope or listening stick, leak noise correlators, noise loggers, etc. Some techniques are able to approximate or localize the position of a leak while others can find exact locations. Often a tool-box approach is used, where multiple technologies are deployed. (HAMILTON; CHARALAMBOUS, 2013).

In this thesis some software for a leak noise correlator is developed. The methodology applied today to detect and locate water leaks using leak noise correlators is based on the principles of underwater acoustics. It was extremely important to develop anti-submarine listening systems in world war I and II. The correlators were introduced commercially into the marketplace in the late 1970s. Basically, it has a receiver and two radio transmitters with sensors and/or hydrophones. However, that technology has advanced quickly, putting this type of equipment in the realm of new technology with changes every year (THORNTON *et al*., 2008).

In 1979, The Fraunhofer Institute for Building Physics (IBP) in Germany started to improve known acoustical inspection techniques using modern sensors and signal processing so that leak detection could be made more effective. At that time, acoustical correlation techniques to locate leaks were not considered promising. The American Water Works Association (AWWA) considered it too expensive and time consuming for commercial application. In about 1990 a compact electronic device was developed using an effective acoustical technique of leak detection by correlation analysis (FUCHS; RIEHLE, 1990).

The effectiveness of the correlation technique for locating leaks depends on several factors including pipe size, type, and depth, soil type and water table level, leak type and size, system pressure, interfering noise, and sensitivity and frequency range of the equipment. It has been found that hydrophones can locate leaks with lower acoustic signals than can be located with accelerometers. In general, the greater the sensitivity of the sensor and the lower its noise floor, the smaller the leaks that can be located. Hydrophones would be the most suitable for locating leaks, having a small Signal to Noise Ratio (SNR). Accelerometers are suggested in multi-leak and coherent noise situations (HUNAIDI, 2000).

Saqib *et al*. (2017) introduced a novel multiscale approach to leak detection and localization in water pipeline network using pressure and vibration data for detection and localization of leaks in a pipeline network. This does not require an extensive knowledge of the

network parameters, such as diameters of all pipe sections and flow rates. Pressure data were used with the indicator Head Loss Ratio (HLR) developed by Ishido and Takahashi, (2014) to detect the leak. Once the leaky segment of the pipe has been identified, vibration data is used to select the best possible nodes around the leak and then cross-correlated to localize the leak.

1.2.2 Overview of time delay estimation Methods

Time delay estimation between two received signals has several applications, such as locating and tracking the position of a signal source (CARTER, 1981), indicating a transit time, or estimating some other process time. It is a research topic in many fields (radar, sonar, hands-free communications, pipe leak detection, etc.) Several approaches with different points of view have been proposed and studied, for example: parameter estimation, generalized cross correlation function (GCC) and using phase data (WUU; PEARSON;1984).

The GCC method is a two-sensor technique common in passive systems based on the ideal single-path acoustic propagation model. This is the case for nondispersive propagation waves. It performs fairly well in moderate noise and reverberation conditions when the two pre-filters are properly selected. However, it suffers severe performance degradation in the presence of strong noise and heavy reverberation (HUANG; BENESTY; 2004).

Gao *et al*. (2004) developed an analytical model to predict the cross-correlation function of leak signals in plastic pipes. This model was used to explain some of the features of correlation measurements made in actual water pipes. The model is used to demonstrate the importance of the cut-off frequency of the high-pass filter and the insensitivity of the correlation to the cut off frequency of the low pass filter.

Basic cross-correlation is the most well-known GCC Method. Gao *et al*. (2004) have shown that, for application in leak detection, the GCC is strongly affected by The SNR at the measurement positions and it can be enhanced by the correct selection of a bandwidth. Phase data obtained from the cross-power spectral density can be used to calculate the time delay estimate between two signals. It has a linear behaviour; whose slope gives the time delay between two sensors (BRENNAN *et al*., 2007).

Gao *et al*. (2006) compared GCC time delay estimators including the ROTH impulse response, the smoothed coherence transform (SCOT), the WIENER, the phase transform (PHAT) and the maximum likelihood (ML) estimators for the purposes of leak detection in buried plastic water pipes. Although the PHAT estimator gives a well-differentiated peak. In

the practice, the SCOT and ML estimators additionally take account of effect of background noise in the estimation procedure, which will probably be more beneficial to water leak detection. Also is shown that the random error in the time delay estimates due to random noise on the measurements is generally insignificant compared to the resolution of the time delay estimate for leak detection in typical plastic pipes.

1.2.3 Overview of vibroacoustic characteristics in buried water pipes

The following works were used as the basis for the vibroacoustic characterization of buried plastic water pipes in São Paulo.

Hunaidi and Chu (1999) investigated the effectiveness of correlators of leak noise signals and one objective was the characterization of leak noise in plastic pipes in a test rig under controlled conditions in Canada. It was a research project sponsored by the American Water Association Research Foundation (AWWARF) and the National Research Council of Canada. Results showed that leak noise correlators in automatic mode rarely succeeded in locating leaks. With the flow variation, vibration sensors were only effective with flow rates greater than 20l/min. Hydrophones have to be used to locate small leaks e.g. joint leaks at flow rates of 6 l/min.

Muggleton *et al*. (2002) presented a theoretical model of a buried fluid filled pipe to predict both wavespeed and attenuation, equations for $n = 0$ axisymmetric wave motion were derived for a fluid-filled pipe, surrounded by an infinite elastic medium which can support both longitudinal and shear waves. These equations were solved for two wave types, $s = 1,\ 2$, which correspond to a fluid dominated wave and an axial shell wave, and expressions for a complex wavenumber for each wave were given. Muggleton *et al*. (2004) validated that model later, experimentally. Wavenumber measurements, encompassing both wavespeed and wave attenuation were made on a water-filled pipe in vacuo and on a buried water-filled pipe. In general, the measurements showed good agreement with the theoretical predictions. In the case of acoustic leak detection in plastic pipes two conclusions can be obtained. The soil surrounding the pipe had little direct effect on the wavespeed of the ‘fluid-borne’ wave compared with the in vacuo case. The elastic properties of the pipe wall are temperature dependent and must be taken into account in calculating the expected wavespeed. Leak location errors are liable to be large if it is not used. The finding that the surrounding soil markedly increases the wave

attenuation compared with the in vacuo case suggests an additional difficulty, in that the signal to noise ratio will be substantially reduced.

Muggleton and Brennan (2004) investigated the effect of the wavespeed and attenuation when the pipe is submerged, it was found that in this case the wavespeed decreases marginally with corresponding small increase on the wave attenuation.

Muggleton *et al*. (2006) developed a signal processing procedure with a novel sensor for measuring the acoustic pressure which means an improvement on the standard cross-correlation technique to locate and detect leak in a buried water filled plastic pipe.

Muggleton and Brennan (2008) designed and implemented an instrumentation of an experimental test rig, as a part of the Mapping the Underworld Programme in UK. This was used to develop and prove the efficacy of a multi-sensor device for remote buried service detection, location and identification and to investigate acoustic methods for the detection and location of underground piping systems. In particular, the rig was designed with the excitation and propagation of one particular wavetype in the pipe in mind: the axisymmetric, fluid-dominated mode. For plastic pipes, this mode is well coupled to the pipe wall and also the surrounding ground; furthermore, it is often the main carrier of energy at low frequencies.

Almeida (2013) investigated an improved acoustic method for leak detection in buried plastic water distribution pipes, and as a part of the PhD research a pipe rig was built at Blithfield reservoir in the UK by South Staffs Water PLC. The behaviour of this pipe rig was investigated, by controlling the location and the strength of the leak.

Almeida *et al*. (2014) investigated the filtering effect of the pipe and sensor in a buried plastic water pipe and its effect on leak detection. Three types of sensors were compared: hydrophones, geophones and accelerometers. Analytical models reported previously (GAO *et al*., 2005) were validated in this work experimentally. The main features were that the hydrophone-pipe system is more sensitive at low frequencies with the pipe acting as a low-pass filter, and the geophone and the accelerometer combined with the pipe effect results in band-pass filter behaviour for these systems. These sensors were capable to detect the leak noise, however for a weak leak, only the accelerometer could clearly detect the leak noise in this case.

Gao *et al*. (2016) developed for the case of $n = 0$ mode and with the $s = 1$ an analytical method for investigating the dispersion characteristics of the wave propagation in a buried fluid-pipe. Whilst these can be found in the literature, they are generally calculated numerically. It

has been found that although the wavespeed is not significantly affected by the inclusion of the frictional stress at the interface between the pipe and the soil, the wave attenuation increases markedly.

Gao *et al*. (2017) extended the analysis on the propagation characteristics to study the loading effects of surrounding elastic medium, acting as a combination of mass, stiffness and radiation damping. It facilitates insight into the loading effects of surrounding medium on the propagation characteristics at low frequencies.

Brennan *et al*. (2018) studied the wavespeed and the attenuation of the wave responsible for leak noise propagation. For this wave, an expression to predict the wavespeed which is dependent upon both fluid loading and soil loading factors, and one for wave attenuation has been derived based in Gao *et al*. (2016) and (2017). It has been shown than the flexibility of the pipe slows down he wave compared to a rigid-wall pipe. the shear stiffness of the soil plays an important role in counteracting this effect, increasing the wavespeed. This has been found to be particularly relevant for the type of soil found in Brazil.

1.2.4 Overview of the distortion effects on the accuracy of the time delay estimate

In signal processing, distortions are normally an undesirable effect. They usually can appear for example when a signal is converted from analogue to digital (A/D) in the quantization process or when a signal is clipped by the effect of exceeding the maximum limits of amplitude of an A/D converter. in the next part the literature that was used as the basis to determine the effect of the distortions in applications of leak detection, is reviewed.

Bennett (1948) of Bell Laboratories discussed the relationship between distortion or error and the step size to determine the number of quantized steps required to transmit specific signals. He analysed the number of quantized steps required to transmit specific signals.

Widrow (1956) and in subsequent work done in 1960 elaborated the quantization theorem, which indicates that the quantization noise is uniformly distributed random noise under the condition that the input random variable has a certain band-limited characteristic. This theorem shows that there are actually several quantization conditions all pertaining to the probability density function (PDF) and the characteristic function (CF) of the signal being quantized.

Watts (1961) presented a general theory of amplitude quantization and used it to investigate the effects of signal quantization on the determination of correlation functions. Theoretical expressions were obtained for the cross-correlation between signals and quantization noise and for the cross-correlation between quantization noise.

Cooper (1969) discussed the properties of correlators for partially coherent noise signals employing two-bit quantization of the input signal, specifically aspects such as the SNR, the relationship between the two bit and the continuous correlation coefficients, and the stability requirements for the quantizers. Two-bit quantization of the input signals has been shown by Cole (1968) to improve the SNR, for low levels of correlation. The availability of inexpensive integrated circuit logic results an attractive proposition in applications for radio astronomy where observing time is at a premium.

Sripad and Snyder (1977) described the necessary and sufficient condition for quantization errors to be considered uniform and white noise, for a Gaussian input.

Work by Widrow and Kollár (1996) modelled the effect of uniform quantization by an additive noise which is uniformly distributed, uncorrelated with the input signal with a white spectrum. The statistical theory behind this model was presented and validated.

Widrow and Kollár (2008) described the way in which sampling and quantization affects signals when they are converted from analog to digital form. Sampling and quantization are mathematically commutable operations. It makes no difference whether a signal is first sampled and then the samples are quantized, or if a signal is quantized and the stepwise continuous signal is then sampled. Both degrade the quality of a signal and may irreversibly reduce our knowledge of it.

Van Vleck (1943) wrote “The Spectrum of Clipped Noise”. The clipping of a signal, as will be seen later, is a distortion which is usually undesirable. This work was a classified report that had great impact on the later development of radio astronomy. It was developed at the Radio Research Laboratory of Harvard University, during World War II. At that time, theoretical and experimental study of the factors which governed the electronic jamming of the radar and communication systems was carried out. Twenty-three years later this material was published with the same title by Van Vleck and Middleton (1966). They presented the calculation of the power spectrum of normal, or Gaussian, noise after it has been rectified by a “clipper,” or zero-memory rectifier and a relation between the cross-correlation function of the clipped and the unclipped noise.

Weinreb (1963) presented an indirect method of computing the autocorrelation function of a signal having Gaussian statistics. This method greatly reduces the amount of digital processing that is required. the one-bit technique has the same mathematical form as for severe clipping as discussed by Van Vleck.

Almeida *et al*. (2017) used the signum function to simulate the effects of clipping on the estimation of time delay by severely distorting of the leak signals, observing that there is no profound effect on time delay estimation.

1.3 Objectives

The specific objectives of this thesis are to:

- Investigate the factors that affect the estimate of the wavespeed of the leak noise propagation of typical buried water pipes in São Paulo,
- Investigate the number of bits of quantization required to digitize and send data, and its influence on the accuracy of the time delay estimate.
- Investigate the effect of the clipping in the influence of time delay estimate
- Develop a Quality Index to represent the reliability of the localization of the leak.
- Develop the software of the prototype with a user-friendly interface to detect and locate leaks in buried plastic water pipes.

1.4 Contributions

The following contributions are made in this thesis

- From the measurement of leaks noise in buried plastic water pipes, the bandwidth where the leak noise is presented has been determined. Using the data within this frequency band, the speed of leak noise propagation has been determined. This data has led to new knowledge about the specific vibroacoustic behaviour of a test rig in São Paulo.
- From the investigation of signal distortion due to quantization and clipping, it has been shown that the lowest value of resolution is one bit to obtain a time delay estimation for detecting and locating a leak in buried plastic water pipes. This means that it is possible to

use inexpensive hardware rather than the expensive complex systems generally in use nowadays.

- A Quality Index has been proposed to quantify the quality and reliability of the cross-correlation function. Three levels of reliability have been proposed.
- Some user-friendly software has been developed to detect and locate a leak in buried plastic water pipes, with the following novel characteristics: an automatic selection of bandwidth and an indicator of the quality of the time delay estimate.

1.5 Thesis Outline

This thesis consists of 6 chapters. Chapter 1 contains the general introduction with the background, literature review, objectives and contributions. In chapter 2, the factors affecting the estimate of the wavespeed of the leak noise propagation of buried water pipes in São Paulo-SABESP test ground are presented. Data measured in this test ground are analysed in the frequency domain, calculating the wavespeed in each zone of analysis, and the automatic bandwidth of the leak noise signals selection is introduced. In chapter 3, an investigation of the distortion effects on the accuracy of the time delay estimate is presented. Two effects are analysed. The first effect is the quantization and the second effect is the clipping signal and a combination of both effects is the heavily clipped signal. Simulated and experimental cases are analysed. In chapter 4, the five indices proposed are shown and simulated and experimental cases are analysed. In chapter 5 two prototypes of an acoustic correlator are presented, and the functionalities and principal characteristics are shown. In chapter 6 the conclusions are given. Recommendations for future work are also given in the end of this chapter. There are Appendixes A, B, C and D which contain: wavenumber prediction, Tolerance on the measurement of the distance, Leak signals processed from the test rig in SABESP and an Algorithm in Matlab® code of the prototype 2 of the correlator acoustic respectively.

2 FACTORS AFFECTING THE ESTIMATE OF THE WAVESPEED OF LEAK NOISE PROPAGATION OF BURIED WATER PIPES

2.1 Introduction

The aim of this chapter is to study the factors that affect the wavespeed of the leak noise propagation using leak signals collected under controlled conditions at a test rig located in SABESP in São Paulo. It is shown, that the filtering effect inherent in the sensor-pipe system concentrates the effect of leakage noise in a frequency range gives an initial idea where leak noise is potentially present. In the field, leak noise usually is contaminated by external noise, and it is important to select an appropriate bandwidth to have a good shape of the cross-correlation function. This is important to obtain an estimate time delay and consequently an accurate estimate of the speed of leak noise propagation. This information, is important to elaborate measurement procedures, designing instrumentation to measure leak noise signals, and to develop a low cost acoustic correlator. The leak signals are analysed in the frequency domain with the Power Spectral Density (PSD), modulus and phase of the Cross Spectral Density (CSD) and coherence. The Cross-Correlation Function (CCF), which is used to estimate the time delay between leak noise signals and to calculate the wavespeed, is also studied in detail.

2.2 Leak detection using correlation

Figure 1 shows a typical situation in which leak noise is used to detect and locate its position. Assuming consistent pipe material and diameter, the noise travels from the leak in both directions at a constant speed. Sensors generally located either side of the leak position can then sense leak noise when it is present in the system. It is observed that the distance between the sensor 1 and 2 is $d = d_1 + d_2$, where d_1 and d_2 are the distances between the leak and sensors 1 and 2 respectively. If the leak is equidistant between the two sensors, then they will sense leak noise at the same time. On the other hand, if the leak is not equidistant, there will be a time delay between the signals. This time delay estimated by the CCF of the two measured signals, is used to determine the position of the leak relative to sensor 2, which is

given by (GAO *et al.*, 2004)

$$d_2 = \frac{d - cT_0}{2}, \tag{1}$$

where c is the propagation speed of the leak noise in the buried pipe and T_0 is the difference in arrival times of the leak noise at the sensor positions (time delay).

Figure 1 - A typical diagram of leak detection in buried water pipe.

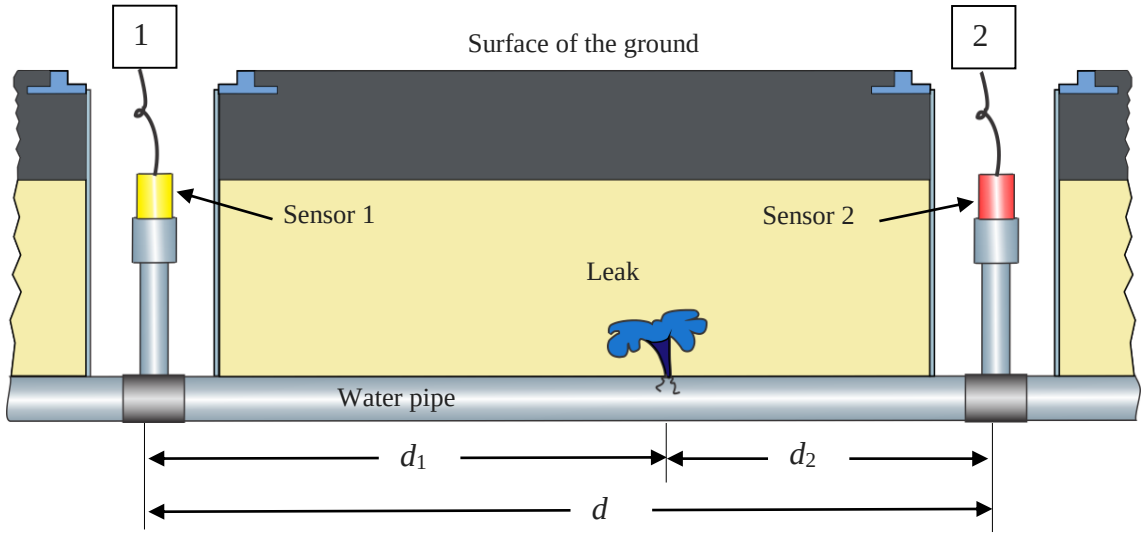

Source: Elaborated by the author.

A typical CCF calculated from two leak noise signals is shown in Figure 2. The time delay T_0 is obtained from the position of the maximum peak of this function.

Figure 2 - Typical CCF of two leak noise signals measure on the system similar to Figure 1.

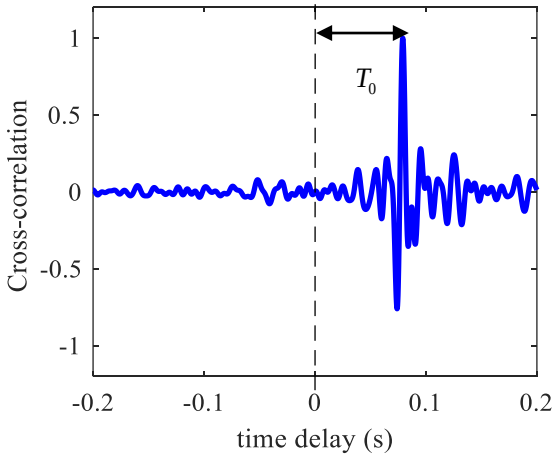

Source: Elaborated by the author.

2.2.1 Basic cross correlation (BCC) Method

The BCC is the most used technique to determine the time delay between the two measured leak signals. This technique uses the CCF where the presence of a leak appears as a maximum peak. This peak gives the time delay estimate.

Assuming that the leak signals are two stationary random signal with zero mean, the CCF is defined by (KIHONG; HAMMOND, 2008)

$$R_{x_1x_2}(\tau) = E\left[x_1(t)x_2(t+\tau)\right] \tag{2}$$

where τ is the time delay and $E[\ ]$ is the expectation operator, and $x_1(t)$ and $x_2(t)$ are the time series of the signals collected by the sensors 1 and 2, respectively (see Figure 1). T_0 is the value to the domain of τ that maximizes Equation 2.

The procedure to obtain the CCF is in the time or frequency domain. In this thesis, the frequency domain method is used with band-limited and sampled data. It is determined from the inverse Fourier transform of $X_1^*(\omega)X_2(\omega)$, where $*$ denote conjugation, ω is circular frequency, $X_1(\omega)$ and $X_2(\omega)$ are the Fourier transforms of the measured signals $x_1(t)$ and $x_2(t)$ (GAO *et al*., 2004). The procedure of the implementation for the BCC is shown in Figure 3. Before the correlation, the signals have to be filtered to have effective performance. This method is susceptible to wave reflections from discontinuities in the system because they affect the modulus and phase spectra of the CSD and appear as spurious peaks in the CCF depending on the magnitude of the reflections (GAO *et al*., 2009) and uncorrelated noise at the receivers (ALMEIDA; 2013), generating problems in the determination of the time delay estimate.

Sometimes, it is useful to use the cross-correlation coefficient (CCC), which is the cross-correlation function in a normalized form with a scale of -1 to +1, given by (KIHONG; HAMMOND, 2008)

$$\rho_{x_1x_2}(\tau) = \frac{R_{x_1x_2}(\tau)}{\sqrt{R_{x_1x_1}(0)R_{x_2x_2}(0)}}, \tag{3}$$

where $R_{x_1x_1}(0)$ and $R_{x_2x_2}(0)$ are the values of the auto-correlation function $R_{x_1x_1}(\tau)$ and $R_{x_2x_2}(\tau)$ at $\tau = 0$.

Figure 3 - Procedure of the Basic Cross-Correlation Method.

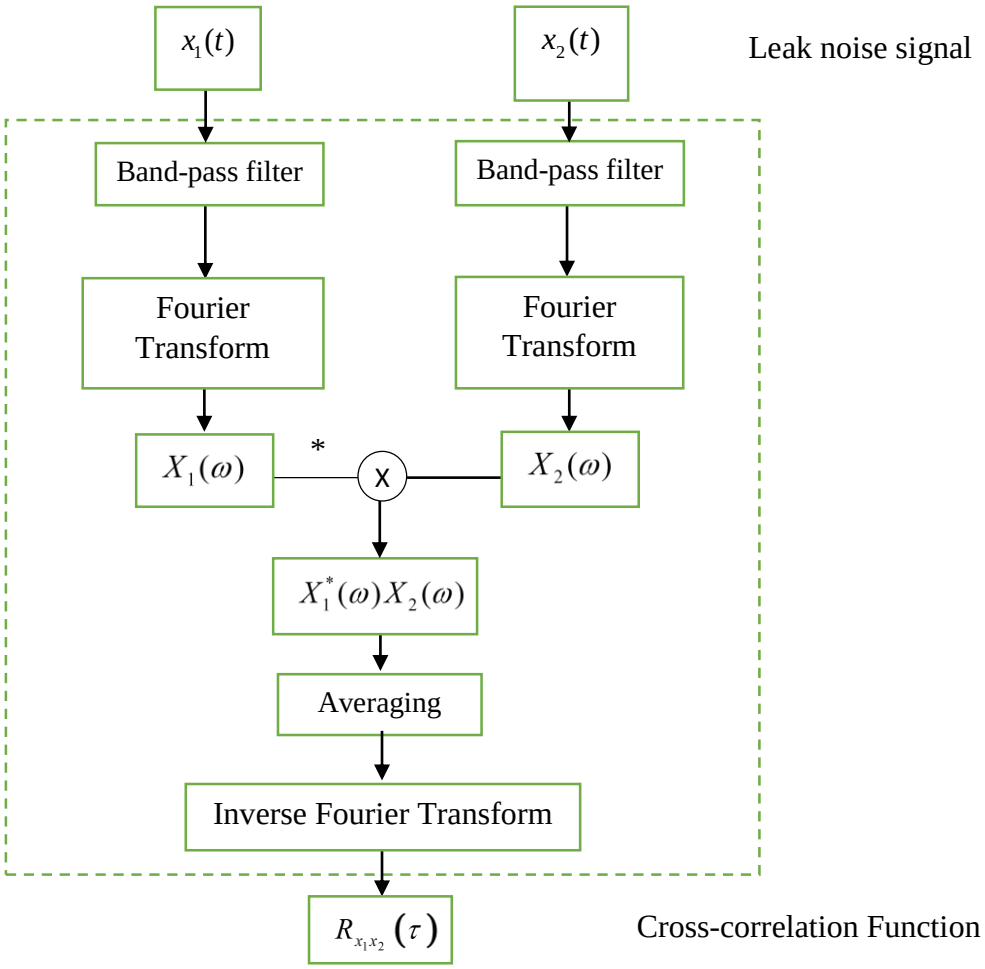

Source: Elaborated by the author.

2.3 Filtering effect of the sensor-pipe system

In this section, the model of the pipe-sensor system proposed by Gao *et al*. (2005) is reviewed to show the bandwidth over which leak noise is potentially present. This frequency band can be used initially to calculate the time delay T_0. With this value and the distances d, d_2 that are known, the speed of the leak noise can be calculated using the Equation 1. This equation can be rearranged as follows $c = d - 2d_2/T_0$.

Figure 4 shows a fluid-filled pipe of arbitrary length. p_{leak} is plane pressure excitation generated in the part where the leak is located. Waves of pressure traveling in the positive x-direction, ignoring the time dependence the internal pressure measured can be represented by

$$p_{\text{measured}} = p_{\text{leak}} e^{-jkx_0}, \tag{4}$$

where p_{leak} is the internal pressure of the leak position, x_0 is the distance from the measurement point to the leak noise, k is the wavenumber and $-j = \sqrt{-1}$.

Figure 4 - Diagram of one dimensional pressure wave in fluid filled pipe.

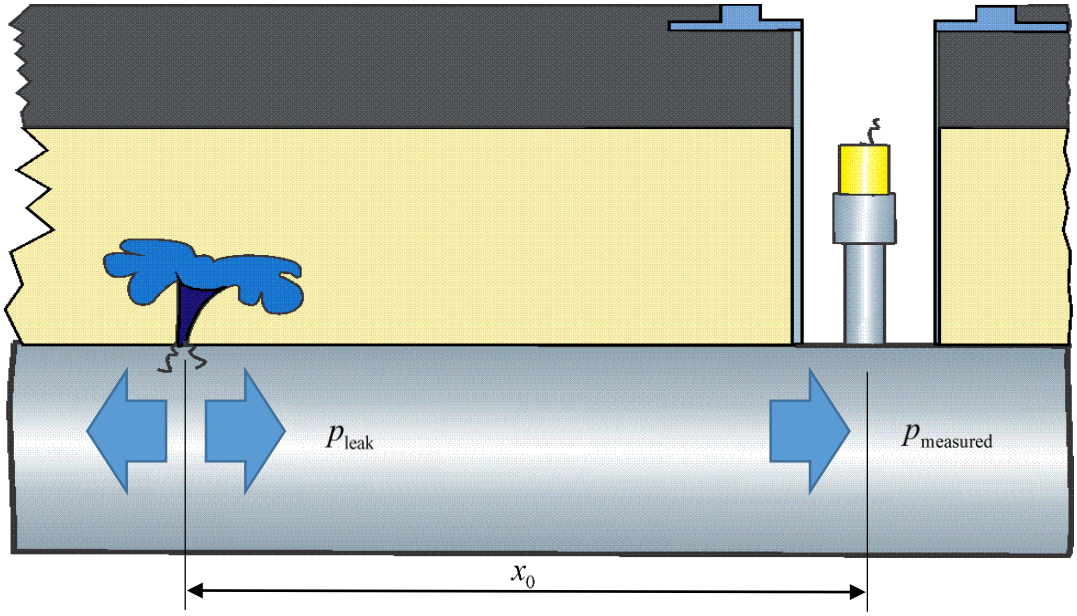

Source: Elaborated by the author.

The wavenumber can be expressed by (BRENNAN *et al.*, 2018)

$$k(\omega) = k_{\text{water}}(\omega)\left(1 + \frac{K_{\text{water}}}{K_{\text{pipe}} + K_{\text{soil}}}\right)^{\frac{1}{2}}, \tag{5}$$

where k_{water} is the free-field wavenumber of the water within the pipe, K_{water} is the dynamic stiffness (pressure/displacement) of the water in the pipe, K_{pipe} is the dynamic stiffness of the pipe-wall and K_{soil} is the dynamic stiffness of the surrounding soil. In Appendix A, the wavenumber and these components are discussed in detail. The wavenumber can also be expressed by

$$k(\omega) = \text{Re}\{k(\omega)\} + \text{Im}\{k(\omega)\}, \tag{6}$$

where the real part of the wavenumber is given by (GAO *et al*., 2004)

$$\mathrm{Re}\left\{k(\omega)\right\} = \frac{\omega}{c}. \tag{7}$$

The imaginary part of the wavenumber is given by (GAO *et al*., 2004)

$$\mathrm{Im}\left\{k(\omega)\right\} = -\beta\omega, \tag{8}$$

where β is a measure of the loss as the wave propagates along the pipe given. Equation 4 can be expressed dividing the wavenumber in its imaginary and real part given by

$$p_{\text{measured}} = p_{\text{leak}} e^{-\omega\beta x_0} e^{-j\omega x_0/c}, \tag{9}$$

where x_0 is the distance between the leak noise and the measurement point.

The frequency response function between the pressure measured at the sensor location and the leak location is given by (GAO *et al*, 2005)

$$H(\omega, x) = e^{-\omega\beta x_0} e^{-j\omega x_0/c}. \tag{10}$$

At low frequencies, well below the pipe ring frequency which is usually at least 1000 Hz, the internal pressure amplitude measured, P_{measured}, is related to the radial displacement amplitude of the pipe, W is given by (PINNINGTON; BRISCOE, 1994)

$$W = \frac{a^2}{E_{\text{pipe}} h} P_{\text{measured}}, \tag{11}$$

where E_{pipe} is the Young's Modulus of the pipe, a is the mean radius of the pipe and h is the thickness of the pipe-wall. This equation shows that there is a linear relationship between the pipe wall displacement and the internal pressure. With this equation and Equation 10 is possible to have the frequency response function of the acceleration measured at the sensor location and the pressure at the leak location, which is given by (GAO *et al*, 2005)

$$H^a(\omega,x) = -\frac{a^2\omega^2}{E_{\text{pipe}}h}H(\omega,x), \tag{12}$$

where the superscript (a) is used to denote acceleration measurement. The CPSD for pressure measurements for a leak between two measurements points as shown in Figure 1 is given by

$$S_{x_1x_2}(\omega) = H^*(\omega,d_1)H(\omega,d_2), \tag{13}$$

where $H(\omega,d_i) = e^{-\omega\beta d_i}e^{-j\omega d_i/c}$, where $i=1$ or 2 and the superscript * denotes the complex conjugate. Thus

$$S_{x_1x_2}(\omega) = e^{-\omega\beta d}e^{-j\omega T_0}. \tag{14}$$

The CPSD for acceleration measurements is given by

$$S^a_{x_1x_2}(\omega) = H^{a*}(\omega,d_1)H^a(\omega,d_2). \tag{15}$$

Combining Equation 10, 12 and 15 gives

$$S^a_{x_1x_2}(\omega) = A\omega^4 e^{-\omega\beta d}e^{-j\omega T_0}, \tag{16}$$

where A is a constant related to the properties of the pipe. Here it is arbitrarily set to 1 without loss of generalisation. The modulus of the CSD is given by

$$\left|S^a_{x_1x_2}\right| = \omega^4 e^{-\omega\beta d}. \tag{17}$$

2.4 Wave propagation in fluid filled pipes

Acoustic energy in buried water pipes generated by a leak propagates at relatively low frequencies (FUCHS; RIEHLE, 1990). Well below the ring frequency of the pipe (usually at least 1000 Hz). Four types are responsible for the energy transfer. Three of them are related to

the axisymmetric mode $n=0$ and one wave related to the beam bending mode $n=1$. Figure 5 shows the modes $n=0$ and $n=1$.

For the mode $n=0$, two waves are plane waves. The first is termed the $s=1$ wave which is a predominantly fluid borne wave with some radial motion associated with the shell compliance, and the second termed $s=2$ which is predominantly a compressional wave in the shell with some associated radial wall motion influenced by the Poisson ratio and the fluid bulk modulus of elasticity. The third wave termed $s=0$ is a torsional wave which does not couple the vibration of the pipe wall and the fluid motion, and can be neglected for leak detection cases (PINNINGTON; BRISCOE, 1994).

For the mode $n=1$, the wave is characterized by lateral movements of the pipe, However, the energy of this type of wave is more concentrated in the pipe wall, and is hence not coupled with the fluid and can also be neglected in leak situations.

For modes $n\geq 2$ have their cut-off frequency generally above the low-frequency region where the leak energy concentrates. As result, only the n = 0 mode with the s = 1 and s = 2 waves propagate in plastic pipes filled with fluid. The energy due to the leak, however, is predominantly transmitted by the s = 1 wave, such that the wave can be considered a plane wave type with a non-dispersive behaviour. (ALMEIDA, 2013)

Figure 5 - The two modal shapes n = 0 and 1.

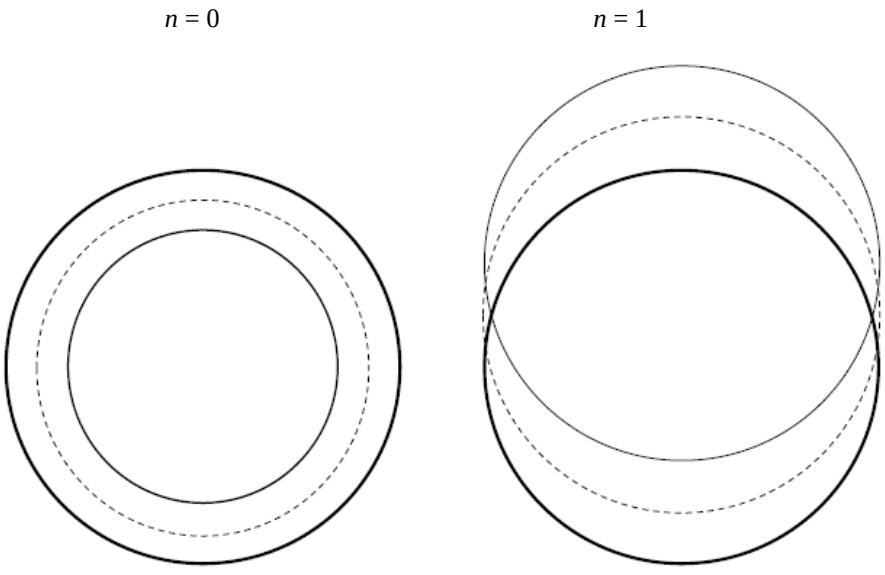

Source: Elaborated by the author.

2.4.1 Wavespeed evaluation

Water escaping through a leak creates a noise. The sound waves propagate along the pipe wall, fittings, surrounding ground and especially via the water inside the pipe. If the pipe wall were completely rigid, the sound would propagate with a velocity of approximately 1485 m/s. However, the pipe material is always elastic to some degree. This elasticity causes a reduction in the velocity of the wave and attenuation of the pressure wave as it progresses down the pipeline.

The sound velocity in water pipes depends on the pipe material and the ratio between the diameter and wall thickness. For metallic pipes, the sound velocity slows down to about 1200 m/s, although the metal absorbs only a fraction of the sound energy and the sound still travels quite far. Plastic pipes are much more elastic, reducing the sound velocity to 300–600 m/s for typical plastic pipes. Furthermore, the sound energy is absorbed more easily causing the sound waves to become weaker and weaker as they travel along the pipeline. (HAMILTON; CHARALAMBOUS, 2013). In steel and iron pipes the leak noise may propagate over 1.5 km, but in plastic pipes the leak noise propagates less than 300 m. (BRENNAN *et al*., 2006)

The wavespeed of the leak can be calculated theoretically by rearranging Equation 5 given

$$c = \frac{\omega}{\mathrm{Re}\{k(\omega)\}}. \tag{18}$$

With the cross-correlation method is possible to calculate the wavespeed experimentally. It is estimated based on the time delay between two signals measured at two points that are a known distance apart. The signals are generated with an artificial device or a simulated leak, both in-bracket or out-bracket of the sensors. The velocity is then calculated by dividing the distance travelled of the measured signals and the time delay. In contemporary correlators, the estimated velocity with which the leak noise propagates in a pipe is stored in tables. The user selects a value from this table according the characteristics of the pipe.

In Figure 6 a comparison of wavespeed for different correlators is shown. It can be seen that the wavespeed for the same nominal diameter and the same material vary from one manufacturer to another, sometimes quite significantly. Even for the same manufacturer the values in two tables may differ.

For example, for a PVC pipe with DN100 (Diameter Nominal), values range from about 415 m/s to 450 m/s. Manufacturers often describe the values in their tables as "empirical values", with no further details of their origin (BECKER, 201?).

Figure 6 - Graphic representation of wavespeed of leak noise obtained from tables of different companies.

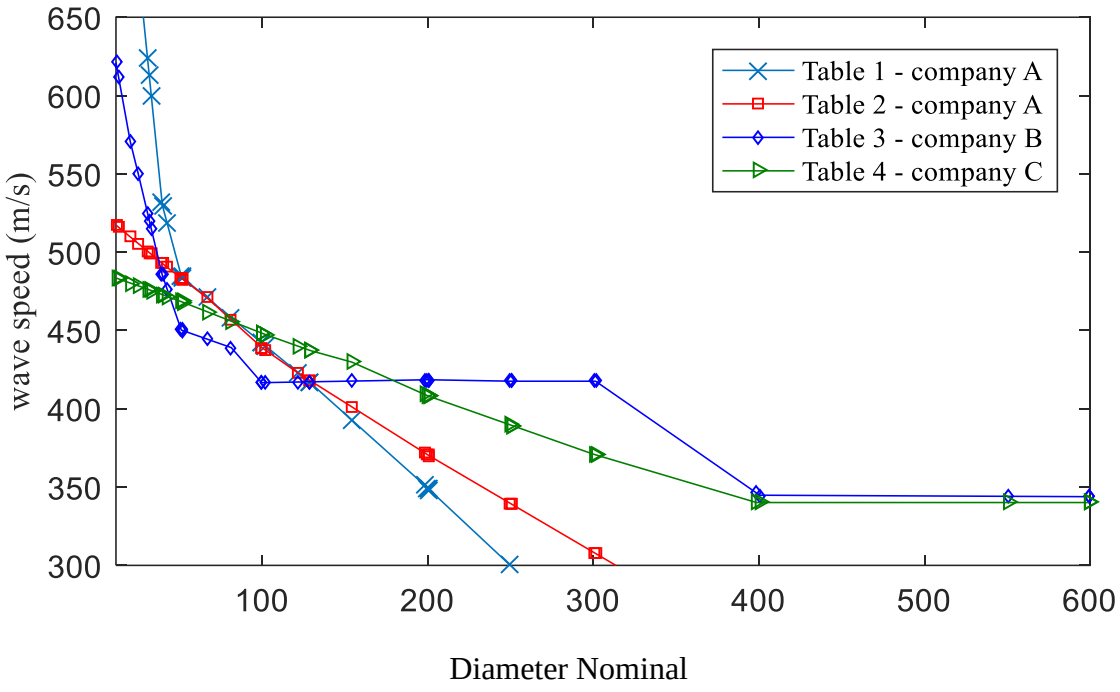

Source: Becker (201?)

2.4.2 Bandwidth prediction

In Table 1 some parameters from São Paulo and Blithfield test rig are given. To determinate the bandwidth over which the leak noise propagates, two half power point frequencies are set as a reference when $\left|S^{a}_{x_1x_2}\right| / \max\left|S^{a}_{x_1x_2}\right| = 1/2$, obtaining a bandwidth with lower and upper limit for each case. To calculate β the Equation 8 is rearranged to give

$$\beta = -\frac{\mathrm{Im}\{k(\omega)\}}{\omega} \quad . \tag{19}$$

Brennan *et al*, (2018) obtained a simplified expression for the wavenumber *k* given by

$$k = k_{\text{water}} \left(1 + \frac{2B_{\text{water}}/a}{E_{\text{pipe}} h/a^2 + 2G_{\text{soil}}/a} \right)^{1/2} , \tag{20}$$

where B_{water} is the bulk modulus of the water and G_{soil} is the shear modulus of the soil. For this simulation the soil effect is not considered, neglecting the term $G_{\text{soil}}/B_{\text{water}} = 0$.

Table 1 - Initial reference of a theoretical bandwidth for Sao Paulo (Brazil) and Blithfield (UK) test rigs.

Data	Material Pipe	d m	Radio a mm	Thickness h mm	Loss factor η	c_{water} m/s	E_{pipe} N/m^2	B N/m^2	βd	lower limit (Hz)	upper limit (Hz)
São Paulo	PVC	6.96	35.8	3.4	0.1	1500	2E+09	2.2E+09	0.001	333	1095
Blithfield	PE	30	84.5	11	0.1	1500	2.4E+09	2.2E+09	0.004	91	300

Source: Elaborated by the author.

The normalized modulus of CSD is shown in Figure 7 for a pipe-accelerometer system with the parameters given in Table 1 for the two cases proposed and using the reference of two half power point frequencies. It is observed graphically, that the combined pipe-accelerometer system acts as band-pass filter with peaks occurring for São Paulo test rig at about 333-1095 Hz and for Blithfield at about 91-300 Hz. With this information is possible to do a theoretical prediction of the bandwidth. These data give an initial idea about where the leak noise signal is potentially present.

Figure 7 - Normalized modulus of CSD for two different test rig. Initial reference of a theoretical bandwidth using the half power point, for Sao Paulo (SP) and Blithfield (BF).

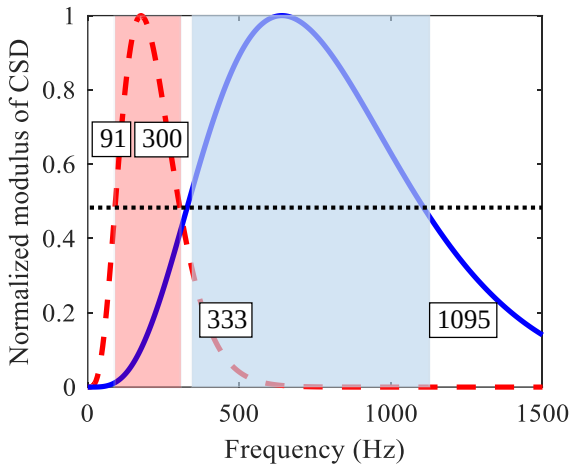

Source: Elaborated by the author.

2.4.3 Description of the test rig

In the project described in this thesis, experiments were carried out in the test rig located in the Qualification Test Center of SABESP (CEQ). This test rig has a zone with a plastic pipe network and another with a metal pipe network and was built buried under the car park, with measurement points for the sensors. Figure 8 a) shows the schematic of the test rig of plastic pipes, points P1-P17 are access points in the pipe network where the sensors can be placed. Between the access points there are output connections V1-V5 to simulate the leak. The diagram of the pipe system to simulate the leak is shown in Figure 8 b) the water from the leak passes to a control center through a narrow pipe. The leak is controlled by closing with valves, the flow of the leak is also regulated. The water that comes out of these valves is collected in a tank and is recirculated through a centrifugal pump to the pipe system, maintaining a constant pressure of about 4 bar. The material of the pipe is PVC (Polyvinyl Chloride) with outer diameter of 71.6 mm and thickness of 3.4 mm.

In Figure 9a) and b) photographs of the test rig are shown. Figure 9c) Shows a photograph of one access point. Figure 9d) and e) show the control room which contain the pump, water tank and the control valves to simulate leaks. Figure 9f) shows a photograph of a measurement station.

Figure 8 - a) Schematic of the SABESP test rig; b) schematic of the leak simulation in a buried plastic water pipe.

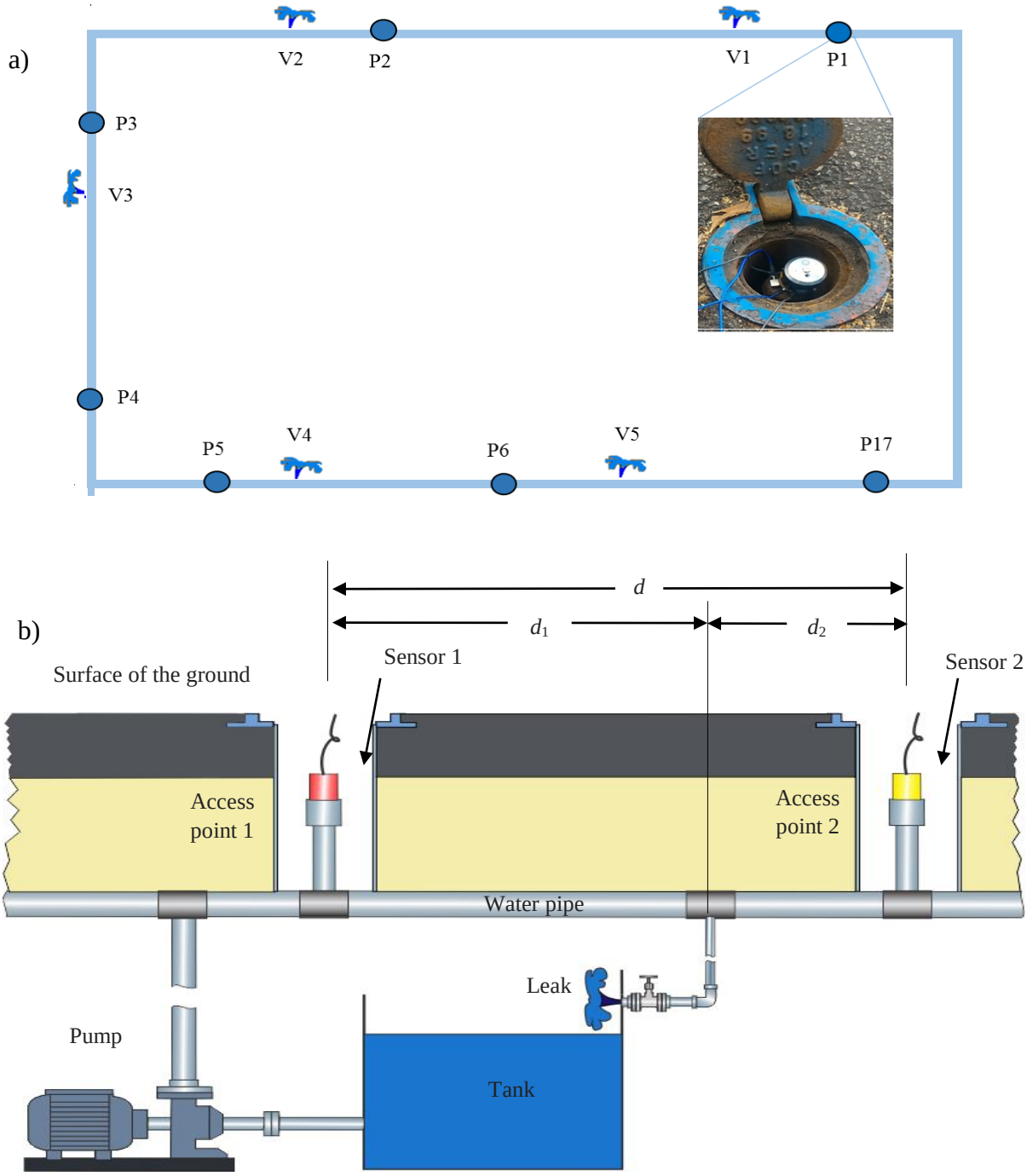

Source: Elaborated by the author.

Figure 9 - a) Qualification Test Center, b) Test rig located in the car parking, c) Access point d) pump and recirculation tank for the test rig, e) valves that simulate the leak in the test rig and f) Mobile measurement station.

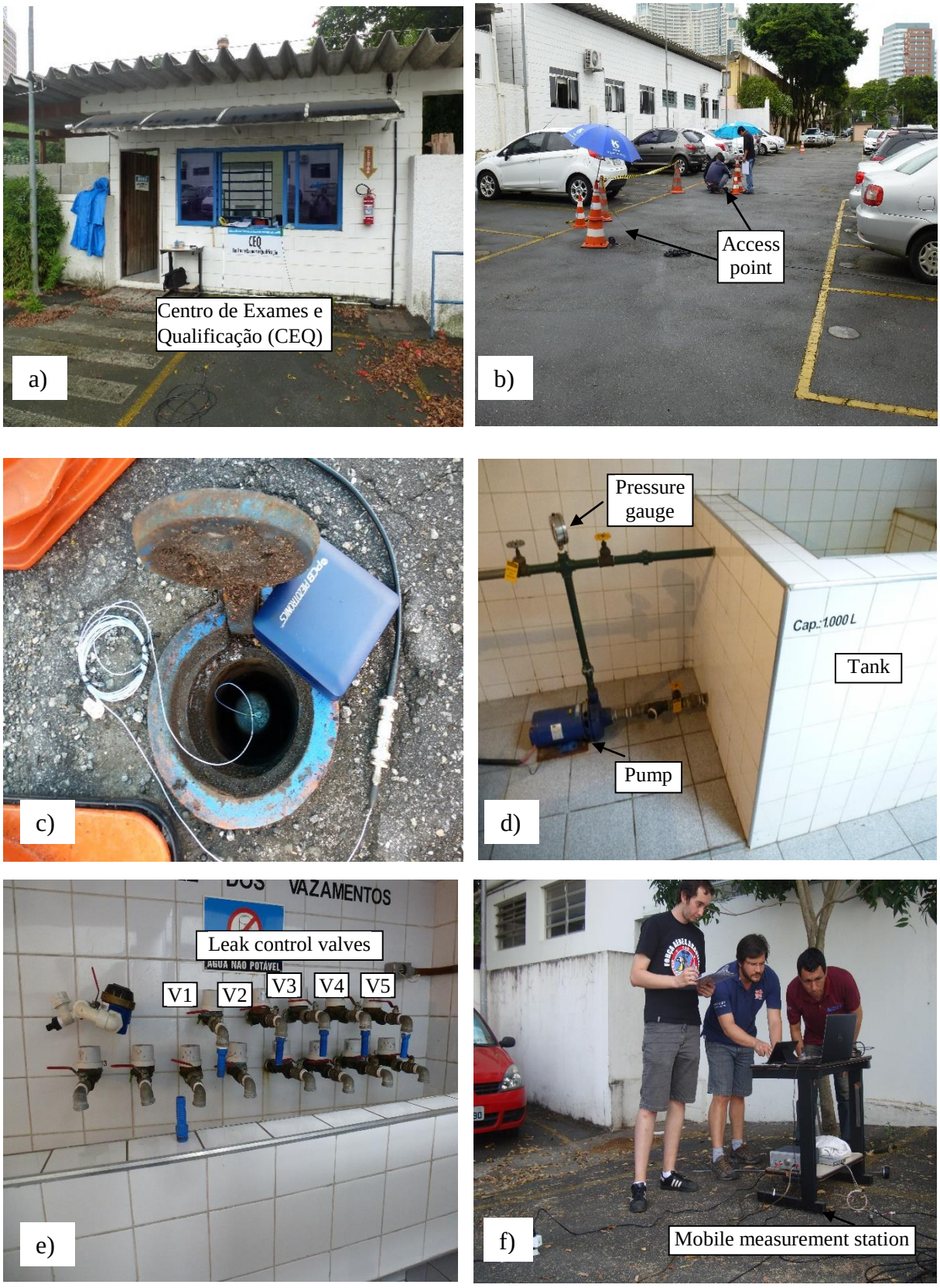

Source: Elaborated by the author.

2.4.4 Bandwidth selection

In previous section was presented, theoretically, an initial idea where the leak noise is potentially present. In the field, leak noise signals usually are contaminated with coherent noise and it is necessary to filter to increase the SNR. In order to have an effective performance, the signals have to be filtered prior to correlation. The selection of the bandwidth to filter the signals, that are of interest, is based on the coherence between the signals. The coherence function $\gamma^2_{x_1x_2}$ is given by (KIHONG; HAMMOND, 2008).

$$\gamma^2_{x_1x_2} = \frac{\left|S_{x_1x_2}(\omega)\right|^2}{S_{x_1x_1}(\omega)S_{x_2x_2}(\omega)}, \tag{21}$$

where $S_{x_1x_1}(\omega)$ is the CSD between the measured signals, $S_{x_1x_1}(\omega)$ and $S_{x_2x_2}(\omega)$ are the PSD function $x_1(t)$ and $x_2(t)$ respectively and ω is circular frequency. This function which represent the linear association between the measured signals has limits of $0 \leq \gamma^2_{x_1x_2} \leq 1$. When coherence is unity, then the two signals are highly linear associated, and 0 otherwise. Muggleton *et al*. (2011) showed that if the coherence is higher than 10^{-3} the phase could be unwrapped successfully. The data analysed in this chapter uses this condition to select the initial bandwidth in which the analysis is carried out.

2.5 Measurement procedure on the test rig

The aim of the experiment carried out on the test rig in Sao Paulo was to study the behaviour of the leak noise through the buried plastic water pipe. This means specifically locating the frequency bandwidth where the leak noise can be measured. The equipment used and the measurement procedure is described below.

Piezoelectric accelerometers from PCB Piezotronics, Model: 333B30 with a sensitivity of 100 mV/g. were connected to the access points and used for vibration measurements. The sensors were mounted by using wax on their bases to guarantee the contact. Figure 10 shows the schematic of the experimental setup with the equipment used on the field. The signals from the sensors were transmitted through cables of approximately 20 m of length to the Supervisory

Control and Data Acquisition (SCADA) from LMS and were collected simultaneously for 2 minutes with a sampling frequency of 8192 Hz. Three conditions were measured. The first one was the background noise only. The second one was the vibration pump when the pipeline was pressurized and the third one was when the leak noise was simulated by opening the valve shown in Figure 8 a). These data signals were passed through a fourth order band pass Butterworth filter, using an appropriate selection of the bandwidth, it was set so that for all frequencies between the upper and lower frequency the coherence was > 10^{-3}. These data signals were processed and analysed in the frequency domain (PSD, CSD and coherence), and by using the CCC.

The cross-correlation coefficient (CCC) was computed according the procedure in Figure 3 and using Equation 3. The time delay estimate T_0 was obtained from the peak of the CCC and with the known distances d_2 and d the speed of propagation of the leak noise can be calculated transposing in to make c the subject in Equation 1, $c = (d - 2d_2)/T_0$.

Figure 10 - Schematic of the experiment to be carried out in SABESP.

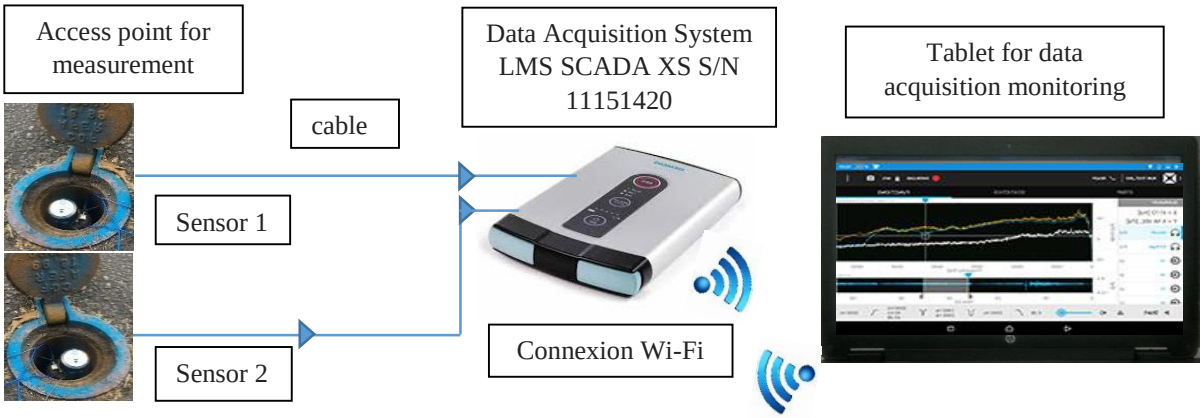

Source: Elaborated by the author.

2.6 Data analysis

In this section, the signals measured and processed are summarized in Table 2. They were collected from access points P1, P2, P3, P4, P5 and P6 (see Figure 8 a). Valves V1, V2, V4, V5 and V6 were used to control the simulated leak in each sector. Once collected the leak signal. They were processed using Matlab®. A Hanning window was used with 50% of overlap in the determination of the PSD and CSD. The processed leak signals from all the measurements are

shown in Appendix C. Taking section P3-P4 as an example, the first set of measurements carried out on 18/04/16 were processed, and as a result wavespeeds of 521, 387 and 541 m/s were obtained. The pump of the circulation system is near to this section and has an effect at low frequencies up to about 300 Hz (It is shown later), so the bandwidth was selected manually. The second set of measurements carried out on 13/03/17 were processed and as result wavespeeds of 497 and 540 m/s were obtained. A new pump was fitted and for these measurements together with a new connection for the water supply with a high-pressure hose. The pump noise was attenuated with this installation. The third set of measurements carried out on 28/06/17 were processed and as a result wavespeeds of 448, 510 and 551 m/s were obtained. For these two last set of measurements, the bandwidth was set so that for all frequencies between the upper and lower frequency the coherence was > 10^{-3}.

Table 2 - Summary of the experiments carried out in the test rig (Figure 3a),

Id		Case	Date	d (m)	d_2 (m)	bandwidth selection	Bandwidth (Hz)	T_0 (s)	c (m/s)
1	1	P1P2-v1	13/03/16	6.96	1.25	lim. 10^{-3}	399-456	17.7	252
2	1	P1P2-v1	18/04/16	6.96	1.25	manual	500-700	9.5	469
	2	P3P4-v2		7	0	manual	414-600	13.4	521
	3	P3P4-v3		7	1.54	manual	300-420	10	387
	4	P3P4-v4		7	0	manual	300-600	12.9	541
	5	P5P6-v4		5.5	1.25	manual	300-600	5.6	534
3	1	P1P2-v1	17/03/17	6.96	1.25	manual	450-700	12.7	352
	2	P1P2-v2		6.96	0	lim. 10^{-3}	486-532	18.5	376
	3	P3P4-v3		7	1.54	lim. 10^{-3}	242-648	7.9	497
	4	P3P4-v3		7	1.54	lim. 10^{-3}	272-757	7.9	497
	5	P3P4-v4		7	0	lim. 10^{-3}	272-506	12.97	540
	6	P5P6-v4		5	1.25	lim. 10^{-3}	211-639	5.9	512
	7	P5P6-v5		5	0	manual	400-600	10.4	531
4	1	P1P2-v1	28/06/17	6.96	1.25	manual	300-600	10.5	463
	2	P1P2-v2		6.96	0	lim. 10^{-3}	467-474	12.7	548
	3	P3P4-v2		7	0	lim. 10^{-3}	358-535	15.6	448
	4	P3P4-v3		7	1.54	lim. 10^{-3}	251-665	7.7	510
	5	P3P4-v4		7	0	lim. 10^{-3}	274-584	12.7	551
	6	P5P6-v4		5.5	1.25	manual	400-600	17.2	160
	7	P5P6-v3		5.5	0	lim. 10^{-3}	305-706	14	374
	8	P5P6-v5		5.5	0	manual	300-600	10	525

Source: Elaborated by the author.

2.6.1 Case study 1

In this case was analyzed measurements of leak noise with accelerometers placed at access points P3-P4 with the simulated leak using valve 2 (Out-bracket) carried out on 28/06/17. These measurement points were selected because, it is possible to observe the leak noise and the pump noise effect. The processed leak noise signals are shown in Figure 11.

In Figure 11a) and b) PSD are shown for the background noise with green dot line, pump noise with red dashed line and leak noise with blue solid line. In both figures it can be observed that the pump noise has an effect on the measurement. This is more prevalent at access point 4 because it is closer to the pump than access point 3. The frequency range where it is observed is approximately from 50 to 358 Hz. The effect of leak noise is observed also in both figures from 358 to 535 Hz of bandwidth approximately with high level of vibration in the PSD 3 because of the leak is close to the access point 3 with a distance equal to 1.54 m.

In Figure 11c) the modulus of the CSD is shown. The CSD for the background noise with green dot line, pump noise with red dashed line and leak noise with blue line. A high amplitude related to the two leak noise signal from approximately 358 to 535 Hz is observed.

In Figure 11d) the phase of CSD from approximately 0 to 358 Hz is shown. Here the effect of the pump noise is given by a straight line with a decreasing slope and above 358 Hz it is observed the leak noise with an increasing slope which is proportional to time delay (pure delay) both slopes are opposites because of the position of the acoustic sources.

In Figure 11e) the coherence that exists between the signals is shown. An appropriate selection of bandwidth, with 10^{-3} as a limit of coherence, is used here to filter the background noise and the pump noise before the CCC is calculated. The bandwidth obtained is 358-535 Hz. In Figure 11f) the cross-correlation coefficient is shown where the maximum peak indicates the time delay T_0 equal to 15.63ms. The wavespeed calculated is 448 m/s.

2.6.2 Case study 2

In this case was analyzed measurements of leak noise with accelerometers placed at access points P3-P4 with the simulated leak using valve 3 (in-bracket), carried out on 13/03/17. These measurement points were selected because, for this date, it is possible to have two sets of measurements (see in Table 2, Id3.3 and Id3.4). The processed of two sets of measurements of leak signals are shown in Figure 12. The bandwidth selection is carried out with the 10^{-3} as a

limit of coherence.

In Figures 12 a) and b) the PSD 3 and 4 for the data sets 1 and 2 are shown. It is observed that the level of vibration at access point 3 is higher than at access point 4 because of the leak is close to point 3. Moreover, in Figure 12 b) it is observed that data 2 has a higher level of vibration between 250 and 700 Hz in comparison with the data 1, possibly due to system dynamics.

In Figure 12 c) the CSD is shown for the data sets 1 and 2, It can be observed that the data 2 has more ripples than the data 1 (which is possibly due to reflections in the system). This behavior is also seen in the phase of the CSD shown in Figure 12d) for example at a frequency of 354 Hz.

In Figure 12 e) the coherence is shown for the data sets 1 and 2, where ripples are also present, which are due reflections in the system. The bandwidth is 242-648 Hz for data 1 and is 272-757 Hz for data 2. The time delay obtained is 7.9 ms and the wavespeed calculated is 497 m/s for both cases.

Figure 13 shows a comparison between the data set 1 and 2 shown above but using a limit of coherence of 10^{-2}, this restricts the bandwidth to 352-602 Hz for data 1 and 359-464 Hz for data 2. This results in a time delay T_0=7.9 ms for data 1 and a time delay T_0=10.4 ms for data 2. This difference is because for the data 2, the shape of the cross-correlation function was modified, shifting the maximum peak. In the field a wrong value of time delay would result in an incorrect location of leak. The wavespeed calculated is 497 m/s for data 1 and 377 m/s for data 2. Compared with the theoretical wavespeed of 540 m/s, given by Brennan *et al*. (2018), the analysis of data 2 gives a value very different to this.

Figure 11 - Measurement of leak signals, accelerometers are placed at points P3 and P4 with the leak simulated in valve 2 (See Table case P3P4-v2; Date 28/06/17) Using to select the bandwidth (limit of coherence 10^{-3}). (a) and (b) Power Spectral Density (PSD) for the access point 3 and 4. (c) Modulus of cross-spectral density (CSD) for signals recorder from the access point 3-4; (d) Coherence; (e) Phase of the cross-spectral density (CSD). and (f) Cross-correlation Coefficient (CCC) evaluated over the bandwidth selected. (Values in dB ref. V^2).

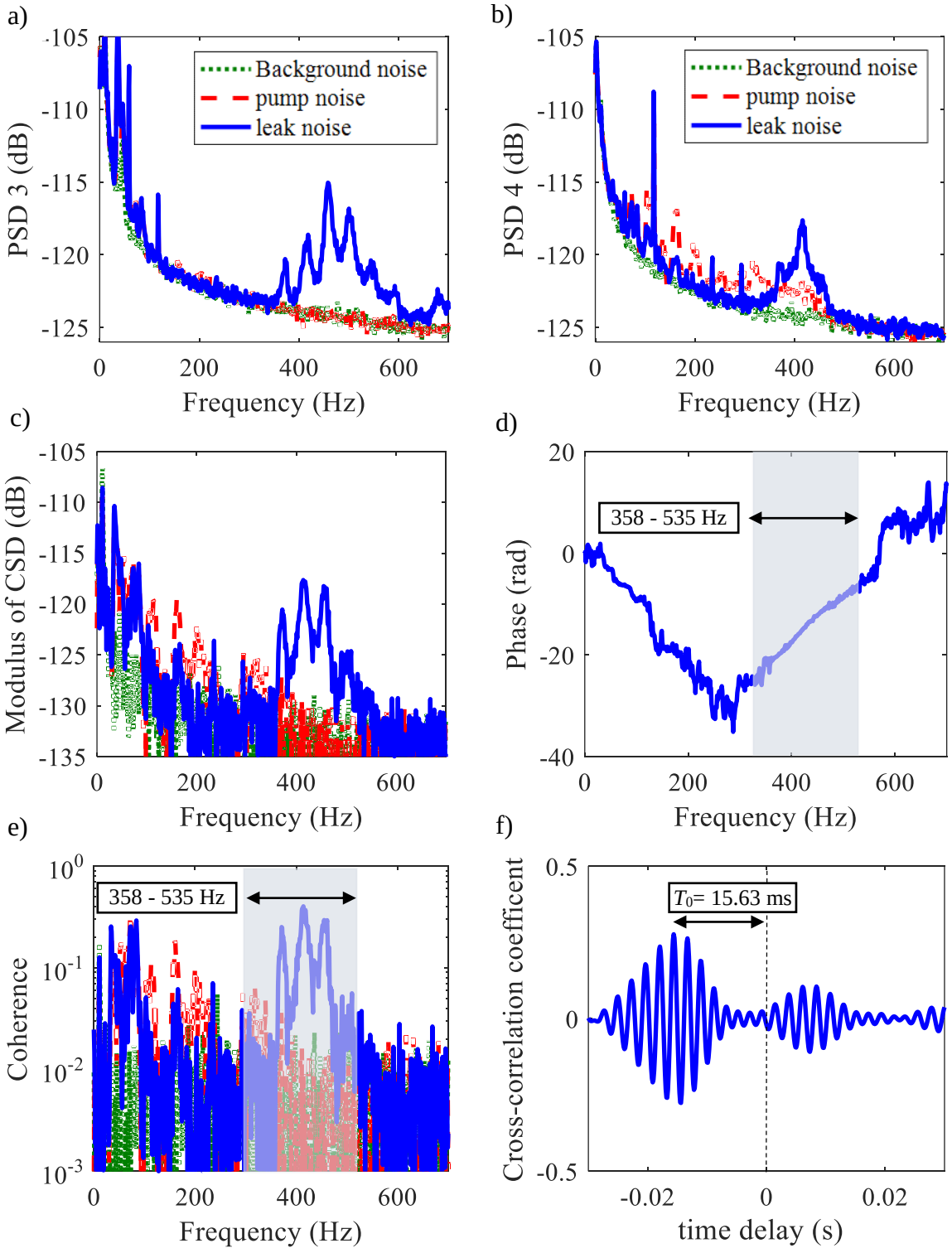

Source: Elaborated by the author.

Figure 12 - Measurement of leak noise signals using accelerometers placed at points P3 and P4 with a simulated in-bracket leak (valve 3) for a known position. Data 1 (solid blue line) and data 2 (dashed pink line), are measurement from date: 13/03/17 at the same position but at a different time. Using an appropriate selection of bandwidth, (limit of coherence 10^{-3}). (a) and (b) Power Spectral Density (PSD) for the access point 3 and 4. (c) Modulus of cross-spectral density (CSD) for signals recorder from the access point 3-4; (d) Coherence; (e) Phase of the cross-spectral density (CSD) and (f) Cross-correlation Coefficient (CCC). (Values in dB ref. V^2).

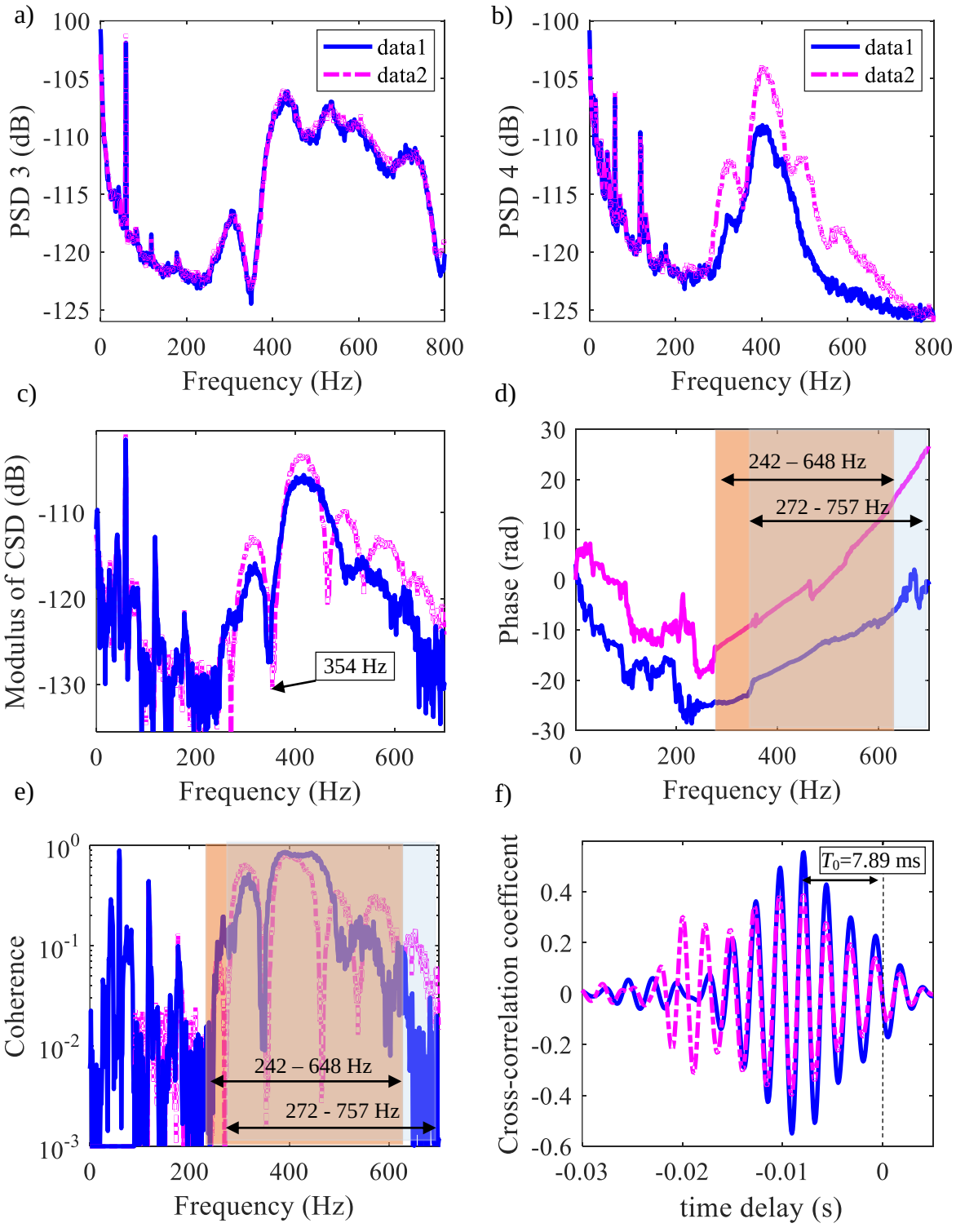

Source: Elaborated by the author.

Figure 13 - Comparison between the two data sets shown in Figure 8. The data 1 and data 2 are from measurements at the same position but with different time. Data 1 (in solid blue line) and Data 2 (in dashed pink line) are from measurement at the same position but at a different time, using an inappropriate selection of bandwidth (limit of coherence 10^{-2}) (a) and (b) Coherence for data A and data B, (c) phase of CSD and (d) Cross-correlation Coefficient.

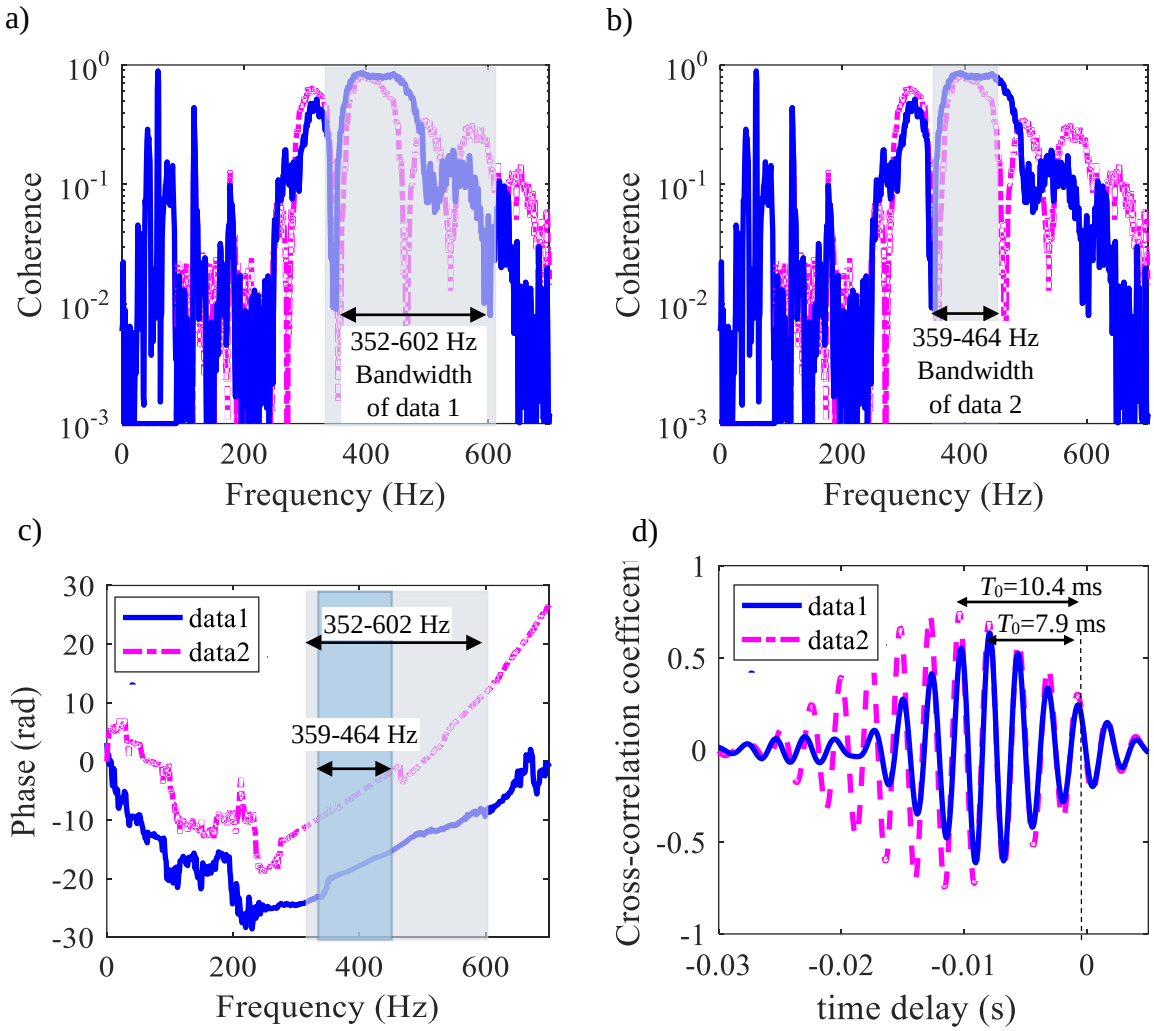

Source: Elaborated by the author.

2.7 Conclusions

In this chapter the factors that affect the estimate of the speed of leak noise propagation has been discussed. The filtering effect of the sensor-pipe system has been described, which gives an initial idea about the bandwidth where the leak noise is potentially present. Leak noise signals under controlled conditions at a test rig located in SABESP-São Paulo were collected. Their time delay and wavespeed were estimated.

The data processed are given in the Appendix C. From one section, two cases of study with out-bracket and in-bracket leak were analysed. For the first case the effect of the pump was shown. Using an appropriate method to select a bandwidth (with a coherence limit of 10^{-3}), the bandwidth to filter the background noise and the pump noise was selected, obtaining T_0=15.6 ms and 480 m/s. In the second case, two sets of data for the same section of the pipe were considered with a condition of 10^{-3} for the coherence function, obtaining a wide bandwidth, with a good result of time delay and thus wavespeed. For the same data sets, a condition of 10^{-2} was used for the coherence function. It was shown that this resulted in two-time delay estimates, which corresponded to two different wave velocities in the pipe, one of which was very different from the value expected. This shows the importance to filter appropriately the leak signals from external coherent noise (pump noise, mains, etc.). In the next chapter this information will be important in the analysis of the distortions that can occur when measurements are made with an acoustic correlator.

3 AN INVESTIGATION OF DISTORTION EFFECTS DUE TO INSTRUMENTATION ON THE ACCURACY OF THE TIME DELAY ESTIMATE

3.1 Introduction

Signals due to environmental noise (traffic, airplane passing near to measurement points, etc.), harmonics, electronic devices can lead to distortions and with that, misinterpretations of the results. In the case of this thesis, attention is focused on the effect of the distortion of water leakage signals such as quantization and clipping.

In the field, when leak detection is carried out with an acoustic correlator with two accelerometers, the following distortion effects may appear: Quantization effects can appear due to low resolution in the leak signals when it is converted from analogue to digital form. Clipping can occur if the leak noise signal is large compared to the dynamic range of the instrumentation. The selection of an appropriate gain is important to preserve the shape of these signals, and this gain is dependent upon local conditions. In some cases, the signals can become saturated.

It is also possible to have both cases in a measurement such as in the situation shown in Figure 14. If a leak is close to one point of measurement, then the level of the signal can be very large and is prone to clipping as a result of limited dynamic range in the measurement. at the other point of measurement, the level of the signal can be very small and is prone to a low resolution because of the quantization process from the analogue to digital signal.

Figure 14 - Diagram of leak detection in buried water pipe with the leak very close to measurement point 1.

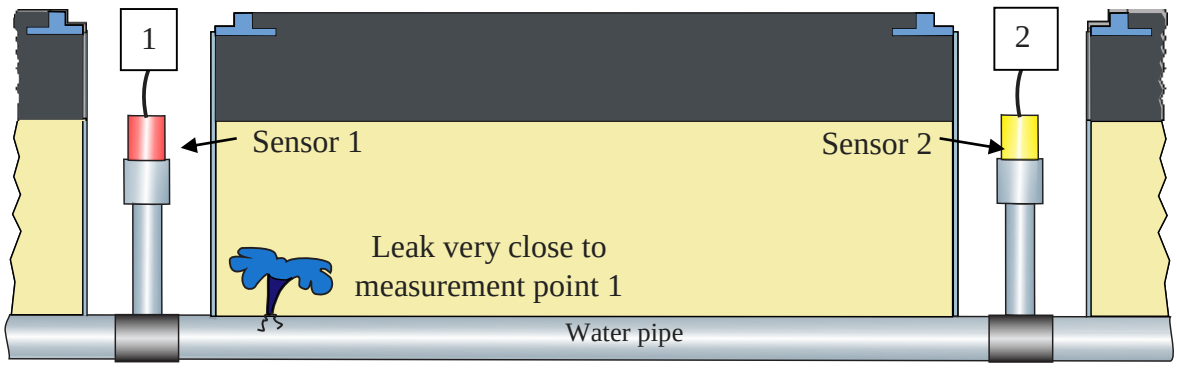

Source: Elaborated by the author.

This Chapter has two aims, the first one is to study the quantization effects with the quantization theory of an analogue/digital converter for different numbers of bits (which is related to the resolution) and a model of quantization is discussed. This model is applied to acceleration signals obtained from an analytical model for a buried water pipe system and using experimental data collected from the SABESP test rig. They are processed and analysed in the frequency domain (PSD, CSD and coherence), and in the time domain by using the CCC. The second one is to study the clipping effects. The dynamic range is set to a fixed value and the gain of the signals is increased. The same experimental data used in the quantization case is used here. Finally, the heavy clipped signal which can describe both effects is analysed, using the signum function. The relationship between the cross-correlation function of severely clipped with unclipped signals is used to compare the cross-correlation function of the signals modified with signum function.

3.2 Quantization effects on the time delay estimate

Physical measurements in leak detection, for example acceleration obtained from an accelerometer, ground movement (velocity) obtained from a geophone, pressure obtained from a hydrophone, etc. are often represented digitally. For processing, conversion of these signals into digital form is necessary.

The process of analog to digital (A to D) conversion is shown in Figure 15. It can be seen that sampling occurs first, which is where the continuous-time signal is converted to discrete-time signal x by sampling at discrete time instants. If an analog signal is not correctly sampled, aliasing can occur (KIHONG; HAMMOND, 2008). For aliasing not to occur, the sampling rate has to be at least twice that of the highest-frequency component of the analog signal. The second operation in the A to D converter is quantization. This is the conversion of each sample into a digital word, which has a value from a finite set of possible values. In binary format the bits take values of 0 and 1. A large number of bits is required for good resolution (WIDROW; KOLLAR, 2008). In this conversion process as result of the quantization, an error or noise appears which is undesirable. This error is controlled by having a good resolution, increasing the processing time and storage space for the data collected. In order to establish a balance between accuracy and economy for the digitized signal, it is important to study the effects on

the accuracy of the time delay estimate. The aim is to find the minimum number of bits required to have an accurate an estimation of the time delay, and thus to use inexpensive electronic components which have an ADC with a small number of bits.

Figure 15 - Block diagram of the conversion of Analog signal to Digital signal (A/D).

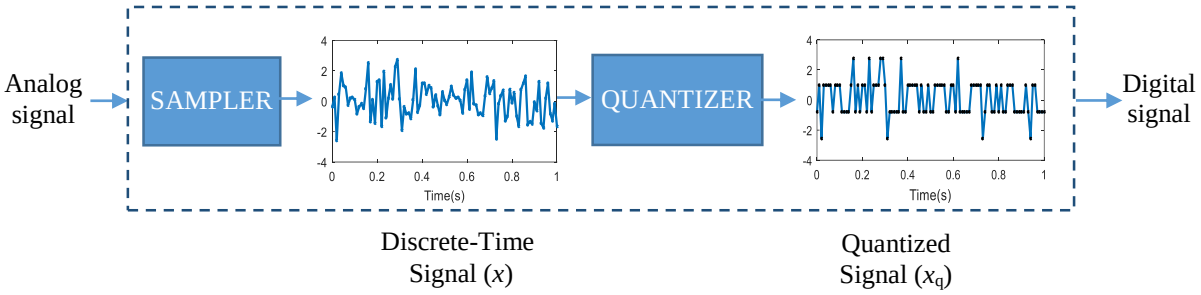

Source: Elaborated by the author.

In the following subsection, the basic concepts of the quantization process are described and applied to a simple signal and later applied to a leak signals, studying its accuracy in time delay estimation.

3.2.1 Quantization

There are different methods for quantization depending on the requirements of the system. The offset or unipolar method (ISEN, 2008) is shown here, in which a typical analog signal having both positive and negative voltage values is given a DC offset so that it is entirely nonnegative. It has 2^N quantization levels, where N is the number of bits.

The quantized step is given by

$$\Delta = \frac{\text{Dynamic range}}{2^N - 1}, \tag{22}$$

where the dynamic range determines the full-scale level of the quantizer (ISEN, 2008). For example, if the dynamic range is ± 1 and the number of bits is 12, the number of levels are 2^{12} and the step Δ is $4.9e^{-4}$.

Figure 16 shows the process of quantization for 2 bits using the offset method. In Figure 16 a) a sampled sinusoidal signal is shown with an amplitude 1 volt. The dynamic range is equal to the twice the amplitude of the sinusoidal signal. In Figure 16 b) for this signal there is a DC offset and the quantization steps are computed by dividing the peak amplitude (2 volts) of the input signal by (2^2 -1), which is the number of increments above zero needed to reach the peak amplitude from the minimum amplitude, which is set at zero in accordance with the offset method. The signal is quantized in (2^2) levels represented by the blue circle marks. In Figure 16 c) the quantized signal is shown in an AC offset form.

Figure 16 - Process for quantizing signal with offset method. dotted black line —●, sampled signal and blue circles marks —o, quantized signal.

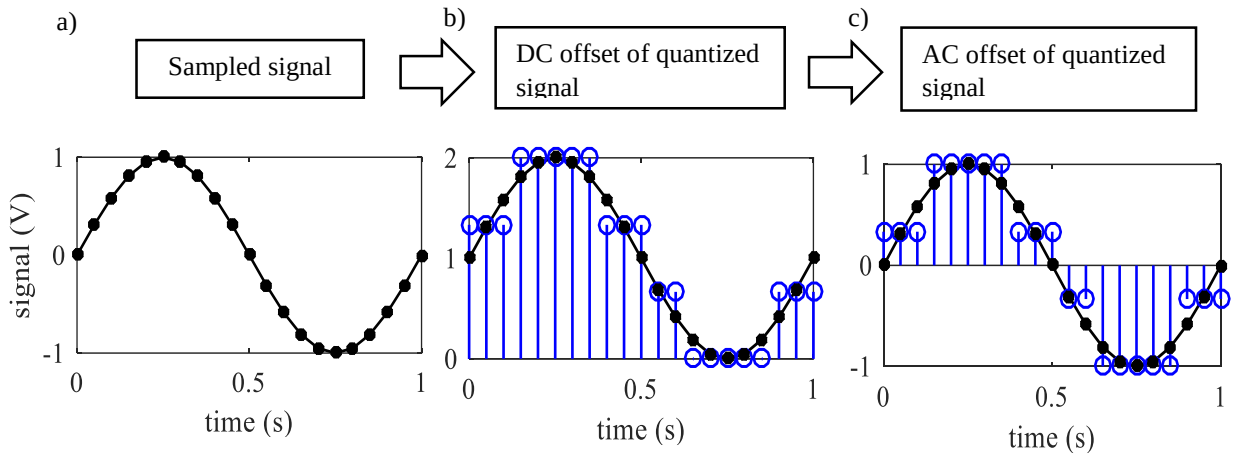

Source: Elaborated by the author.

3.2.2 Quantization Error

Quantization error or noise is the difference between the quantized signal value and the sampled signal value given by (OPPENHEIM; SCHAFER, 2013)

$$e = x_q - x, \tag{23}$$

where x_q is the quantized signal and x the sampled signal.

In Figure 17 a quantization of a sinusoidal signal with 2 bits presented previously is shown. The dynamic range is also 2, which is the full-scale level of the converter. It has 4 quantization

levels. In Figure 17 b) the quantization error or noise as a function of input signal is shown. It is observed that the values of the error are between [-Δ/2, Δ/2].

Figure 17 - a) A uniform quantizer of two bits for sampled sinusoidal signal. Thick black line —, sampled signal and blue circles marks —o, quantized signal; b) Quantization error for 2 bits.

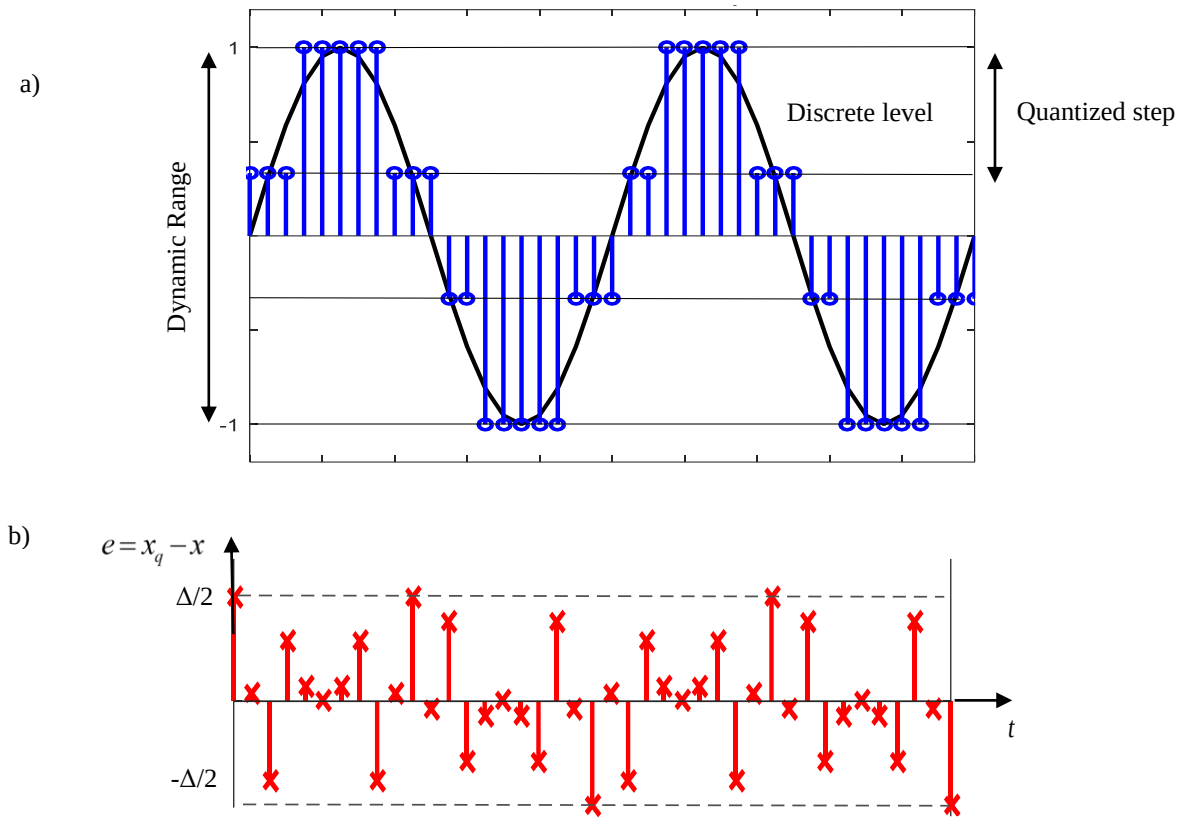

Source: Elaborated by the author.

3.2.3 Signal to quantization Noise Ratio (SQNR)

The effect of additive noise in the sampled signal desired can be quantified with the signal-to-quantization noise ratio *SQNR*. Which is given by (OPPENHEIM; SCHAFER, 2013)

$$SQNR = \frac{\sigma_s^2}{\sigma_e^2}, \tag{24}$$

where σ_s^2 and σ_e^2 are the variances of the signal and the quantization error. The SQNR can be expressed in dB as

$$SQNR_{dB} = 10\log_{10}\left(\frac{\sigma_s^2}{\sigma_e^2}\right). \quad (25)$$

The variance is derived for the quantization error is given by (PELGROM, 2013)

$$\sigma_e^2 = \int_{-\Delta/2}^{\Delta/2} e^2\, p(e)\mathrm{d}e = \frac{1}{\Delta}\int_{-\Delta/2}^{\Delta/2} e^2 \mathrm{d}e = \frac{\Delta^2}{12}, \quad (26)$$

where $p(e)$ is Probability density function of quantization error which is assumed to be constant and uniformly distributed. Combining equations (3.4) and (3.5) gives

$$SQNR_{dB} = 10\log_{10}\left(\frac{\sigma_s^2}{\Delta^2/12}\right) = 20\log_{10}\left(\sqrt{12}\right) + 20\log_{10}\left(\frac{\sigma_s}{\Delta}\right). \quad (27)$$

Simplifying equation (27) gives

$$SQNR_{dB} = 10.79 + 20\log_{10}\left(\frac{\sigma_s}{\Delta}\right). \quad (28)$$

This equation is used in the next section to calculate the SQNR of a sinusoidal signal and some experimental data from SABESP test rig.

3.2.4 Quantization of a sampled sinusoidal signal

Many systems use or are based on sinusoidal signal specifications. A sine wave can be easily generated with high quality. Therefore, in A/D converters, a sinusoidal signal is used to characterize the performance (PELGROM, 2013).

Figure 18 shows the quantization of a sampled sinusoidal signal using the offset method for different numbers of bits. For this example, the dynamic range is considered to be equal to twice of the amplitude of the sampled sinusoidal signal. The sampled sinusoidal signal, quantized signal and quantization noise are shown in thick solid black line, blue circle mark and red cross mark respectively.

It is observed that the quantized signal has 2, 4, 16 and 256 levels for 1, 2, 4 and 8 bits respectively. The quantization noise has an amplitude between ± a half of the quantization step. It is observed that for one bit the quantization noise is highly correlated with the signal. It can be seen that when the number of bits increases the quantization noise amplitude diminishes and there is a better signal resolution.

Figure 18 - Quantization of a sampled sinusoidal signal with f_s=20 samples/cycle; and comparison between sampled sinusoidal signal and error for a) 1 bit, b) 2 bits, c) 4 bits and d) 8 bits. thick solid black line —, sampled sinusoidal signal, thick solid blue line —o quantized signal, and dashed red line ---x, quantization error.

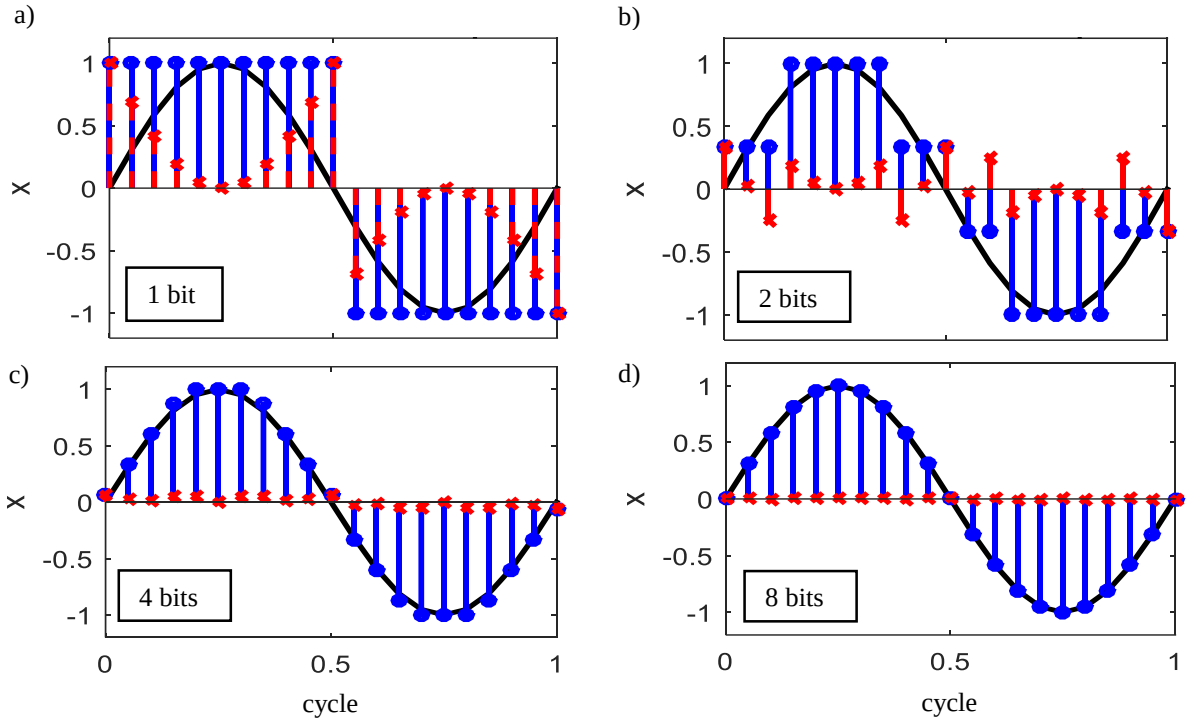

Source: Elaborated by the author.

The SQNR for sinusoidal signals is calculated using equation 3.7, replacing the step Δ obtained with the equation 3.1 which is $\Delta = 2X/(2^N - 1)$, where X is the amplitude of the sine wave and the variance of the sine wave is $\sigma_s^2 = X^2/2$. The resulting equation is given by (PELGROM, 2013).

$$SQNR_{dB} = 1.76 + 20\log_{10}\left(2^N - 1\right). \quad (29)$$

Table 3 shows the signal to quantization noise ratio (SQNR) for the sinusoidal signal with its respective number of bits. In this table is observed that the SQNR increases by approximately 6dB for each increase of a bit. It is observed that if the signal amplitude of the sine function is for example 6% of the dynamic range of an eight-bit analog-to-digital converter, this converter functionally is equivalent to a five bit analog-to-digital converter (see in Table 3 for 31.5 dB of SQNR is approximately 5 bits).

Table 3 - Signal to quantization noise ratio numerical for different number of bits with 20 sampled/cycle.

Bits	1	2	3	4	5	6	7	8	9	10	11	12	13	14	15	16
SQNR (dB)	1.8	11.3	18.7	25.3	31.6	37.8	43.9	49.9	56	62	68	74	80.1	86.1	92.1	98.1

Source: Elaborated by the author.

3.2.5 Quantization of a leak signal

In this section a leak is generated theoretically using a model for a leak in a buried water pipe, then it is quantized and using the model of cross-correlation function is analysed the accuracy in time delay estimate. Finally, an experimental case of leak detection from SABESP test rig also is quantized and analysed.

Figure 19 shows the procedure to model the correlation function of a quantized leak signal in buried plastic water pipe. As a first part, a white noise is used as acoustic pressure to simulate leak noise in the time domain. The Fourier transform is used to change to the frequency domain which is then multiplied by the transfer function *H* to obtain the measured leak noise signal in the frequency domain. Finally, to change to the time domain the inverse Fourier transform is applied. With the theoretical leaks generated, the leak signals are processed by applying the quantization model, to these leak signals. They are then transformed to the frequency domain using the Fourier transform. Then these signals in frequency domain are multiplied, one of them by the conjugate. Finally, it is averaged and applied the inverse Fourier transform to change on time domain, obtaining the cross-correlation function.

Figure 19 - Schematic of the procedure to model the correlation function of a leak quantized signal in buried plastic water pipe.

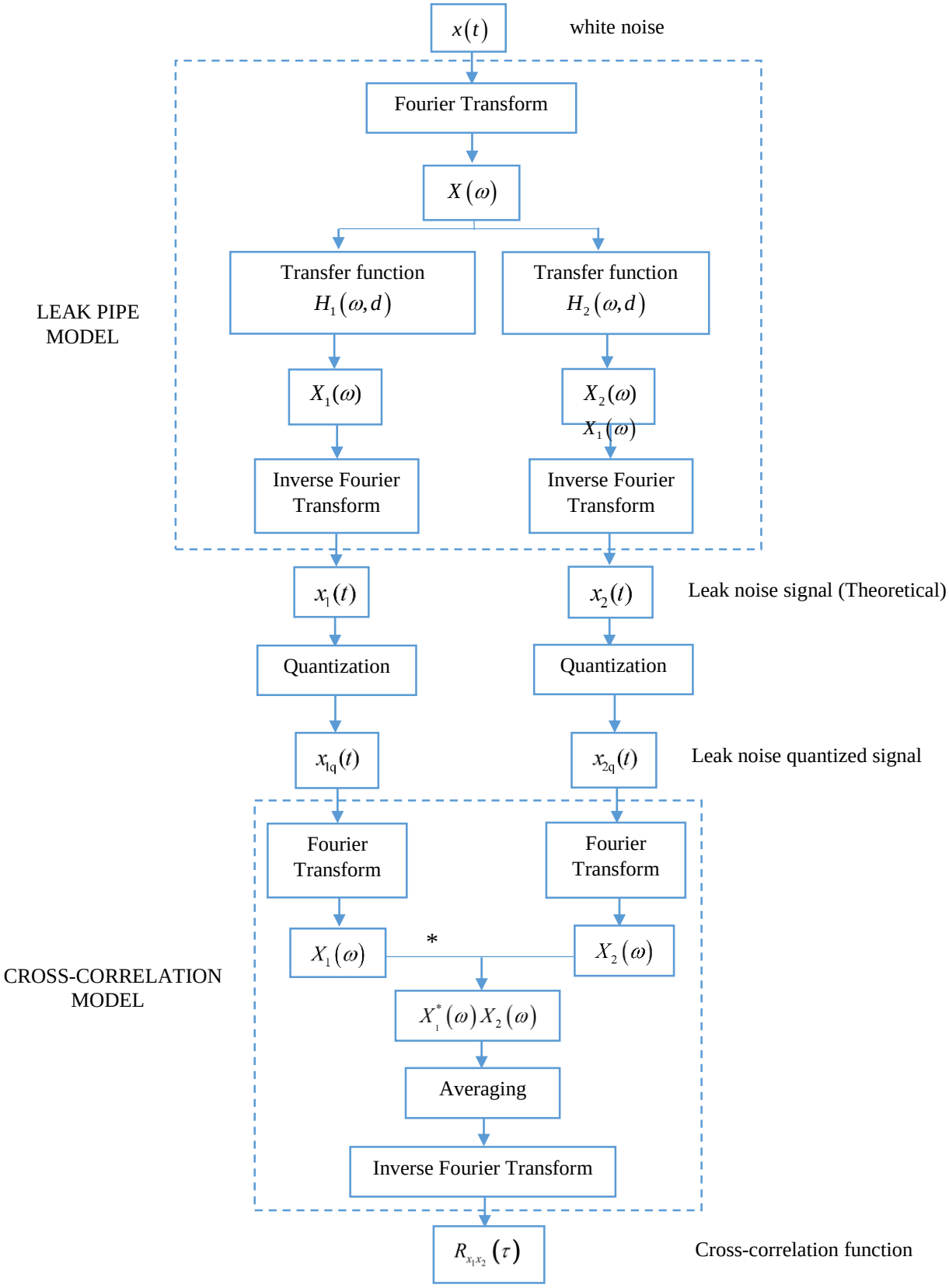

Source: Elaborated by the author.

3.2.5.1 Simulation

A typical leak detection problem is simulated (see Figure 1-Chapter 2) adding a quantization model. Properties of the leak pipe model are shown in Table 4. These properties are taken to simulate a test rig located in Canada. The distances are chosen arbitrarily.

Table 4 - Physical properties of the pipe-model from a test rig in UK with $d_1 \neq d_2$.

Mean radius of the pipe	75 mm
Pipe-wall thickness	9.85 mm
Pipe Young's modulus	$2x10^9$ N/m^2
Pipe loss factor	0.1
Bulk modulus of water	$2.2x10^9$ N/m^2
Free-field wave-speed in water	1500 m/s
d_1; d_2	20 m, 30 m

Source: Elaborated by the author.

The sampling frequency for 10 second of acceleration time histories is 8 kHz. The transformation to the frequency domain is carried out using a 4096 point FFT and a Hanning window with 50% overlap.

For this example, the dynamic range of the quantizer is ±1V. Figure 20 shows the time history of theoretical leak signals sampled and quantized for 1, 2, 4 and 8 bits. It is observed that sensor 1 has signals collected with amplitudes greater than at the sensor 2 due the proximity of the leak to the sensor 1. Quantization levels are shown as gray lines and it is observed, for example for the sensor 2 for 1 and 2, the behaviour is as a 1 bit converter. It is observed not all the levels of quantization are used, showing a low resolution. For 8 bits, it is possible to observe more quantization levels increasing the resolution. In the following section the influence of the quantization and its resolution is analysed for the estimation of the time delay in the detection and location of water leaks.

Figure 20 - Simulation of leak noise signals acquired by the sensor 1 and 2 with the leak pipe model, quantized for a) and ai) 1 bit; b) and bi) 2 bits; c), ci) 4 bits; d), di) 8 bits. Gray lines —, quantization levels; red dashed-dotted line ---, sampled signal; thick solid blue line —, quantized signal.

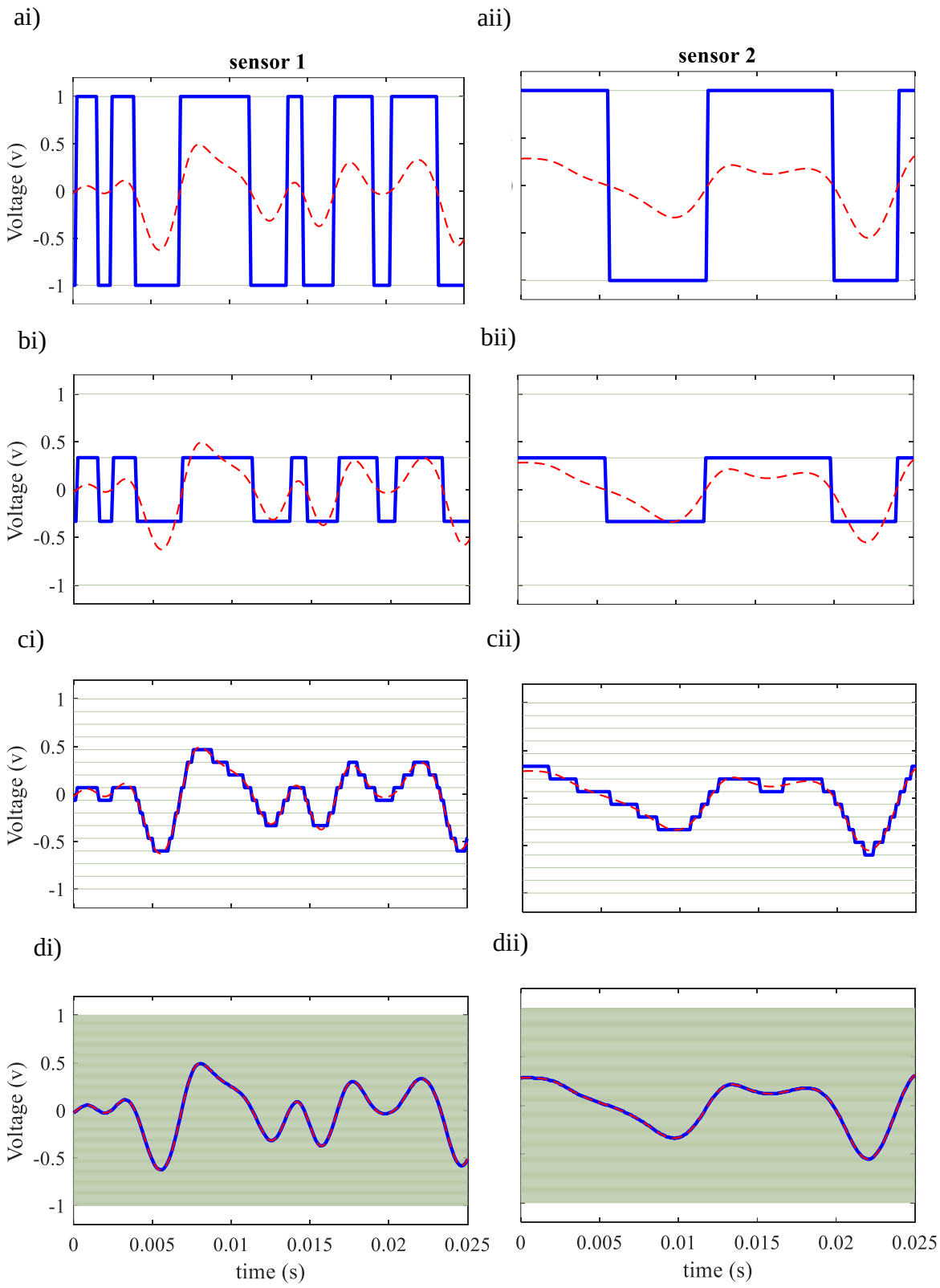

Source: Elaborated by the author

3.2.5.2 Analysis of the cross-correlation coefficient

In this section the effect of quantization on the processing of quantized signals is investigated. The PSD from sensors 1 and 2, the modulus and phase of the CSD, the coherence and the cross-correlation coefficient are shown in Figure 21 a), b), c), d), e) and f) respectively. They are calculated for the case study with the model of quantization for 1, 2, 4 and 8 bits chosen arbitrarily and with numerical solutions for comparison of results.

In Figure 21 a) and b) the PSD obtained from the sensor 2 and 1 is shown. They were normalized. It can be seen that in general, they have the same trend between the frequency range where the leak is present. Working with more resolution (8 bits) is possible to get a good approximation respect to the numerical solution.

In Figure 21 c), the module of the CSD is shown for different number of bits in the quantizer. They have the same trend and they are according with the analytical solution between 50 to 200 Hz (here the energy associated between the signals with the largest amplitudes are located), then over 200 Hz the behaviour is flat in contrast with the analytical solution which decreases when the frequency increases. In Figure 17 d), the phase of the CSD is calculated for different number of bits. For all the cases, in comparison with the numerical solution, there is a bandwidth from approximately 10 to 200 Hz with the same trend.

In Figure 21 e), it is observed that the coherence decreases when the number of bits decrease. That is because with low number of bits, the signals obtained from the sensor 1 and 2 lose the degree of linear association between them.

Figure 21 f) is shown the cross-correlation coefficient for different numbers of bits and compared with the numerical solution it can be seen that the peak decreases when the number of bits decreases, but the time delay obtained where the peak is maximum is the same for all cases. That’s mean that the accuracy for the time delay estimate is not affected. In the next section a real case will be presented.

.

Figure 21 - a) PSD of signal from point P1 (b) PSD of signals from point P2 (c) Modulus of the CSD (d) Coherence (e) Phase spectrum (f) Cross-correlation coefficient over the frequency range. —1bit; ---2 bits; ....4 bits; -·-· 8 bits, — numerical solution.

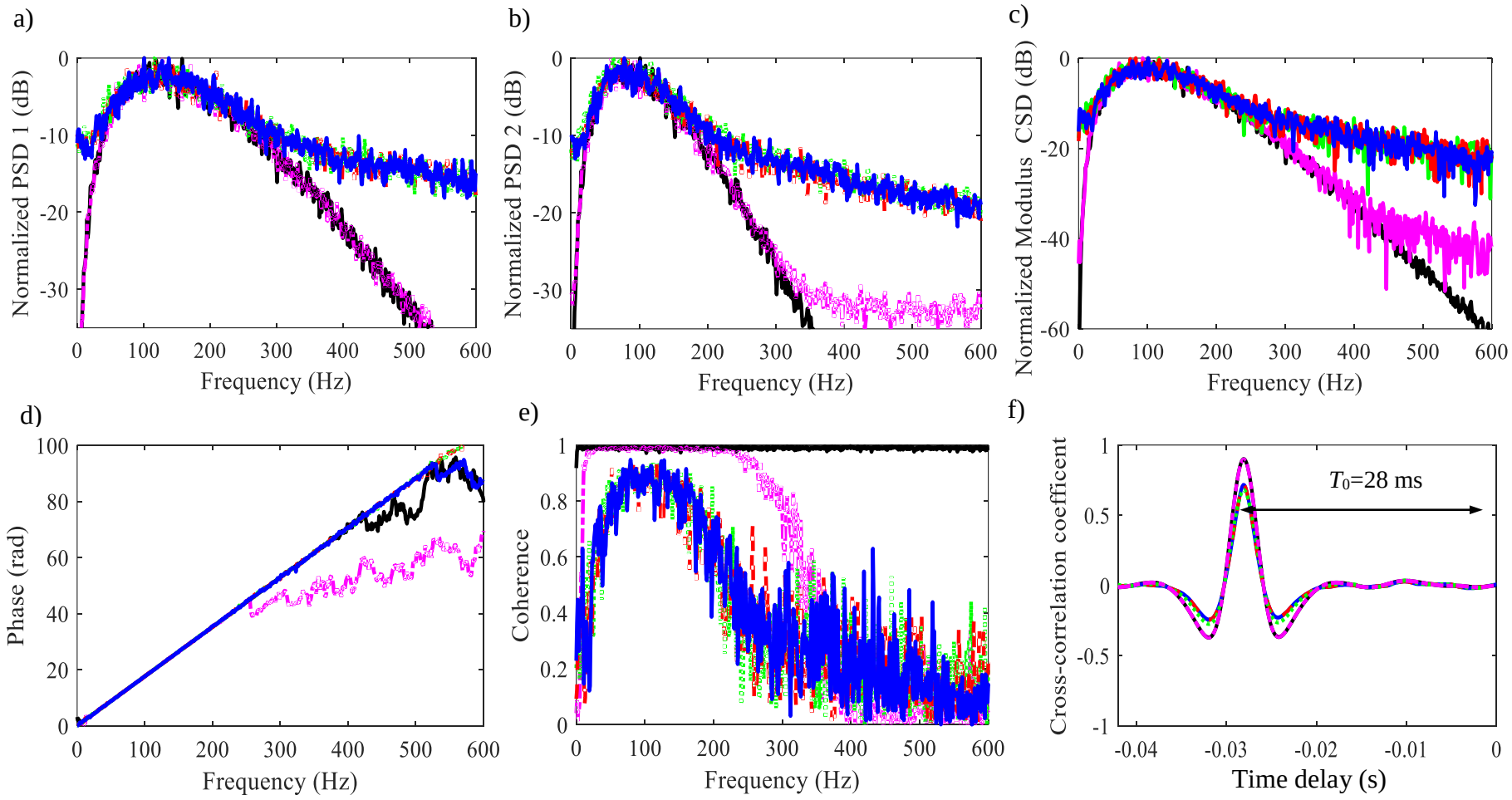

Source: Elaborated by the author.

3.2.5.3 Experimental case

Data that were collected on SABESP test rig (Figure 8 a) from access points P5-P6 with leak simulated in valve 4 on 18/04/16 (Table 1 Id. 2.4) is analysed in this section. The quantization effects are shown here as in the theoretical case. The material of the pipe is PVC and the distances d_1 and d_2 are 4.25 m and 1.25 m. These signals were sampled with 8192 Hz and with an acquisition time of 2 minutes. They are then filtered through a fourth order band pass Butterworth filter. The bandwidth was chosen manually from 300 to 600 Hz, as it was mentioned in chapter 2 in this date, the effect of the pump is observed until 300 Hz. The signals were then passed through an algorithm of quantization with a dynamic range of ±1 V, for 1, 2, 4, 8 bits chosen arbitrarily.

In Figure 22 sampled signals and quantized signals for 1 and 8 bits from the sensors placed at access point 5 and 6 are shown. It is observed for 1 bit that is used, for all the levels (2 levels of quantization), the signals are quantized effectively. Similar to the theoretical analysis the resolution increases when the number of bits increases. This resolution does not affect the analysis of the processed signals as was seen in the theoretical case for different numbers of bits.

Figure 23 is shown the normalized PSD obtained from these quantized signals, modulus normalized and phase of the CSD, coherence and cross-correlation coefficient, for 1, 2,4 and 8 bits. The sampled signal was passed through a band pass fourth order Butterworth filter, with lower and upper limits of 300 Hz and 600 Hz, respectively before applying the quantization process. The cross-correlation coefficients were computed using a 10240-point FFT, 5120 of overlap and applying a Hanning window.

It is observed in Figure 23 a), b) and c) that the tendency of the PSD and the modulus of the CSD obtained from the signals have the same tendency for 1, 2, 4, 8 bits for the sensors placed at P5-P6. Figure 23 d) shows the phase of CSD that has the same slope for all cases. It is observed in Figure 23 e) that the coherence increases when the number of bits increases, this is because the signals have good resolution when the number of bits increases and the distortion disappears. Figure 23 f) shows the cross-correlation coefficient (CCC). It is observed that the height of the maximum peak varies in all the cases, increasing the height of the maximum peak when the number of bits increases (resolution). From the CCC the time delay estimate (T_0) is obtained which is 5.6ms with wavespeed of 534m/s for all numbers of bits analysed.

Figure 22 - Quantization of leak signals collected in SABESP test rig from access points P5-P6 with leak simulated in valve 4 on 13/03/16; ai) and aii) 1 bit; bi) and bii) 2 bits; ci) and cii) 4 bits; di) and dii) 8 bits. Gray lines —, quantization levels; red dashed-dotted line---, sampled signal; thick solid blue line —, quantized signal.

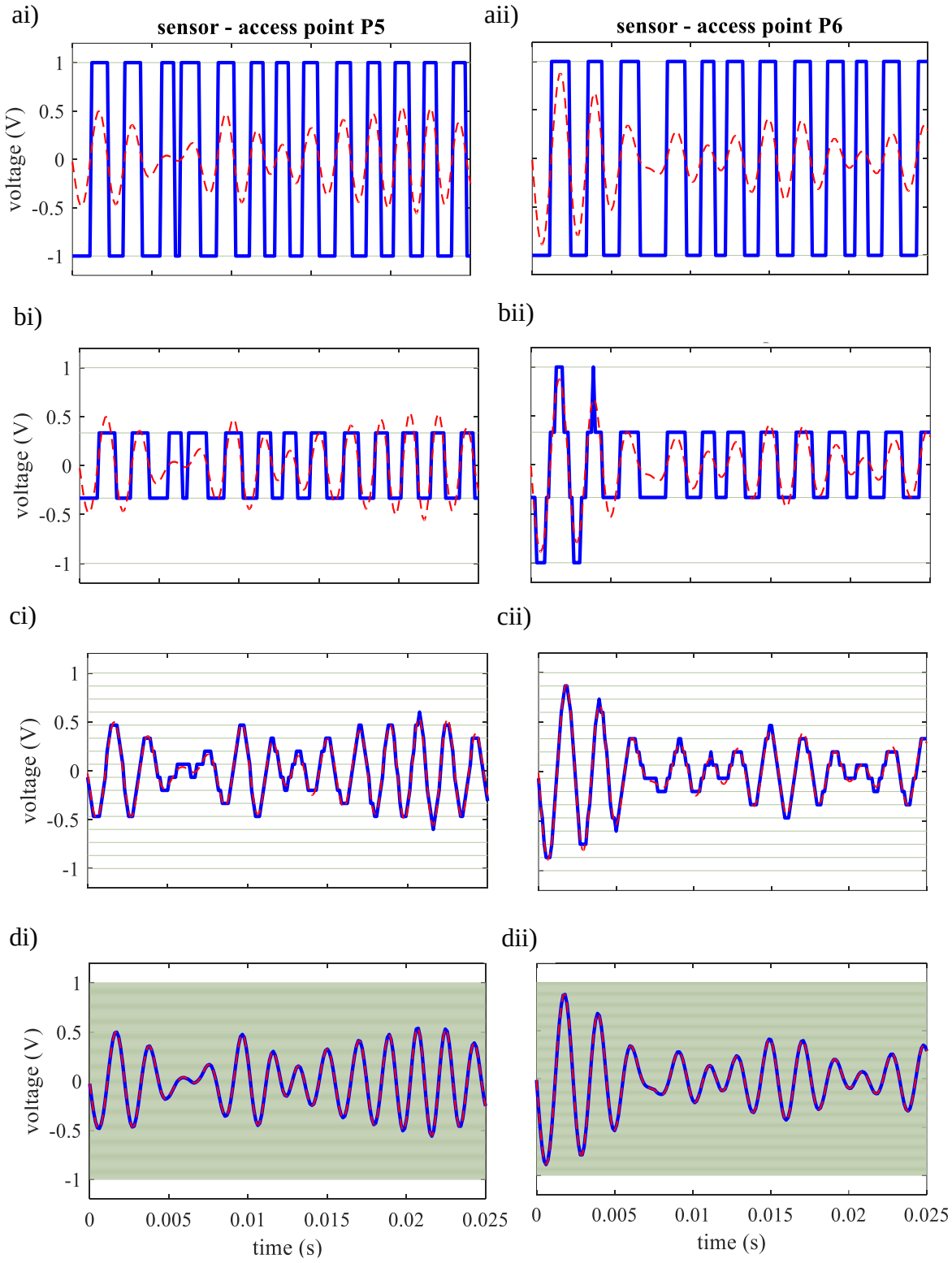

Source: Elaborated by the author.

Figure 23 - a) Normalized PSD of signal collected from access point P5, (b) Normalized PSD of signal collected from access point P6, (c) Normalized Modulus of the CSD, (d) Coherence, (e) Phase spectrum and (f) Cross-correlation coefficient. —1bit; ---2 bits; ....4 bits; -·-· 8 bits.

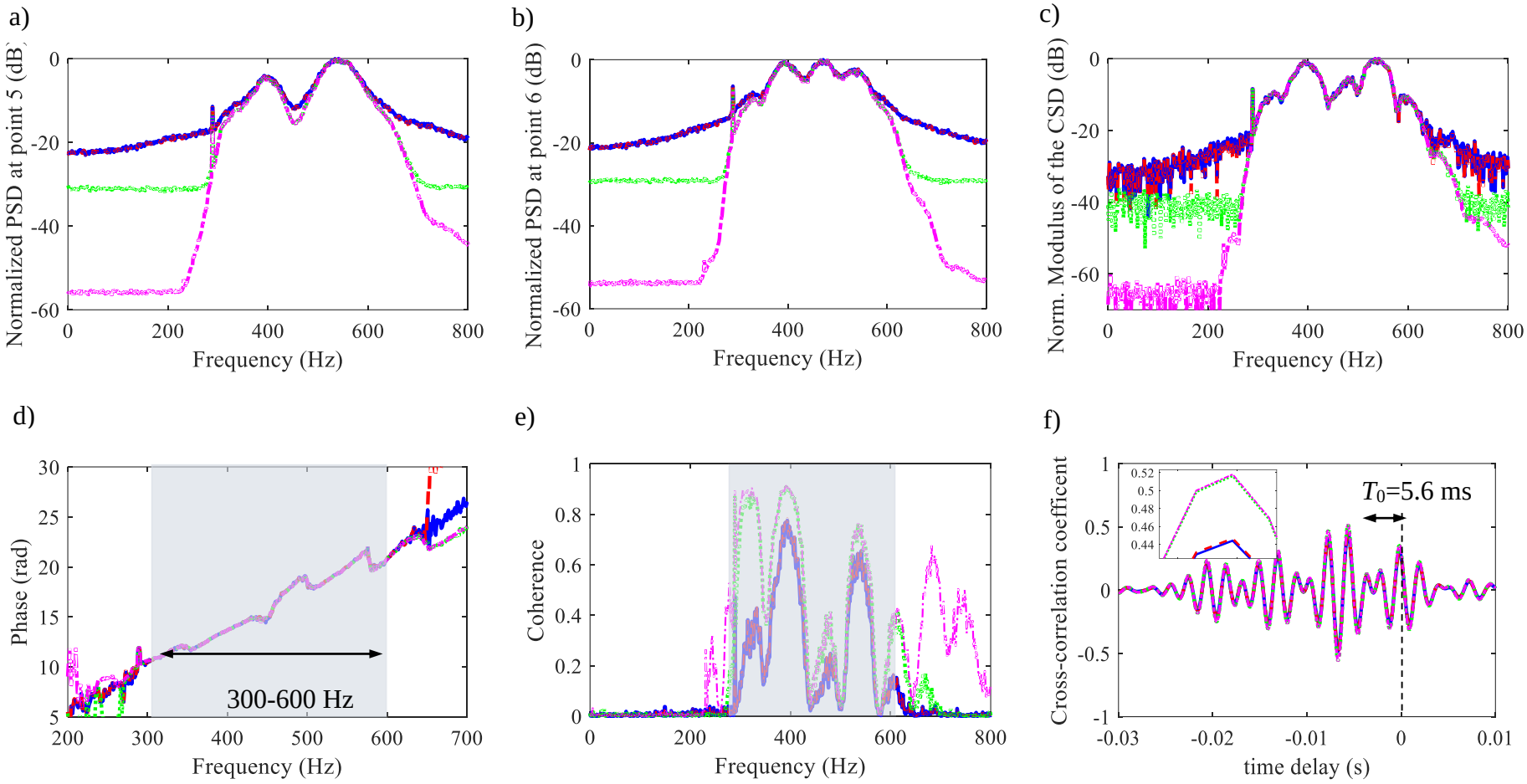

Source: Elaborated by the author.

3.3 Clipping effects in time delay estimate

Leaks signals from plastic pipes can be affected by high attenuation levels in the system during propagation, which means that the background noise can mask these signals. The selection of appropriate gain is important to improve these signals and have no problems in the processing. In some cases, this can cause that the signals to become saturated (clipped). In this section the clipping effect on the time delay estimate is investigated.

3.3.1 Experimental case

In Figure 24 the experimental case shown in the last section is analysed here, the leak signal is amplified (multiplying by 4000). With this value it was possible to show the clipped signal due to the limits of the dynamic range of ±1V.

Figure 24 a) and b) are shown the clipping in both signals in blue thick line and the original signal in red dashed line. It is observed that the leak signal in P5 is larger than the leak signal in P6, exceeding in some parts the dynamic range and because of that P5 suffers more peaks cut than P6.

In Figure 24 c) and d) are shown the PSD of leak signals from the point P5 and P6 respective. It is observed that PSD 5 has a slight variation in low frequencies than PSD 6 when are compared the clipped and unclipped signals. That is because it is observed that there are more peaks cut in P5 than P6. In Figure 24 e) and f) are shown the modulus and phase of the CSD and it is observed that there is apparently no variation.

In Figure 24 e) and f) it is shown the coherence and the CCC respectively. It is observed that the coherence for the clipped signal decreases a bit at low frequencies. The distortion generated by the clipped signals causes the similarity of their decreases in comparison with the unclipped signals. Because of that it is also observed that some peaks in the cross-correlation function increased their height.

Using the normalized CCC is obtained the time delay estimate (T_0) from the maximum peak, which is 5.6ms and a wavespeed of 534m/s which are the same results when the signal is quantized for 1 and 16 bits in the previous analysis.

Figure 24 - Clipping of leak signals sampled. Leak signal sampled, red dashed line; leak signal clipped, blue thick line; from a) access point P6 and b) access point P5; c) PSD of leak signal from point P6 d) PSD of leak signals from point P5; d) Normalized Modulus of the CSD; f) Phase spectrum; g) Coherence; h) Basic cross-correlation.

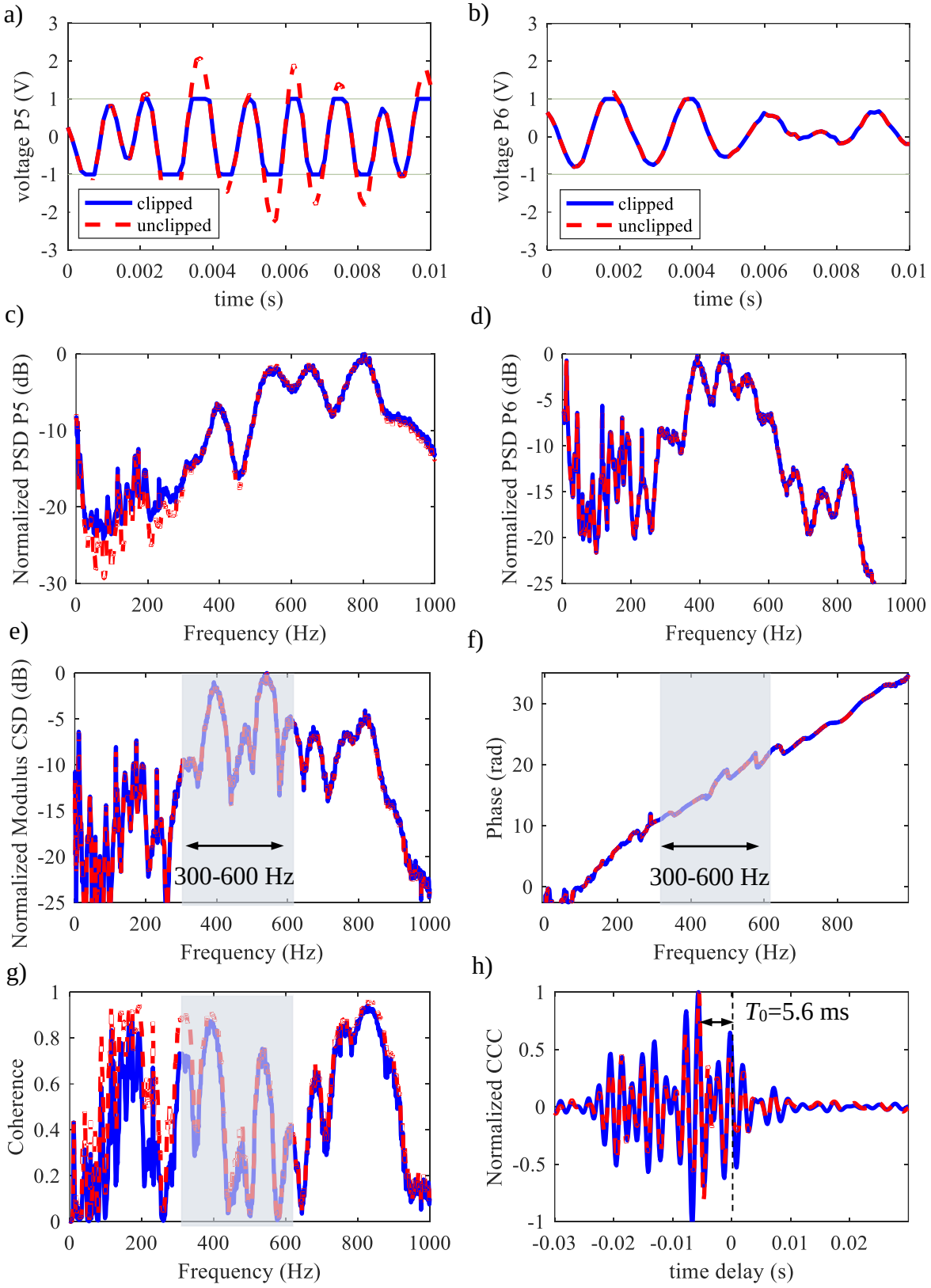

Source: Elaborated by the author.

3.3.2 Heavily clipped signal

In the introduction it was mentioned that in the field it is possible to have high amplitude of the leak signals, depending of the strength of the leak and the distance of the measurement position from the leak. When the dynamic range is fixed due to conditions of the electronic device, two extreme situations make the signals quantized or clipped. In this section, Van Vleck theory is used to study the relation between the CCC of clipped and unclipped signals. This theory, elaborated in 1943 was applied at that time to enhance the radar and communications processes. Nowadays, for the leak detection community it is not well known. To simulate the severely clipped signals, the signum function is applied to acceleration signals of leak noise obtained from the data collected in the test rig, so that they take a value of -1 if the value of signal is negative and +1 if the value signal is positive. An example of an original leak noise signal, and the same signal modified by the signum function is shown in Figure 25.

Figure 25 - A typical leak noise signal. Unclipped signal and severely clipped signal with red dashed line and blue solid line respectively.

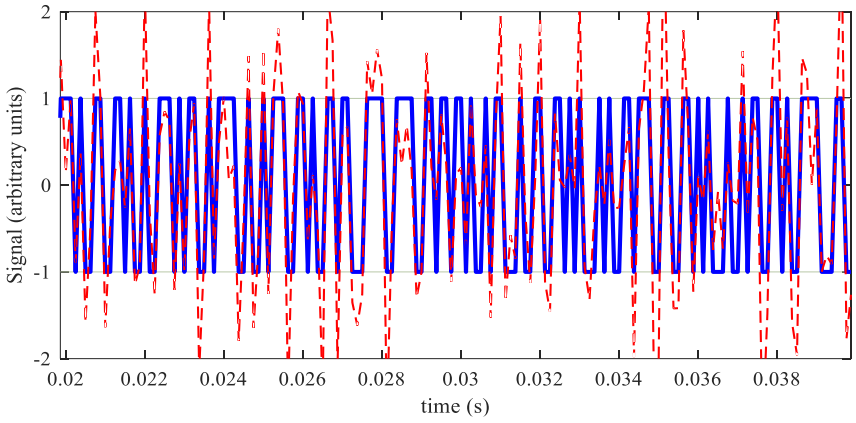

Source: Elaborated by the author.

For the case where the sensor is close to the measurement point, it is possible to have severe clipping as mentioned in the introduction. For this case, there is an equation which relates the CCC of extreme clipping and an original CCC before clipping. It is given by (VAN VLECK; MIDDLETON, 1966)

$$\rho_{x_1x_2}(\tau)\Big|_{\text{clipped}} = \frac{2}{\pi}\sin^{-1}\left(\rho_{x_1x_2}(\tau)\right). \tag{30}$$

The relationship between the CCC with severe clipping and CCC original is given by

$$\alpha = \frac{\rho_{x_1x_2}(\tau)\big|_{\text{clipped}}}{\rho_{x_1x_2}(\tau)}, \tag{31}$$

and is plotted in Figure 26 a) to observe the effects. For values of $\rho_{x_1x_2}$ less than about 0.4, to obtain the effect of severe clipping $\rho_{x_1x_2}$ is simply multiplied by $2/\pi$. For values greater than this, the value varies between $2/\pi$ and 1. If the maximum value of $\rho_{x_1x_2}$ < 0.4, It is possible to observe negligible distortion of the CCC. The maximum value of $\rho_{x_1x_2}(\tau)$ is influenced by the background noise and the position of the leak. An expression which relates the maximum peak and the distance derived by (GAO *et al*. 2005) is obtained from the CCF given by

$$R_{x_1x_2}(\tau) = \frac{\beta d}{\pi\left[(\beta d)^2 + (\tau - T_0)^2\right]}. \tag{32}$$

The autocorrelation function $R_{x_ix_i}(\tau)$ at distance d_i from the leak position is given by

$$R_{x_ix_i}(\tau) = \frac{2\beta d_i}{\pi\left[(2\beta d_i)^2 + \tau^2\right]}. \tag{33}$$

Calculating the fourth derivative of Equation 32 results in (GAO, *et al* 2005)

$$R^{(a)}_{x_1x_2}(\tau) = \frac{24\beta d}{\pi}\left(\frac{5(\tau - T_0)^4 - 10(\beta d)^2(\tau - T_0)^2 + (\beta d)^4}{\left((\beta d)^2 + (\tau - T_0)^2\right)^5}\right), \tag{34}$$

where $R^{(a)}_{x_1x_2}(\tau)$ is the cross-correlation function for acceleration measurements. Calculating the fourth derivative of Equation 33 and combining with Equation 32 and 3, the resulting CCC for acceleration measurements is given by

$$\rho^{(a)}_{x_1x_2} = \left(\frac{2\sqrt{d_1d_2}}{d}\right)^5 (\beta d)^6 \left(\frac{5(\tau - T_0)^4 - 10(\beta d)^2(\tau - T_0)^2 + (\beta d)^4}{\left((\beta d)^2 + (\tau - T_0)^2\right)^5}\right), \tag{35}$$

In Equation 35 setting $\tau = T_0$ results in

$$\rho_{x_1x_2}^{(a)}(T_0) = \left(\frac{2\sqrt{d_1 d_2}}{d} \right)^5 . \tag{36}$$

This equation may be rewritten in function of d_1 and normalizing with d is obtained

$$\max\left\{ \rho_{x_1x_2}^{(a)}(T_0) \right\} = \left(2\sqrt{\hat{d}_1\left(1-\hat{d}_1\right)} \right)^5 , \tag{37}$$

where $\hat{d}_1 = d_1/d$. This equation is plotted in Figure 26 b). The reason for this behaviour is because the band-pass filtering effect of the sections of the pipe either side of the leak. When the d_1 is equal to d_2 the peak in the CCC is 1 and when $d_1 = 0$ or $d_2 = 0$, the peak in the CCC is 0. From these two graphics, it is clear to observe in figure 26 b) that a leak close of the measurement position $\hat{d}_1 = 0.2$ gives $\max\left\{ \rho_{x_1x_2}\left(T_0\right) \right\}$ about 0.4 and with this value is observed in Figure 26 a) the severe clipping practically has no effect on the shape of the CCC.

Figure 26 - Effects on the cross-correlation coefficient for acceleration measurements. a) Effect of the CCC due to severe clipping; (b) Effect on the maximum value of the CCC of the unclipped signal as a function of the position of the leak.

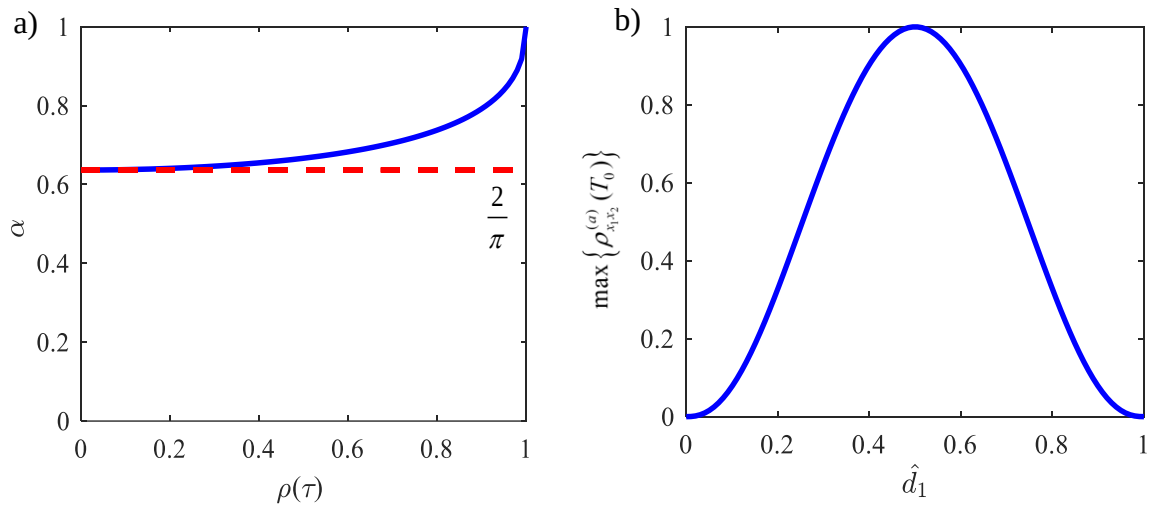

Source: Elaborated by the author.

3.3.2.1 Simulation

A typical leak detection problem is simulated (see Figure 1-chapter 2). Properties of the leak pipe model using the data from the test rig in P5P6 V5 are shown in Table 5. The sampling frequency for 10 second of acceleration time histories is 8 kHz. The transformation to the frequency domain is carried out using a 4096 point FFT and a Hanning window with 50% overlap. The cases for unclipped and severely clipped data are compared in Figure 27. Before any leak noise signal were processed, they were normalised so that they had zero mean and a standard deviation of unity.

Table 5 - Physical properties of the pipe-model from a test rig in São Paulo

Mean radius of the pipe	35.8 mm
Pipe-wall thickness	3.4 mm
Pipe Young's modulus	$2x10^9$ N/m^2
Bulk modulus of water	$2.25x10^9$ N/m^2
Shear modulus	$2.41x10^8$ N/m^2
Free-field wave-speed in water	1500 m/s
d_1; d_2	1.25 m, 4.25 m

Source: Elaborated by the author.

In Figure 27 a), b) and c) are PSD 5, the PSD 6 and the modulus of the CSD in which the effect of a band pass filter can be seen as result of the effect of the pipe and the accelerometers. That effect is not observed for the clipped signal because the poor effect of the coherence at low and high frequency. In Figure 27 d) a problem of unwrapping issue at low frequency for the clipped signal can be seen, but in general the effect of severe clipping has only a small effect on the phase spectrum. In Figure 27 f) an unclipped CCC is shown as a solid blue line; clipped CCC as a dotted green line and using the Van Vleck theory for the CCC as a dashed red line. The severe clipped signal matches with the Van Vleck theory. These plots have a difference with the unclipped signals in the height of the maximum peak which was indicated before in the Figure 21 a). There is no effect of severe clipping on the time delay estimation and only has a small effect on the shape of the CCC.

Figure 27 - Processed data from simulated acceleration signals (parameters according Table 5); a), b) PSD 5 and 6, respectively; c) Normalized modulus of the CSD, d) Phase of the CSD, e) coherence, f) CCC. Numerical unclipped, thick solid blue line; Numerical clipped, dotted green line; Van Vleck theory for the CCC, dashed red.

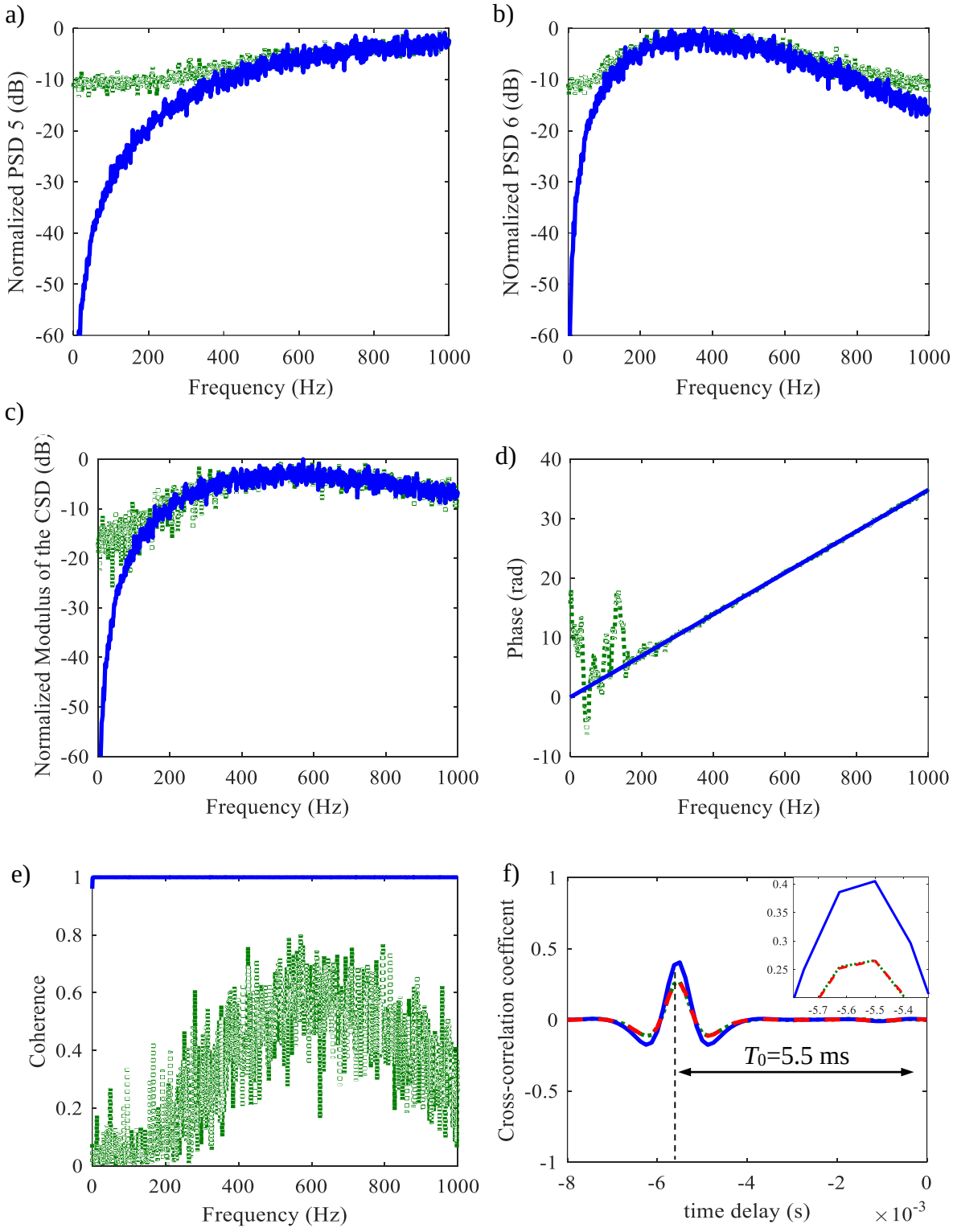

Source: Elaborated by the author.

3.4 Conclusions

In this chapter the effects of the quantization, clipping of signals on the accuracy of the time delay estimate and hence in the leak detection and location of leaks in buried plastic water pipes were investigated. For the case of the quantization, this has been achieved, by studying the theory that involves the process of quantization and applying in the theory to simulate and experimental leak data. It has been shown that varying the number of bits of quantization does not have an effect on the time delay estimation. For the case of clipping, the same experimental leak data was amplified, in order to saturate the signal. It has been shown, as well as in the last case, that it does not have an effect on the time delay estimation. A heavily clipped signal was studied using the signum function. Van Vleck theory was used to compare the unclipped and the heavily clipped data, and it was also found not have effect on the time delay estimation. This result can lead to significant improvements in the design and development of leak noise correlators. First, saving in processing time and storage of leak data, because of the possibility of using of converter A/D with low resolution (number of bits). Second, electronic circuits for automatic gain control are unnecessary in the correlator device.

4 QUALITY INDEX

4.1 Introduction

In previous chapters leaks signals collected from the test rig in SABESP were processed and from these data, the effect of the bandwidth, the effects of the background noise and the pump, the filtering effects of the pipe, wave reflections in the pipe and distortions of the leak signal due to instrumentation were studied. In particular, the influence on the shape of the CCF was of interest as the maximum peak gives the value of the estimated time delay. CCF with a larger peak with respect to the other peaks is considered to be a good form of CCF to give a reliable and accurate time delay estimate. The aim of this chapter is to study different features that influence the reliability and accuracy of the time delay estimate, hence the location of the leak. The modulus and phase of the CSD, coherence and the CCF are used in the study. They are quantified in indices to then be integrated in an overall quality index that includes all of them. Simulations are carried out together with experimental data from SABESP test rig to investigate the concept.

4.2 Proposed indices

4.2.1 Bandwidth index

The correct choice of bandwidth to supress external noise is important in the accurate estimate of the time delay measured from leak noise signals. In this section the relationship between the bandwidth and the CSD, and its effect in the shape of the CCC is studied. A good shape of the CCC is when the maximum peak is higher than the other peaks. Normally there is a maximum peak amongst other peaks. Later the height of the maximum peak is compared with the height of the peak that has a value close to this to obtain an expression to formulate the index. Gao *et al*. (2003) showed that acceleration measurements made either side of the leak have a modulus of the CSD given by the equation 2.17. The maximum value of this occurs when $\omega = 4/(\beta d)$. Setting $\hat{\omega} = \omega\beta d$, Equation 2.17 can be written as

$$\left|\hat{S}_{x_1x_2}\right| = \frac{\left|S_{x_1x_2}\right|}{\max\left|S_{x_1x_2}\right|} = \frac{\hat{\omega}^4 e^{-\hat{\omega}}}{2^8 e^{-4}}. \tag{38}$$

To determinate the bandwidth over which the leak propagates, two half power point frequencies $\hat{\omega}_{\text{lower}}$ and $\hat{\omega}_{\text{higher}}$ are set as follows

$$\left|\hat{S}_{x_1x_2}\right|_{lower,\, higher} = \frac{\hat{\omega}^4 e^{-\hat{\omega}}}{2^8 e^{-4}} = \frac{1}{2}. \tag{39}$$

Equation 39 has the following solutions, $\hat{\omega}_{\text{lower}}$ = 2.083 and $\hat{\omega}_{\text{higher}}$ = 6.83. The ratio of these frequencies $\hat{\omega}_{\text{higher}}/\hat{\omega}_{\text{lower}} = \omega_{\text{higher}}/\omega_{\text{lower}} = 3.28$ which is independent of βd. Later this value will be shown to be important in determining the shape of the CCC. Figure 28 represents the normalized modulus of the CSD as function of the normalized frequency $\hat{\omega}$. This last parameter is a function of βd. The half power point at frequencies $\hat{\omega}_{\text{lower}}$ and $\hat{\omega}_{\text{higher}}$, and the centre frequency $\hat{\omega}_c$ are shown as is the band-pass effect of the sensor-pipe system. as mentioned in chapter 2.

Figure 28 - Normalized modulus of CSD as function of normalized frequency $\hat{\omega}$. Showing the two half power point frequencies and centre frequency.

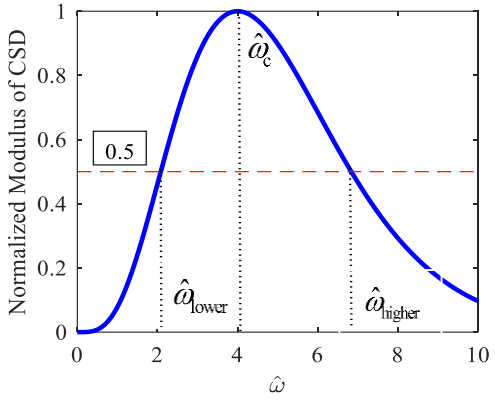

Source: Elaborated by the author.

The analysis below shows how the bandwidth influences the shape of the CCC. Figures 29 a) i, ii, iii show the original normalized CSD and the additional band pass filter limits shown as solid blue line and dashed red line respectively. Figures 29 b) i, ii, iii show the normalized CCC

for the bandwidth shown, setting $T_0 = 0$ to show the effects of the bandwidth better. With a mark on the second peak. In all cases $\hat{\omega}_x$ is the lowest frequency of the filter and it is varied, keeping $\hat{\omega}_{higher}$ fixed with a value of 6.84 to show the effect of the bandwidth on the shape of the CCC. In row i) with $\hat{\omega}_x = 2$, a broad bandwidth in the CSD is observed with a good shape in the normalized CCC. A good shape means that the maximum peak is distinguishable with respect to the other peaks. In row ii) with $\hat{\omega}_x = 4$, the second peak of the CCC is increased its height. In row iii) with $\hat{\omega}_x = 6$, a narrow bandwidth in the CSD with a poor shape of the normalized CCC.

Figure 29 - a) Normalized modulus of CSD as function of $\hat{\omega}$; b) Normalized CCC, $\hat{\omega}_x = 2$, row 1 i) ; $\hat{\omega}_x = 4$; row ii); $\hat{\omega}_x = 6$; row 3 iii), with $\hat{\omega}_{higher} = 6.84$ fixed for the three cases.

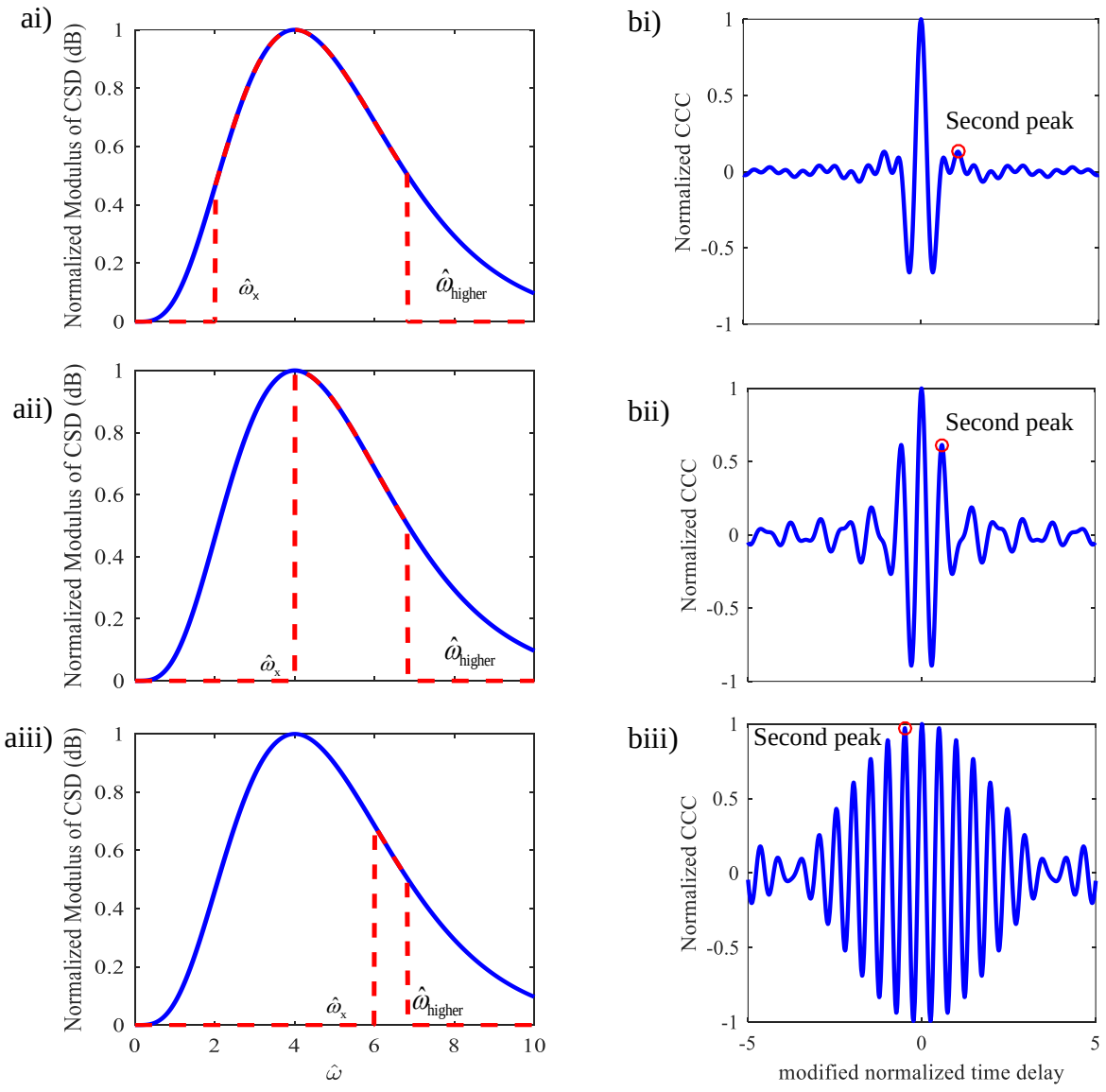

Source: Elaborated by the author.

4.2.1.1 Formulating the bandwidth index

In the last section, the effect of the bandwidth in the shape of the CCF was studied, observing the variation that in the shape of the CCF that occurs when the bandwidth changes. In this section, special emphasis is given to the second peak of the CCF and an analytical expression is obtained for the second peak in the frequency domain. If the second peak is lower than the maximum peak, the shape of the CCF is good. On the other hand, if the second peak is closer in height to the maximum peak the shape is not good. This bandwidth index is determined from simplified CCC without considering attenuation of the leak noise in the pipe, for simplicity (BRENNAN *et al*., 2018).

$$R_{x_1x_2}(\tau)=\frac{\Delta\omega}{\pi}\frac{\sin\left(\Delta\omega(\tau-T_0)/2\right)}{\Delta\omega(\tau-T_0)/2}\cos\left(\omega_c(\tau-T_0)\right), \tag{40}$$

where $\Delta\omega=\omega_{\text{higher}}-\omega_{\text{lower}}$ is the bandwidth over which there is leak noise is present and $\omega_c=\left(\omega_{\text{higher}}+\omega_{\text{lower}}\right)/2$ is the centre frequency of the band. This can be written in non-dimensional form as

$$\hat{R}_{x_1x_2}(\hat{\tau})=\frac{R_{x_1x_2}(\tau)}{\Delta\omega/\pi}=\frac{\sin(\hat{\tau})}{\hat{\tau}}\cos\left(\frac{2\omega_c\hat{\tau}}{\Delta\omega}\right)=\frac{\sin(\hat{\tau})}{\hat{\tau}}\cos\left(\left(\frac{\omega_{\text{higher}}/\omega_{\text{lower}}+1}{\omega_{\text{higher}}/\omega_{\text{lower}}-1}\right)\hat{\tau}\right), \tag{41}$$

where $\hat{\tau}=\Delta\omega(\tau-T_0)/2$.

Equation 41 is plotted in Figure 30 for two cases with thin blue line for a) $\omega_{\text{higher}}/\omega_{\text{lower}}$ = 1.2 which has a bad shape and b) $\omega_{\text{higher}}/\omega_{\text{lower}}$ =3 which has a good shape. The envelope $\sin(\hat{\tau})/\hat{\tau}$ is also plotted as a thick red dashed line. It is observed that $\omega_{\text{higher}}/\omega_{\text{lower}}$ controls the oscillations of $\hat{R}_{x_1x_2}(\hat{\tau})$ and when $\omega_{\text{higher}}/\omega_{\text{lower}}$ increases, the maximum peak can be identified clearly in comparison with the second peak of the cross-correlation function. For all cases, the maximum peak of the cross-correlation function is at $\hat{\tau}=0$, which corresponds to $\tau=T_0$.

Figure 30 - Normalized cross-correlation function (CCF) with the time delay set to zero, a) $\omega_{\text{higher}}/\omega_{\text{lower}} = 1.2$ and b) $\omega_{\text{higher}}/\omega_{\text{lower}} = 3$; thin solid blue line, CCF; thick red line, envelope of CCF.

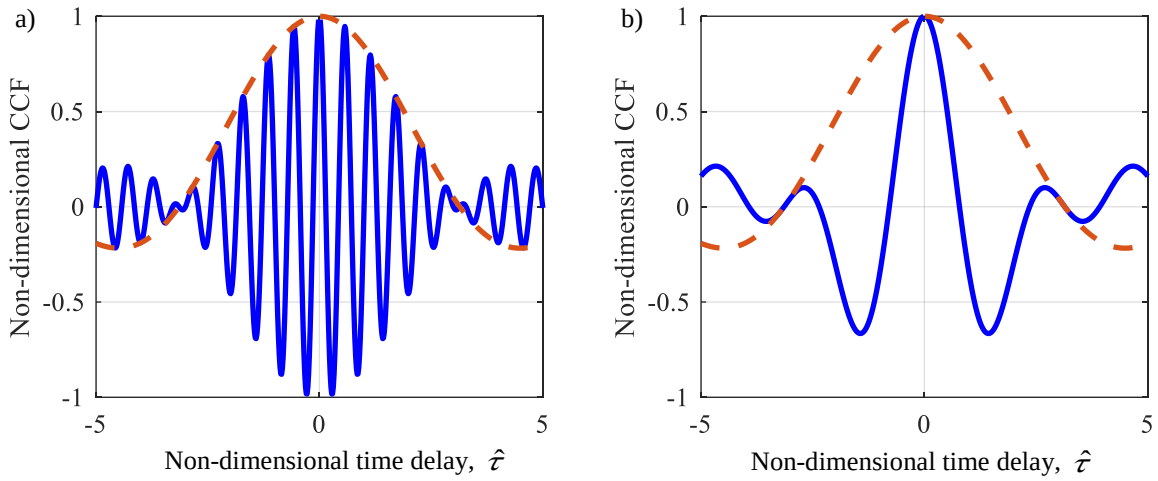

Source: Elaborated by the author.

Considering the maximum peak as the first peak, an approximate value of the peak close to this is determined by setting the second term of Equation 41 to 1 which occurs when $\hat{\tau}$ is a multiple of 2π, obtaining

$$\hat{\tau} = 2\pi\left(\frac{\omega_{\text{higher}}/\omega_{\text{lower}} - 1}{\omega_{\text{higher}}/\omega_{\text{lower}} + 1}\right). \tag{42}$$

Replacing the first term of Equation 41, the second peak is given by

$$\hat{R}_{x_1x_2}\left(\hat{\tau}\big|_{\text{second peak}}\right) = \frac{\sin\left(2\pi(\omega_{\text{higher}}/\omega_{\text{lower}} - 1)/(\omega_{\text{higher}}/\omega_{\text{lower}} + 1)\right)}{2\pi(\omega_{\text{higher}}/\omega_{\text{lower}} - 1)/(\omega_{\text{higher}}/\omega_{\text{lower}_{\omega}} + 1)}. \tag{43}$$

For small values of $\omega_{\text{higher}}/\omega_{\text{lower}}$, the second peak has the same amplitude that the first peak and also close to the value of 1. For high values of $\omega_{\text{higher}}/\omega_{\text{lower}}$, the second peak has a value close to zero. A bandwidth index that is low when the shape is not good and high when is the opposite is given by

$$k_b = 1 - \hat{R}_{x_1x_2}\left(\hat{\tau}\big|_{\text{second peak}}\right). \tag{44}$$

Equation 4.6 is plotted in Figure 31 a). It is observed that with values close to a $\omega_{\text{higher}}/\omega_{\text{lower}}=1$, a second peak close to 1 is obtained. High values of $\omega_{\text{higher}}/\omega_{\text{lower}}$ as for example, 3 gives a small second peak, which the first peak of CCF to be identified clearly. Equation 4.7 is plotted in Figure 31 b). Note that the bandwidth index varies between 0 and 1. width a good shape being with frequency close to 3. A poor shape is obtained with a low frequency ratio close to 1.

Figure 31 - a) Approximation of the second peak as a function of $\omega_{\text{higher}}/\omega_{\text{lower}}$, b) bandwidth index k_b as a function of $\omega_{\text{higher}}/\omega_{\text{lower}}$.

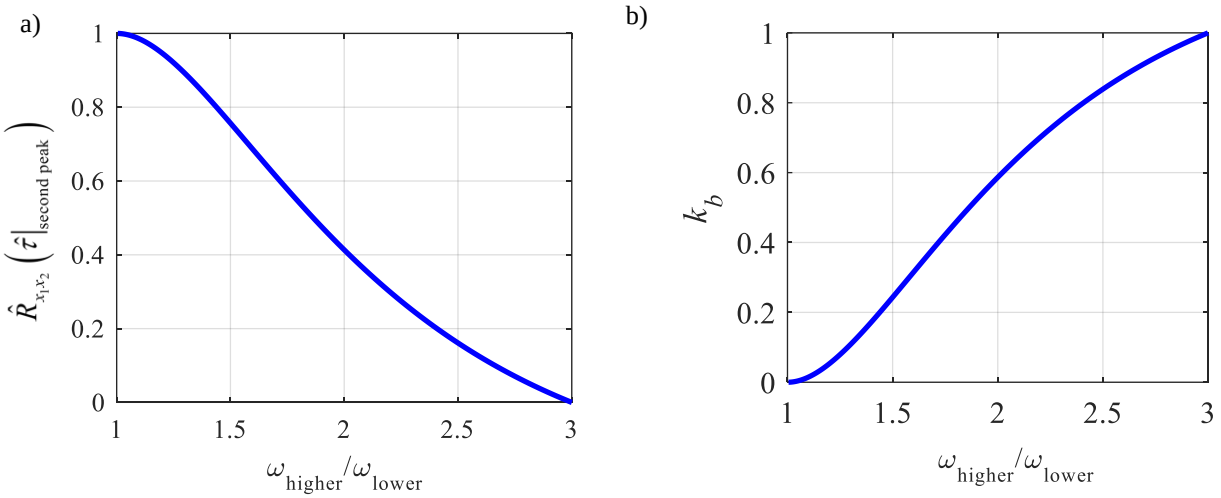

Source: Elaborated by the author.

4.2.2 Coherence index

This index is determined from the coherence function, using a bandwidth where the leak is present. As it was mentioned in chapter 2 this function has limits of $0 \le \gamma^2_{x_1x_2} \le 1$. If the leak noise signals are linearly related the coherence is 1, which would be an ideal case, but always there is noise present in the system so they are partially linearly related.

Figure 32 a) shows the ideal coherence of two leak signals, coherence equal to one. Figure 32 b) shows the same leak signal with noise.

Figure 32 - Coherence function as function of the frequency a) ideal case, b) A experimental case with noise in the system.

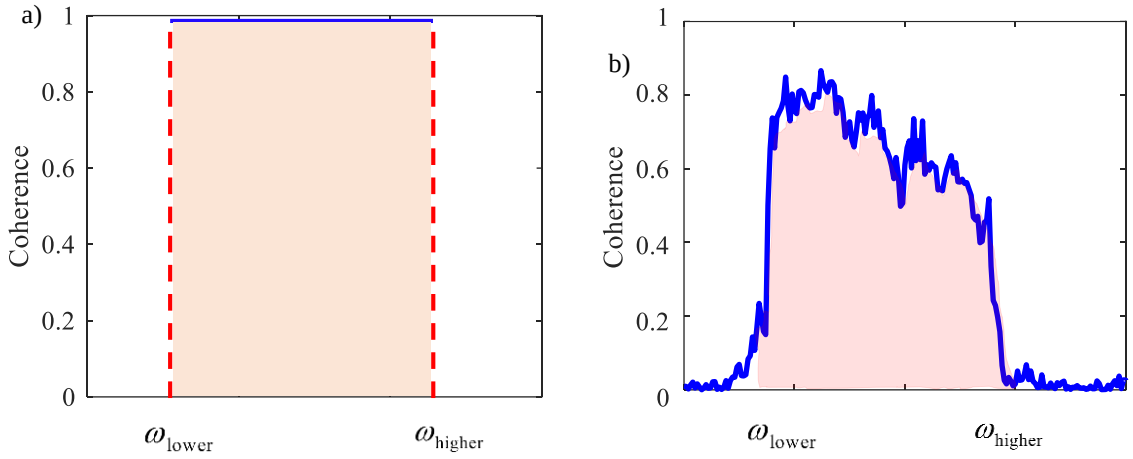

Source: Elaborated by the author.

The coherence index is considered as the ratio of the coherence signal power to coherence signal power plus coherence noise power given by

$$k_{co} = \frac{\sum_{j=1}^{m-1} \gamma^2_{x_1 x_2}(\omega_j)}{m-1}, \tag{45}$$

where m is the number of points, ω is the j-th frequency in the bandwidth limited by ω_{higher} and ω_{lower} which are the frequencies where there is leak noise. This section shows how the noise affects the coherence between two leak signals collected from a point 1 and 2 and how this influence in the CCF. Figure 33 shows a simulation of three cases which noise was added gradually increased to one of the acceleration measurements from a typical leak made with a correlator (see Figure 1-Chapter 2). Properties of the leak pipe model are shown in Table 4-Chapter 3. These properties are taken to simulate a test rig located in Canada. This was modelled as $x_1(t) = s_1(t) + n_1(t)$ and $x_2(t) = s_2(t) + n_2(t)$, where $s_1(t)$, $s_2(t)$ and $n_1(t)$, $n_2(t)$ are the leak signals without noise and noise signals respectively. For this example $n_2(t) = 0$. The signal noise ratio (SNR) for point 1, for these three cases are 0, -5 and -20 dB. In Figure 33 a) for these three cases the CSD is calculated. The transformation to the frequency domain of the leak signals is carried out using a 4096-point FFT and a Hanning window with 50% overlap. The same tendency is observed for all the three cases but with an increment of the noise in the modulus of CSD. In Figure 33 b) the phase of the CSD has the same tendency with some small

unwrapping problems. In Figure 33 c) the coherence is significantly reduced when the noise is increased. In Figure 33 d) The CCC reduces the height of its maximum peak.

Figure 33 - a) Normalized modulus of CSD, b) Phase of CSD c) coherence d) Cross-correlation coefficient. SNR = 0, solid blue line; SNR = -5, dashed red line; SNR = -20, dotted green line.

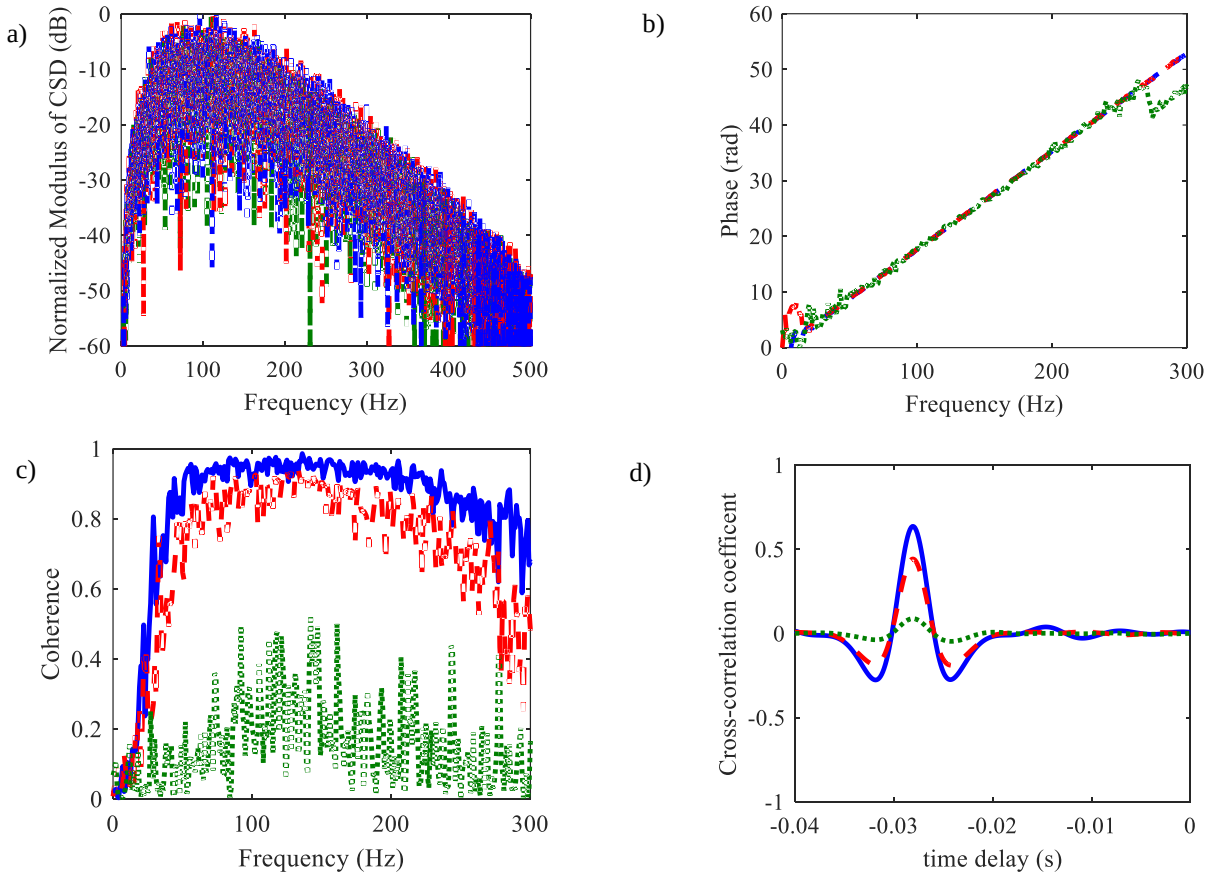

Source: Elaborated by the author.

4.2.3 Phase index

The phase index is related to the phase of the CSD. A pure time delay between the signals results in a phase that changes linearly with frequency. However, in practice, it often does not pass through the origin and distortions are observed. This can be due several reasons, including noise, structural dynamics of the pipe system (ALMEIDA *et al.*, 2013), and wave reflections from discontinuities in the pipe system (GAO *et al.*, 2009). The index is obtained by comparing the phase of the CSD with the fitted phase using a least squares method. For this comparison, the standard deviation is calculated. The data used are within the frequency bandwidth where the leak noise is present. This value is zero whether there is no variability, so this is modified

to have 1 as maximum and zero as the minimum value of the index. Thus, the phase index is given by

$$k_{ph} = 1 - \sqrt{\left(\frac{1}{m-1}\right)\left(|r| - \mu_r\right)^2}\ , \tag{46}$$

where m is the number of points, $r = \left|r_{ph} - 1\right|$, μ_r is the mean of r and r_{ph} is the ratio between the experimental phase to the best fit (least squares) of it. The fitted phase is given by $\phi_f(\omega_j) = p\omega_j + b$ (CHAPRA, 2018) where

$$p = \frac{m\sum_{j=1}^{m}\left(\omega_j\phi\left(\omega_j\right)\right) - \sum_{j=1}^{m}\omega_j\sum_{j=1}^{m}\phi\left(\omega_j\right)}{m\sum_{j=1}^{m}\left(\omega_j^2\right) - \left(\sum_{j=1}^{m}\omega_j\right)^2}, \tag{47}$$

$$b = \frac{\sum_{j=1}^{N}\left(\phi\left(\omega_j\right)\right)\sum_{j=1}^{N}\omega_j^2 - \sum_{j=1}^{N}\left(\omega_j\phi\left(\omega_j\right)\right)\sum_{j=1}^{N}\omega_j}{N\sum_{j=1}^{N}\left(\omega_j^2\right) - \left(\sum_{j=1}^{N}\omega_j\right)^2}, \tag{48}$$

where $\phi\left(\omega_j\right)$ is the experimental phase and ω_j is the j-th frequency in the interval where the leak is present. In Figure 34 a) is shown an experimental case where the original phase is fitted. Figure 34 b) shows the value of the phase index.

Figure 34 - a) original and fitted phase in solid blue line and dashed red line respectively. b) Phase index in dashed red line.

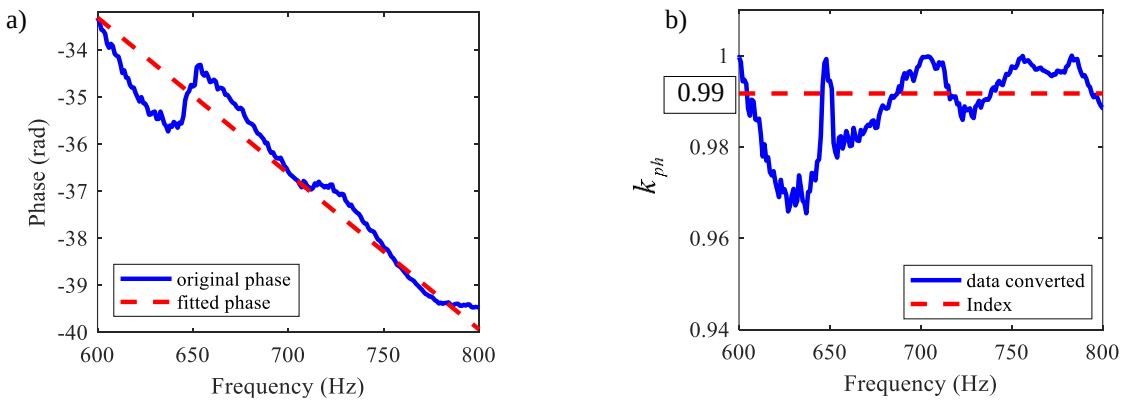

Source: Elaborated by the author.

4.2.4 Peak Index

This index is determined from the CCC which is the cross-correlation function expressed in a normalized form given by (KIHONG; HAMMOND, 2008)

$$\rho_{x_1x_2}(\tau) = \frac{R_{x_1x_2}(\tau)}{\sqrt{R_{x_1x_1}(0)R_{x_2x_2}(0)}}, \tag{49}$$

This equation was mention before in Equation 2.3 chapter 2. The peak in the CCC can vary because of the noise, reflections (peak apparent), attenuation, etc. The peak index is given by

$$k_{pk} = \max\left(\rho_{x_1x_2}(T_0)\right). \tag{50}$$

This occurs when $\tau = T_0$, and the value of the index is between 0 to 1. Figure 33 d) shows how the noise influences in the maximum peak of the CCC.

4.2.5 Shape Index

This index was constructed using the relationship between the normalized peak of the CCC and the second highest peak. It is observed in practical situation that because of reflections or correlated noise, the shape of correlation function can be suffer some change. The value of the ideal index is when the difference between these values is near to one. Thus, using the Normalized CCC is obtained

$$k_{sh} = 1 - h_{\text{second peak}}, \tag{51}$$

where $h_{\text{second peak}}$ is the height of the second highest peak.

This section shows the bandwidth index k_b and shape indices k_{sh} for simulated cases for a wide and narrow bandwidth which correspond to a good and poor shape. The influence of a wave reflection in the shape index is analysed. These indices use the second highest peak of the CCC as reference. k_b, as it was mention before, relates theoretically the second highest peak with the bandwidth where the leak noise is present and k_{sh} uses the second highest peak of the

signal measured which could be affected by reflections or correlated noise. In Figure 35 a diagram of a simulated case is shown in which the distances from the leak to points 1 and 2 are equal to give zero-time delay. In the left side of the access point 1, there is a deviation of an elbow at 90° which creates wave reflections in the pipe. This simulation is carried out using the physical properties of the pipe-model showed in Table 6, the soil effect is not considered. The sampling frequency for 10 second of acceleration time histories is 8 kHz. The transformation to the frequency domain is carried out using a 4096 point FFT and a Hanning window with 50% overlap. In the next section the CCC is shown, discussing the behaviour of the second highest peak with the reflections.

Figure 35 - Schematic of leak detection with a leak noise located in the centre. The test rig has a deviation of an elbow in 90° which creates a reflection.

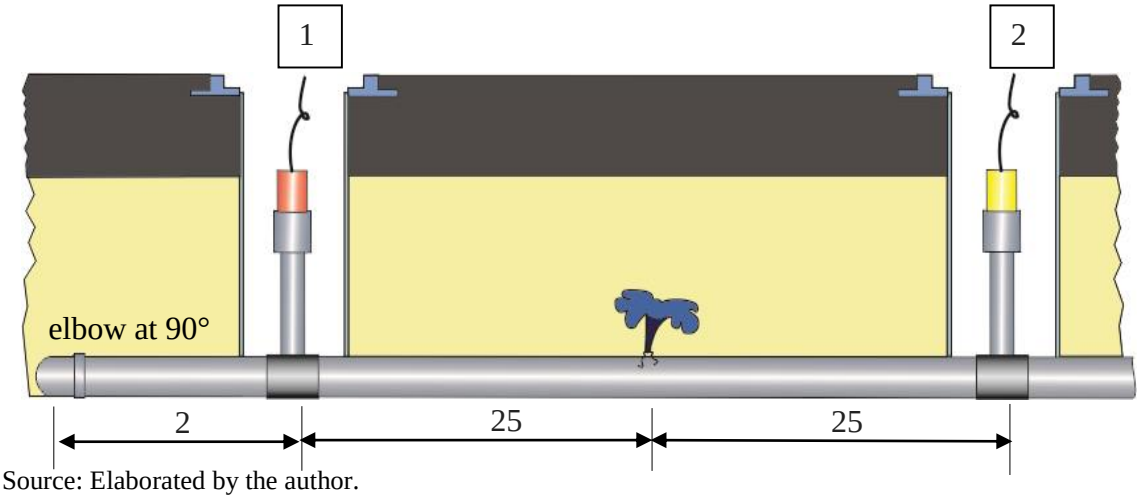

Source: Elaborated by the author.

Table 6 - Physical properties of the pipe-model from a test rig in UK with $d_1 = d_2$.

Mean radius of the pipe	75 mm
Pipe-wall thickness	9.85 mm
Pipe Young's modulus	$2x10^9$ N/m^2
Pipe loss factor	0.1
Bulk modulus of water	$2.2x10^9$ N/m^2
Free-field wave-speed in water	1500 m/s
d_1; d_2	25 m, 25 m

Source: Elaborated by the author.

Figure 36 a) shows the CCC with a good shape because of a wide bandwidth from 100 to 300 Hz, without reflection (solid blue line) and with reflection (dashed red line). For these

cases, the maximum peak is located at 0 seconds, because the distances from the leak to points 1 and 2 are equal. When the system does not have reflection, it is observed that, the second highest peak is smaller than the maximum peak. However, when it is affected by the reflection, the height of the second highest peak increases.

Figure 36 b) shows the CCC with poor shape because of a narrow bandwidth from 100 to 150 Hz, without reflection (solid blue line) and with reflection (dashed red line). For these cases, the maximum peak is located in 0 seconds, because the distances from the leak to points 1 and 2 are equal. It is observed that the height of the second highest peak of the CCC without wave reflection increases when the wave reflection influences in the system, and an appreciable variation of the position of the maximum peak is observed.

Figure 36 - a) CCC with a wide bandwidth b) CCC with a narrow bandwidth. CCC with reflection and without reflection in solid blue line and dashed red line respectively.

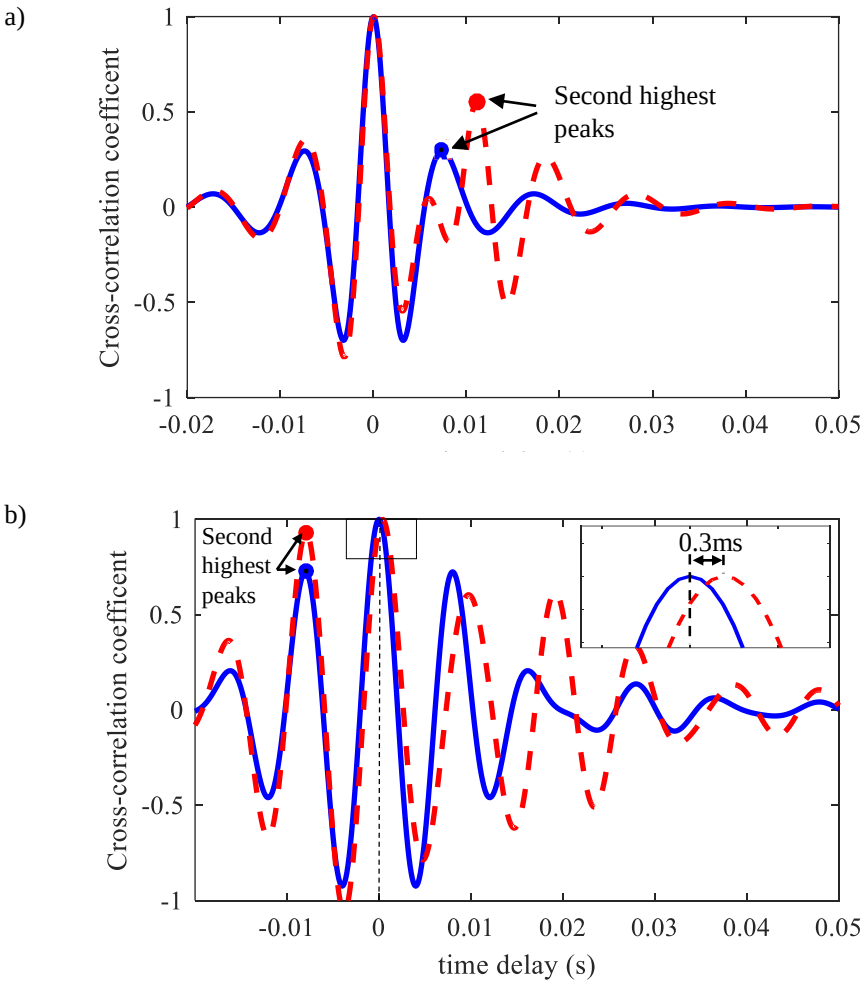

Source: Elaborated by the author.

The bandwidth and shape indices k_b and k_{sh} are determined for the cases shown below, they can be observed in the Table 7. The bandwidth index which depends of the bandwidth does not change when a reflection is added to the system, but the shape index decreases because of the second highest peak increases when the reflections is added to the system.

Table 7 - Indices of two cases using a narrow and wide bandwidth with reflection and without reflection.

Case	Bandwidth (Hz)	Index without reflection		Index with reflection	
		k_b	k_{sh}	k_b	k_{sh}
1	100-300	1	0.72	1	0.44
2	100-150	0.24	0.28	0.24	0.07

Source: Elaborated by the author.

4.3 Integration of the indices

In the last section five indices have been proposed, which represent different variables. the geometric mean was used to integrate these variables as this is less susceptible to major variations as a result of violent fluctuations in the values of the individual items. It is determined that the values are positive and it behaves well to algebraic operations. Compared with the arithmetic mean, which is more often used when constructing indices, the geometric mean is preferred wherever possible to have greater accuracy. (SHARMA, 2005).

Therefore, the overall quality index *K* is given by

$$K = \sqrt[5]{k_b k_{co} k_{ph} k_{pk} k_{sh}} \ , \tag{52}$$

In general, the indices are positioned into levels: 0-0.2 poor quality, 0.2-0.7 good quality and 0.7-1 excellent quality.

4.4 Experimental cases

The overall quality index is calculated for 5 cases, the components of which are listed in Table 8. The phase of CSD, the coherence, CCC and the quality indices proposed for data from test rig in Brazil and for data from test rigs in Canada and UK are shown in Figure 37 and 38 respectively. For Brazil the cases considered are from access points P1P2-V2, P3P4-V2, P5P6-V3, carried out on 28/06/17 according with the schematic of SABESP test rig showed in Figure 8 a). They were processed in the appendix A in Figure 63, 64 and 68 respectively. The selection of the bandwidth where the leak is present is with the limit 10^{-3} of amplitude in the coherence.

In Figure 37 a) the first case in Table 8 is shown. It is observed that the bandwidth index is 0 because of the narrow bandwidth selected. The coherence is 0.03 which is poor. There is a low linear association between the leak signal collected and this is possibly because there is coherent noise in the system. The phase index is 0.99 which is excellent because the phase matches with the straight line of the least square fitted in the bandwidth selected. The peak index is 0.18 which is poor, this is possibly because there is coherent noise in the system and the attenuation. The shape index is 0, because of the second peak has a similar amplitude that the maximum peak. The overall quality index *K* calculated is 0, not being reliable the time delay estimated.

In Figure 37 b) the second case in Table 8 is shown. It is observed that the bandwidth index is 0.24 which is good because of the wide bandwidth selected. The coherence index is 0.1 which is poor, this is possibly because there is coherent noise in the system. The phase index is 0.86, which is excellent because the phase matches with the straight line of the least square fitted in the bandwidth selected. The peak index is 0.28 which is good, this is possibly because there is coherent noise in the system and the attenuation. The shape index is 0.05, because of the second peak has a similar amplitude that the maximum peak. The overall quality index *K* calculated is 0.20, being reliable the time delay estimated.

In Figure 37 c) the third case in Table 8 is shown. It is observed that the bandwidth index is 0.76 which is excellent because of the wide bandwidth selected. The coherence index is 0.19 which is poor, this is possibly because there is coherent noise in the system. The phase index is 0.82 which is excellent because the phase matches with the straight line of the least square fitted in the bandwidth selected. The peak index is 0.43 which is good, this is possibly because there is coherent noise in the system and the attenuation. The shape index is 0.13, because of the

second peak is close to the height of the maximum peak. The overall quality index *K* calculated is 0.37, being reliable the time delay estimated.

In Figure 37 d) the forth case in Table 8 is shown. It is observed that the bandwidth index is 1 which is excellent because of the wide bandwidth selected. The coherence index is 0.05 which is poor, this is possibly because there is coherent noise in the system. The phase index is 0.56 which is good. Due to the selection method of the bandwidth there is a small deviation of the phase with respect to the straight line of the least square fitted. The peak index is 0.18 which is poor, this is possibly because there is coherent noise in the system and the attenuation. The shape index is 0.76, which is excellent because of the second peak is close to zero. The overall quality index *K* calculated is 0.33, being reliable the time delay estimated.

In Figure 37 e) the Fifth case in Table 8 is shown. It is observed that the bandwidth index is 1 which is excellent because of the wide bandwidth selected. The coherence index is 0.4 which is good, this is possibly because there is coherent noise in the system. The phase index is 0.85 which is excellent. The peak index is 0.22 which is good, this is possibly because there is coherent noise in the system and the attenuation. The shape index is 0.71, which is excellent because of the second peak is close to zero. The overall quality index *K* calculated is 0.56, being reliable the time delay estimated.

Table 8 - Resume of the cases with indices evaluated.

Case	**Date**	**leak position**	***d*** **(m)**	**d_2 (m)**	**Bandwidth (Hz)**	**T_0 (ms)**	***V*** **(m/s)**	k_b	k_{co}	k_{ph}	k_{pk}	k_{sh}	***K***
P1P2-v2	28/06/17	outbracket	7	-	467-476	12.7	548	0.00	0.03	0.99	0.18	0.00	0.00
P3P4-v2	28/06/17	outbracket	7	-	358-535	15.6	448	0.24	0.10	0.86	0.28	0.05	0.20
P5P6-v3	28/06/17	outbracket	5.5	-	305-706	14.0	374	0.76	0.19	0.82	0.43	0.13	0.37
Canada		inbracket	102	29	11-144	90.0	489	1.00	0.05	0.56	0.18	0.76	0.33
UK		outbracket	30	-	9-188	79.0	379	1.00	0.40	0.85	0.22	0.71	0.56

Source: Elaborated by the author.

Figure 37 - Measurements at points a) P1P2V2, b) P3P4V2 and c) P5P6V3. (i) phase (ii) coherence (iii) CCC and (iv) Quality Index and components.

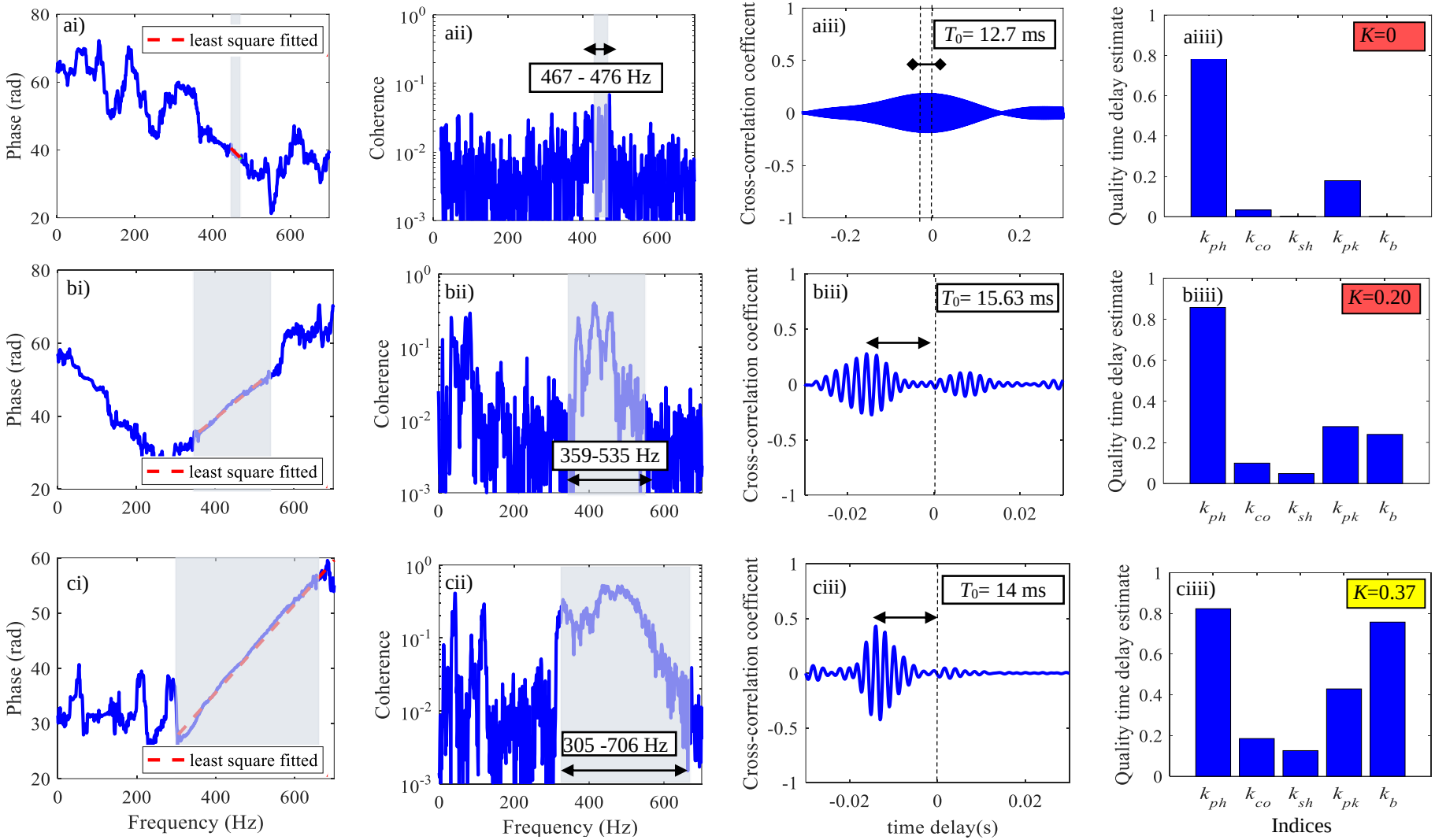

Source: Elaborated by the author.

Figure 38 - Measurements in d) Canada, and e) UK. (i) phase (ii) coherence (iii) CCC and (vi) Quality Index and components.

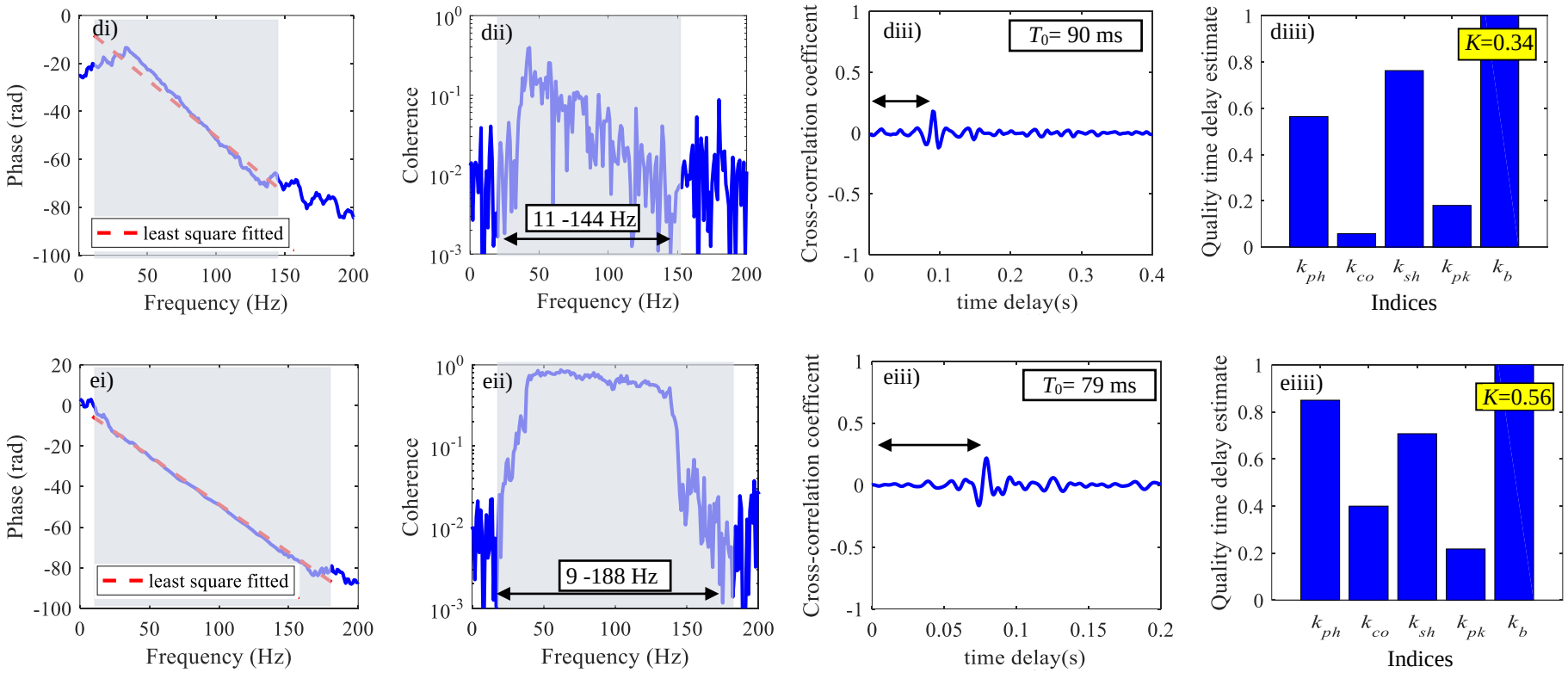

Source: Elaborated by the author.

4.5 Conclusions

In this part was proposed five indices, with different features which are quantified and integrated in one representative value. Then, the indices are integrated into a representative value. Three different levels of quality of the indices have been proposed to identify which one has a reliable estimation of the time delay. The first one, poor with 0 - 0.2, the second one, good with 0.2 - 0.7 and finally excellent with 0.7 - 1.

The first index is the bandwidth index, which relates the shape and the bandwidth in which there is leak noise. The second index is the coherence index, which relates external noise with the shape of the CCC. The third index is the phase index, which relates the noise, structural dynamics of the pipe system, and wave reflections from discontinuities in the pipe system with the least square fitted of the phase in a bandwidth selected. The fourth index is the peak index, which relates noise, the inherent attenuation of the system, reflections, etc. with the height of the CCC. Finally, the fifth index is the shape index, which relates the second highest peak with the maximum peak of the CCC.

Simulations were carried out to show how these features were quantified. In particular, a simulated case of wave reflection in a typical leak detection problem is analysed using bandwidth and shape index. These indices are related directly to the shape of the CCC and they were compared, showing the sensibility of the shape index with the reflections. Bandwidth index keeps the same values because it is directly related to the selected bandwidth. Experimental cases were analysed using the proposed indices, representing different features properly. An overall quality index was obtained for each experimental case, the state of each case is indicated. This state, represented by a value, gives a good representation of the reliability of the time delay estimated.

5 ACOUSTIC CORRELATOR SOFTWARE

5.1 Introduction

The aim of this chapter is to describe the hardware and software components of two prototypes of the acoustic correlator to detect and locate water leaks from buried pipes. The first prototype collected data using a cable and second prototype collected the data using a wireless system. The prototypes were tested with a virtual pipe rig and in the test rig of SABESP. The software was written by the author of his thesis mainly and the wireless data collection system was designed and built by Daniel Obata.

5.2 First prototype of the Acoustic correlator

The first prototype was developed with the aim to carried out the collection of data, process and analyse the information collected. The analysis obtained was used to improve the second prototype: The first prototype is composed of two parts

5.2.1 Hardware

Two sensors are used to collect the leak data from the measurement points. They are accelerometers PCB Piezotronics model 333B30 with sensitivity (±10%) 100 mV/g. They are connected with two low-noise coaxial cables (blue TFE jacket, 10-ft, 10-32 with coaxial plug to BNC plug) with two ICP® sensor signal conditioners model 480C02 (1-chanel, 3 different gains and BNC input/output connector) which supply with a constant excitation current to the sensors (ICP power). The output signals from the signal conditioners are sent through coaxial cables to the line-in connector of the laptop computer. As acquisition system and to process the leak data collected for this first prototype is a laptop computer. The data is collected using the sound card. This contains an A/D converter with 16 bits of resolution and the maximum sampling rate at which the sound card acquires data is around 48 kHz. This acquisition is set with a sampling rate of 8192 Hz with a time of acquisition of 60 seconds.

In Figure 39 the hardware of the first prototype of the acoustic correlator and its components are shown.

Figure 39 - Hardware of the first prototype of the acoustic correlator.

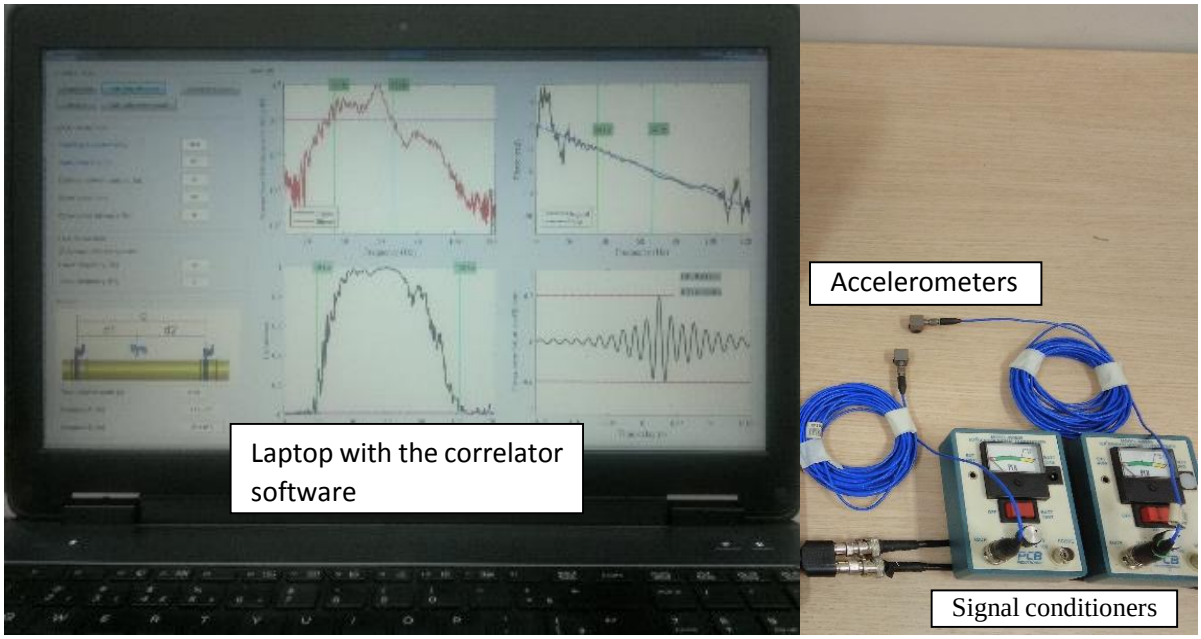

Source: Elaborated by the author.

5.2.2 Software of the correlator

The software was developed in GUIDE (Graphical User Interface Development Environment) which is an application from Matlab®. For this first prototype, the parameters considered by default were the following: The time of acquisition of the leak signals which is 60 seconds, the sampling frequency which is 8192 Hz and the transformation to the frequency domain of the leak signals is carried out using a 4096-point FFT and a Hanning window with 50% overlap.

5.2.3 Interface description

Figure 40 shows the graphical interface and the parts are designated by uppercase letters. The software follows these three main functions:

- First, the distance between sensors placed in the measurement points, the theoretical wavespeed given by Brennan *et al*. (2018), a tolerance for the estimated wavespeed (which

is considered 10%). They are entered in the signal parameter panel (B) and an initial bandwidth is entered in the filter parameters panel (C).

- Second, the acquisition button is used to collect the leak signals with the acquisition time and sampling frequency entered by default of 60 s and 8192 Hz respectively. After 60 seconds the data is saved with the extension .wav.
- Third, the calculate distance button is used to calculate the normalized modulus of CSD, the phase of CSD, the coherence and CCC, and it is shown in E, F, G and H respectively. The resume of the result is shown in D where the time delay estimate, the distances d_1 and d_2 are shown.
- Additionally, there are other secondary buttons such as the open file button, is used to open and load .wav and .mat extension files of leak data. The restart button restarts the program, erasing the interface information. The calculate wavespeed button is disabled for this prototype.

Figure 40 - Interface of the first prototype of the acoustic correlator.

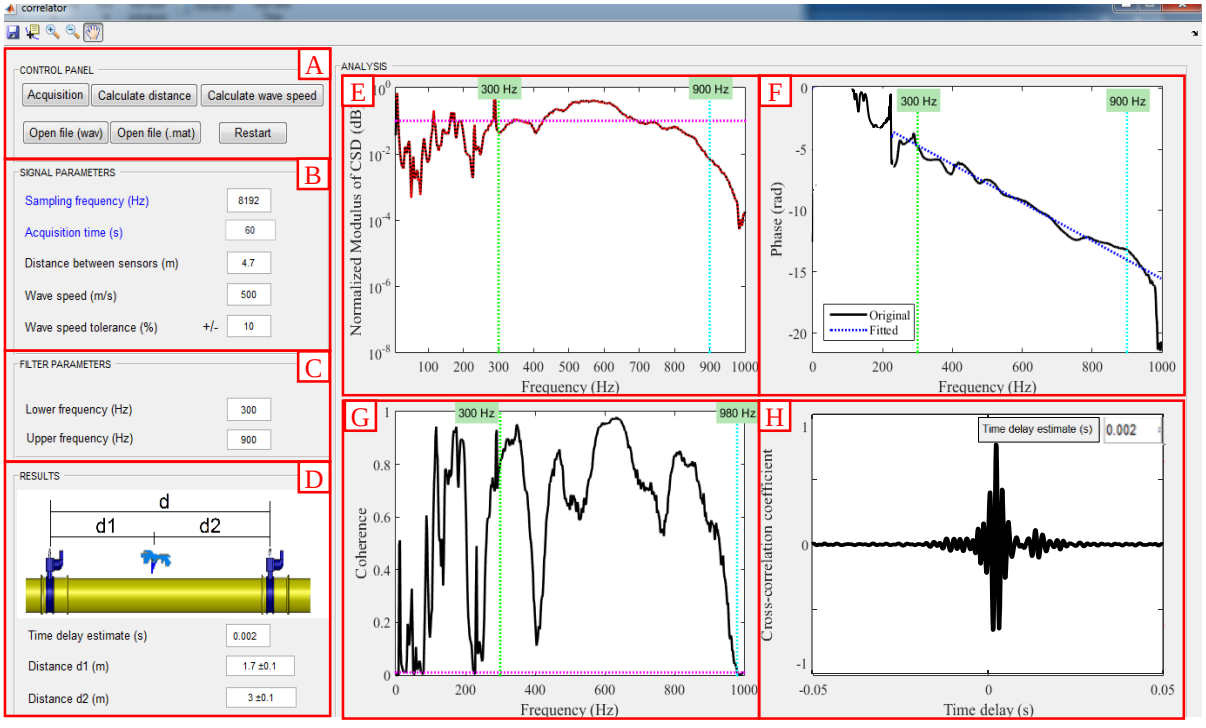

Source: Elaborated by the author.

5.2.4 Tests of the correlator

5.2.4.1 Test with the virtual pipe rig

The virtual leak simulator (BRENNAN *et al*., 2016) was used to test the collection of data and the processing of the time delay estimate using the interface and the prototype with cables. This virtual leak simulator follows the typical model of a leak noise in a buried water pipe of Figure 1 (chapter 2) and reproduces, using the speakers, leak signals depending on the parameters set.

Figure 41 shows the experimental setup of the virtual pipe rig and the prototype of the acoustic correlator. A PC was connected 2 speakers. Each speaker reproduces a leak in an access point. The software of the prototype of the correlator is installed in a laptop computer. This last one, through the line-in connector of the soundcard is connected, with two signal conditioners and cables to the two sensors glued to the diaphragm. The sensors used are accelerometers PCB Piezotronics Model 352A25 with sensitivity (±10%) 2.5 mV/g (only for this case is lighter and does not need much sensitivity).

Figure 41 - Experimental setup of the virtual pipe rig with the prototype of the acoustic correlator.

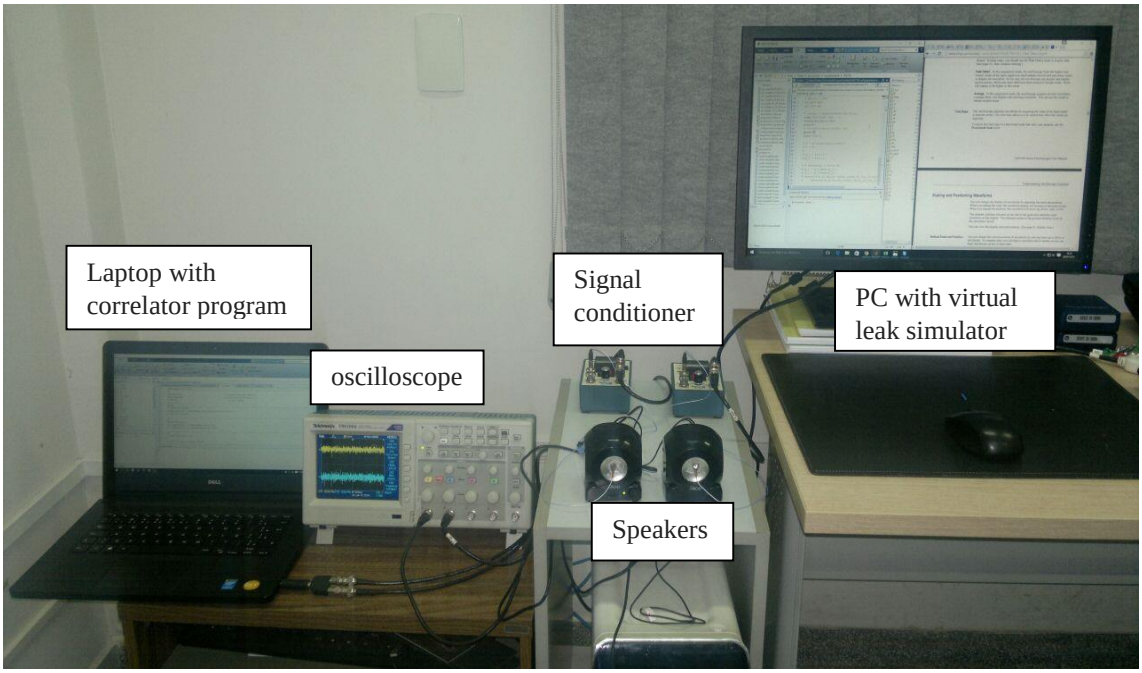

Source: Elaborated by the author.

In this section the interface with a typical leak detection problem (see Figure 1-Chapter 2) is shown. Parameters from Table 4 (chapter 3) are used to simulate the leak signals. The input parameters were set in the interface as d =50 m, c =356 m/s, wavespeed tolerance 10% and from 50 to 200 Hz of bandwidth.

The interface of the prototype of the acoustic correlator is shown in Figure 42. The normalized modulus of the CSD, where within the bandwidth selected there is high signal energy. Then, the phase of the CSD is shown. A deviation approximately at 160 Hz is observed, which can be due to structural dynamics of the speakers. The coherence shows a good similarity between the signals with a decay in 160 Hz as indicated above, this observation will be used to reduce the quantity of plots showed in the prototype 2. The CCC is shown, obtaining the time delay estimate from the maximum peak. In the result panel, the time delay T_0=27 ms, the distances d_1 =20.3±0.5 m and d_2 =29.7±0.5 m are shown.

Figure 42 - Interface of the prototype of the acoustic correlator, showing the results obtained from the leak simulated in the virtual pipe rig.

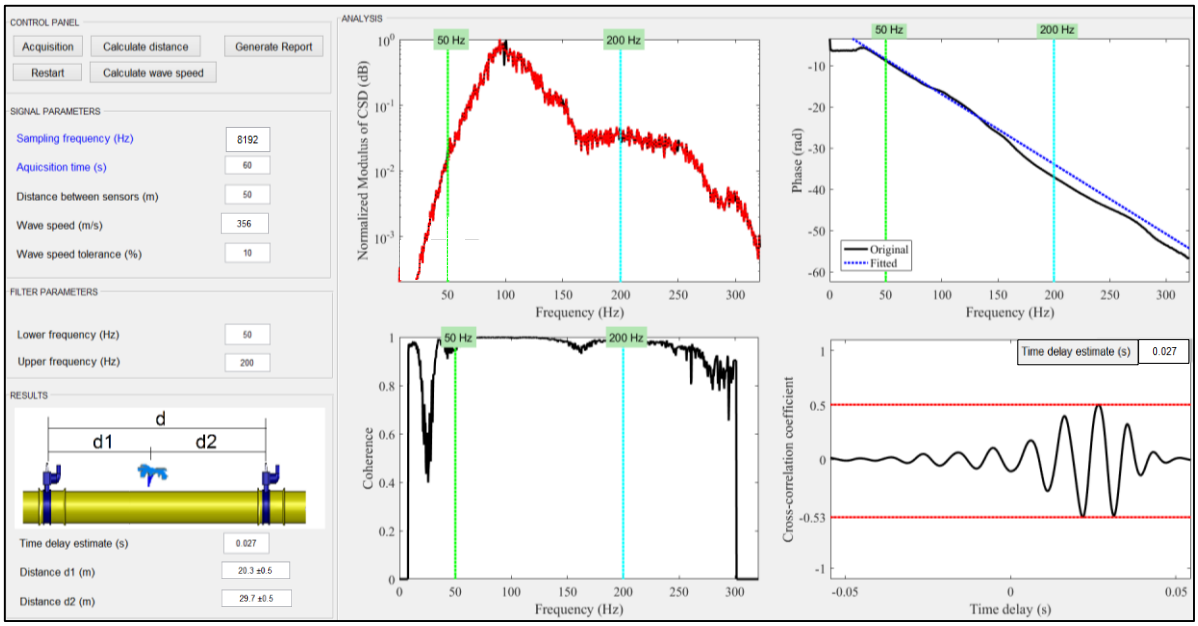

Source: Elaborated by the author.

5.2.4.2 Test in the SABESP test rig

The equipment was taken to the SABESP test rig and tested were conducted at P6, P17 with the open valve V5 to simulate the leak inbracket. In Figure 43 is shown the section of the test rig in which the experiments were carried out marked with a red rectangle. More detail of this test rig is described in chapter 2 page 28.

Figure 43 - Schematic of the SABESP test rig used for the experimental work. The points P5P17 with valve V5 was used to test the prototype.

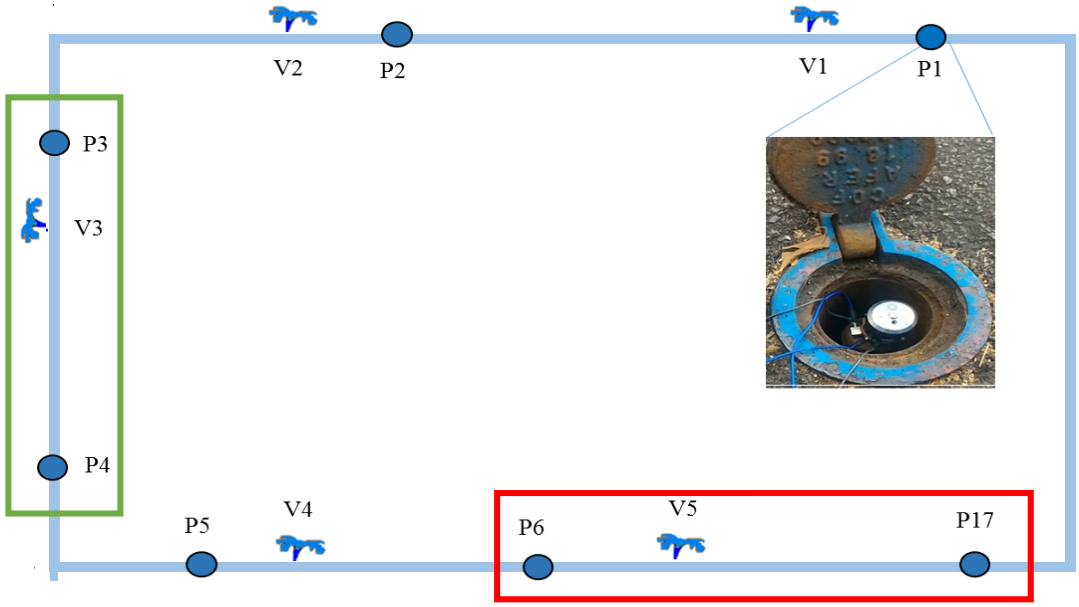

Source: Elaborated by the author.

Figure 44 shows the interface with the processed data from points P6, P17 with the open valve V5. The input data considered are: wavespeed of 500 m/s. with 10% of tolerance of the wavespeed, distance between sensors d =4.7 m, and a bandwidth from 300 to 900 Hz. The modulus of CSD normalized by its maximum value is shown, with large values within the bandwidth selected. The phase of CSD is shown as a black line with the straight blue line corresponding to $\phi = -\omega T_0$, where T_0 is obtained from the maximum peak of the CCC. The coherence is also shown, where it can be seen the bandwidth over which there is potentially time delay information is about 300-900 Hz. Finally, the cross-correlation coefficient is shown

in which the time delay estimated is indicated in the top left-hand corner of this plot. In the results panel, the time delay is 20 ms and the distances with the tolerances obtained are d_1 =1.7±0.5 m and d_2 =3±0.5 m.

In Figure 45, the same experiment, the SCADA from LMS was used to, (equipment used in chapter 2, page 31 to acquire leak data) carry out the test to compare the results obtained with the prototype 1. The bandwidth from 300 to 900 was used. (a) and (b) Power Spectral Density (PSD) for the access point 6 and 17. (c) Modulus of cross-spectral density (CSD) for signals recorder from the access point 6-17; (d) Coherence; (e) Phase of the cross-spectral density (CSD) and (f) Cross-correlation Coefficient (CCC) evaluated over the bandwidth selected. In the PSD for the access point 6 and 17, it is observed that the level of vibration is higher in the access point 6 than the access point 17, because of the leak is close to the access point 6.

In comparison with the plots obtained with the prototype 1, the modulus normalized of the CSD, the phase of the CSD, the coherence and the CCC have equal behaviour and the results of both experiments do not show any difference in the value of the time delay equal to 20 ms, therefore the location of the leaks in both experiments are the same.

Figure 44 - Interface of the prototype of the acoustic correlator, showing the results obtained from the leak simulated in the virtual pipe rig.

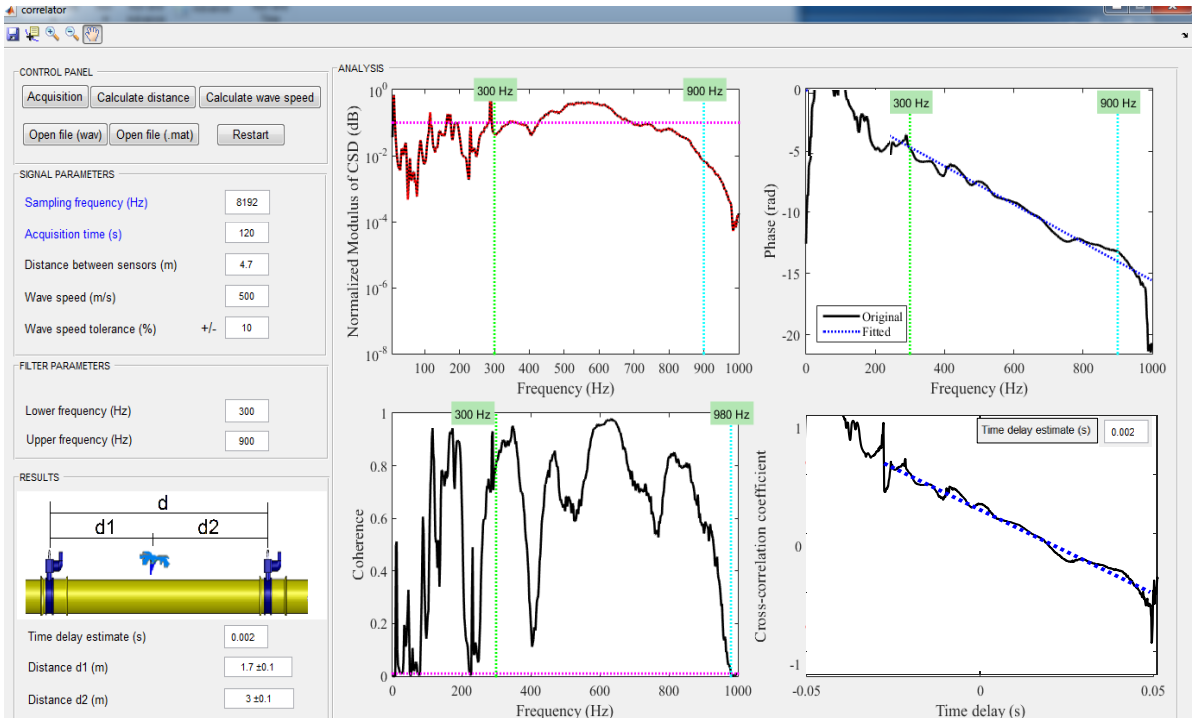

Source: Elaborated by the author.

Figure 45 - Measurement of leak signals using data acquisition system (SCADA) with accelerometers are placed at points P6 and P17 with the leak simulated in valve 5. (a) and (b) Power Spectral Density (PSD) for the access point 6 and 17. (c) Modulus of cross-spectral density (CSD) for signals recorder from the access point 6-17; (d) Coherence; (e) Phase of the cross-spectral density (CSD) and (f) Cross-correlation Coefficient (CCC) evaluated over the bandwidth selected. (Values in dB ref. V^2 for a and b).

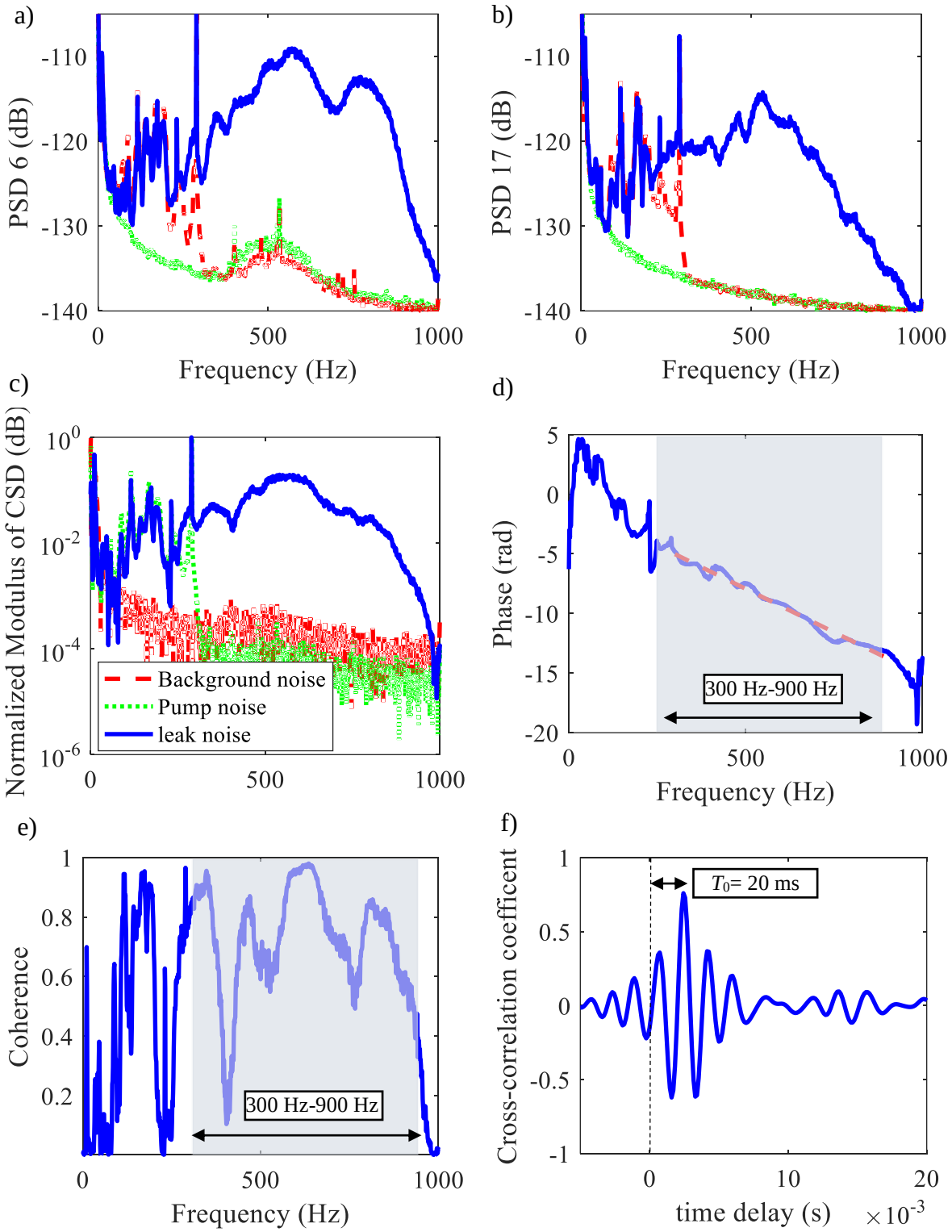

Source: Elaborated by the author.

5.3 Second prototype of the Acoustic correlator

The second prototype of the acoustic correlator has improvements in hardware and software with respect to the first prototype. The aims of this device are to collect efficiently the leak data with a wireless sensing and the operation of the software converting to an interface friendly and of easy operation for the user. Below is explained in detail the improvements.

5.3.1 Hardware of the correlator

The hardware changed with respect to the first prototype in the way how the information is collected. Figure 46 shows a diagram of the complete system. A data acquisition system of low cost using a board with architecture ARM® Orange Pi Zero model is designed, to synchronise the signals, an electronic circuit is designed with a trigger system and for transmission wireless of the data a GPS Ublox NEO-6 is used. (OBATA, *et al*., 2018)

Figure 46 - Diagram of the data acquisition system, circuit for synchronization and signal transmission system.

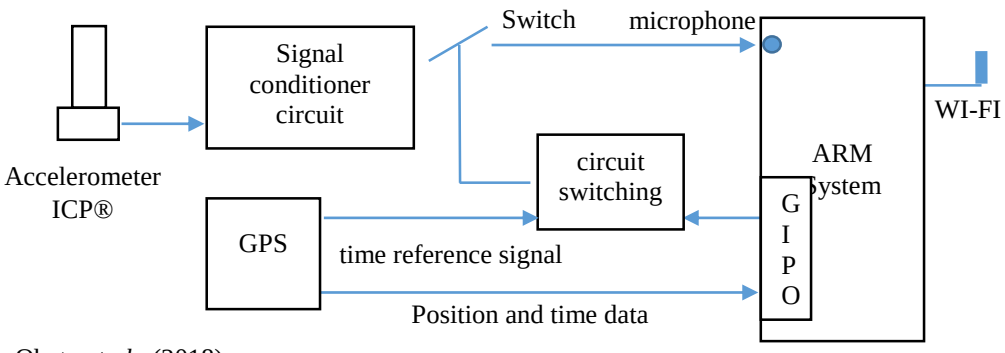

Source: Obata *et al*., (2018)

5.3.2 Software of the correlator

In the software, the parameters considered by default were the following: The time of acquisition of the leak signals which is 60 seconds, the sampling frequency which is 8192 Hz and the transformation to the frequency domain of the leak signals is carried out using a 4096-point FFT and a Hanning window with 50% overlap.

5.3.3 Interface description

Figure 47 shows the graphical interface and the parts are designated by uppercase letters. The update of the software of the first prototype contains improvements in the process of data entry and analysis of the results, they are shown in detail below.

In Figure 47 a) the first interface is shown. Two sections are observed:

- First section, which parameters as distance between sensors (A), diameter (B), thickness of the pipe (C) and selection of the type of Material (D) and soil (E) are entered. With these parameters the wavespeed is calculated (equation 2.18 chapter 2). In this interface is also entered the acquisition time (F).
- Second section, which two buttons are presented. The previous button (G), which is used to returned to initial presentation. And finally, the next button (H), which is used to go to results interface.

In Figure 47 b) the second interface is shown. Four sections are observed:

- The first section is the control Panel (A) containing five buttons which are the following:
  - The acquisition button (A-1), which is used to activate the connexion by wireless. This one collects the leak data from the accelerometers without cable connection. The calculation of the Phase of CSD and the CCC is effectuated internally using an automatic bandwidth selection with the condition of limit of the coherence (10^{-3}).
  - The parameters button (A-2), which is used to return to parameters interface.
  - The open file button (A-3), which is used to open and load .wav and .mat extension files of leak data.
  - The restart button (A-4), which is used to restart the program, erasing the interface information.
  - The filter button (A-5), which is used to reset the values of frequency chosen manually to values initially calculated with the condition of the coherence (10^{-3}). It is also possible to select interactively from the plot of the phase the bandwidth manually and it is recalculated automatically according to the bandwidth selected, updating the results.
- The second section are the plots of the phase of CSD (B), and the CCC scaled in distance (C). These plots are selected as enough to obtain visual information about the system.

- The third section are the results of the distances with a tolerance where the leak is located (D). This tolerance of the distance is calculated assuming a tolerance of 5% of the wavespeed. (see Appendix B for more detail about the distance tolerance). The leak is shown interactively in a diagram. This position of the leak changes depending of the case.
- Finally, the module of the quality index was implemented in the Quality of the correlation panel (E), where a representative value is shown which indicates the reliability of the estimation of the time delay.

Figure 47 - Print screen of the interface of the software a) parameters window b) results window.

a)

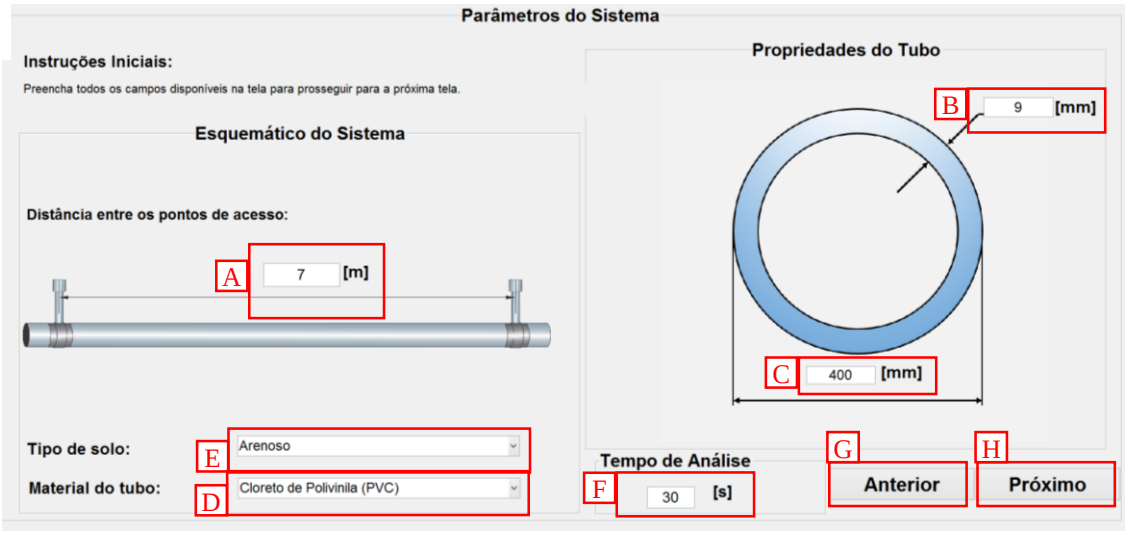

b)

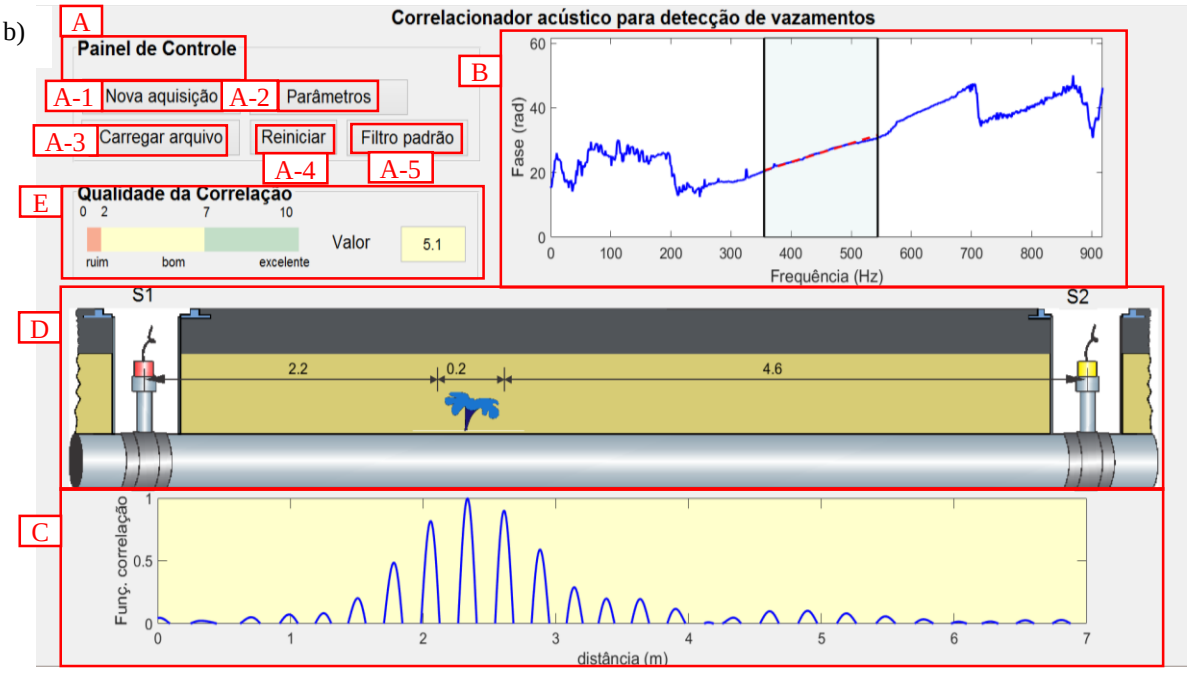

Source: Elaborated by the author.

5.3.4 Tests of the correlator

Prototype 2 is shown in Figure 48. In Figure 48 a) the equipment with the tablet to acquire data and control the software and the portable sensor units A and B is shown. In Figure 48 b) the portable sensor units are shown. This contains a power switch, a wireless antenna, a connector for the accelerometer and a connector for the external GPS.

Figure 48 - a) correlator prototype 2, b) module of sensor A and sensor B.

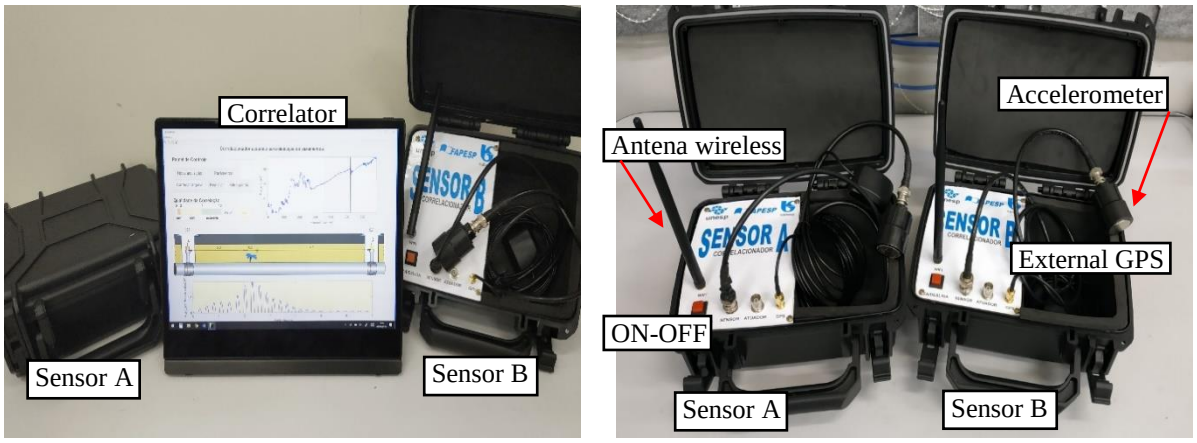

Source: Elaborated by the author.

This equipment was taken to SABESP test rig and tested at points P3P4 with the valve V3 opened to simulate the inbracket leak. Figure 43 is shown the schematic of SABESP test rig. The location of the points to measure with prototype 2 are marked with a green rectangle.

Two cases were analysed, data 1 with maximum flow of leak noise and data 2 with medium flow of leak noise were simulated. The flow of the leak is regulated with a valve. Maximum flow with the valve completely open and medium flow with the valve half open.

The input data were: distance between sensors d =4.7 m, ratio and thickness of the pipe 35.8 mm and 3.4 mm respectively, type of soil considered clay soil and acquisition time equal to 60 s. In Figure 49, these two cases are shown.

In Figure 49 a), The data 1 shows a good phase between the bandwidth selected automatically (350 - 550 Hz) being 1.4m the distance from the measurement point S1 to the possible location of the leak, which has a tolerance of 0.2m. The value of the quality index is equal to 5.5 which in the quality scale presented means that the estimation is good.

In Figure 49 b) the data 2 shows a good phase between the bandwidth selected automatically (350 - 550 Hz) being 1.5m the distance from the measurement point S1 to the possible location of the leak, which has a tolerance of 0.2m. The value of the quality index for the data 2 is equal to 5.2, which in the quality scale presented means that the estimation is good. In the two cases presented it was possible to observe minimal differences in the value of distances.

Figure 49 - Measurement with the prototype, a) Data 1-P3P4 open valve V3 with maximum flow of the leak, and b) Data 2-P3P4 open valve V3 with medium flow of the leak.

a)

b)

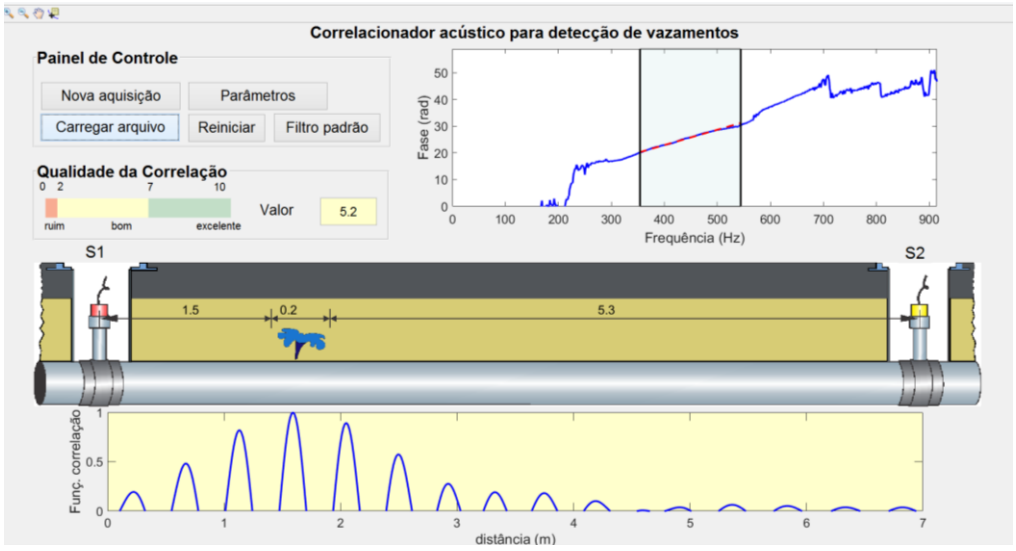

Source: Elaborated by the author.

5.4 Conclusions

In this chapter two prototypes of the acoustic correlator to detect and locate leaks have been described. The features of each one have been presented.

For the first prototype, the leak data is loaded manually after data acquisition using cables, showing the modulus and phase of the CSD, coherence and CCC as information to analyse the behaviour of the leak noise. The leak position is shown in a text box.

For the second prototype, the leak data is collect with a wireless sensing. Two interfaces were designed to enter the parameters and show the result easily. In the first interface the selection of the material and dimensions of the pipe, soil type where was installed the pipe, adjust the time of the acquisition, automatic selection of the bandwidth where the leak is present are entered. In the second interface the phase of the CSD and the CCC are presented for a better analysis of the behaviour of the leak in the system. The bandwidth is shown graphically in the phase of the CSD, the location of the leak noise is shown graphically with a tolerance and the quality of the correlation was quantified and shown.

6 CONCLUSIONS AND FUTURE WORK

6.1 Conclusions

In this chapter the main conclusions of this thesis are summarized with suggestions for future work. Detailed conclusions are given in the end of each chapter. In this thesis, the factors that affect the wavespeed of the leak noise propagation in buried water pipes have been investigated. They involving the filtering effect of the sensor-pipe system and a method to select appropriately a bandwidth to concentrate the effect of the leak noise. The distortion effects on the accuracy of the time delay estimate have been also studied with focus on the quantization and clipping of the leak signals. An attempt to obtain a representative value of quality of the CCF and hence the time delay estimate has been made. Finally, two correlator prototypes have been presented in which the author contributed to the development, being the second prototype better than the first one, with a wireless sensing and interfaces to enter the parameters easily and show the necessary information for a better analysis of the behaviour of the leak in the system.

The main conclusions of this thesis can be summarised as follow:

- The sensor-pipe system acts as a band-pass filter, concentring in a bandwidth the effect of the leak noise. This bandwidth gives an initial idea where the leak noise is potentially present. It was obtained using the two half power point frequencies in the normalized modulus of CSD as a reference. Two cases with simulated data from test rigs on Sao Paulo and Blitfield have been used to shown this effect.
- The importance of the band-pass filter selection, which is used to suppress the undesirable noise on the shape of the CCC, has been presented. It may affect in the estimation of time delay and wavespeed. Leak data collected from the SABESP test rig was filtered, selecting a bandwidth with 10^{-3} as a limit of the coherence. This condition has been appropriated to obtain good results.
- Distortions of the leak noise signals due to quantization and clipping do not have effect on the time delay estimated. This result can lead to significant improvements in the design and development of leak noise correlators. First, saving in processing time and storage of leak data, because of the possibility of using of converter A/D with low resolution (number of

bits). Second, electronic circuits for automatic gain control are unnecessary in the correlator device.

- Five indices have been proposed, each one with different features related to the effects of noise, structural dynamic and wave reflection from discontinuities in the pipe system. These indices have been quantified and integrated in an overall quality index. Experimental cases in different test rigs have been calculated their quality indices. Showing a good representation of the reliability of the time delay estimated.
- Two prototypes have been presented in which the author contributed to the development of the software mainly. The first prototype was developed with the aim to carried out the collection of data, process and analyse the information collected. The analysis obtained was used to improve the second prototype: implementing the wireless sensing, dividing in two friendly interfaces, the first one with the distance between the measurement points some parameters of the pipe, selection of material, soil type and acquisition time, and the second one showing the results of the location of the leak with an automatic selection of bandwidth and an indicator of the quality of the time delay estimate. The plots of phase of CSD and CCC are also shown. These plots are selected as enough to obtain visual information about the system analysed.

6.2 Recommendation for Further Work

This work was part of the FAPESP project to develop a national low cost acoustic correlator optimized to detect and locate leaks in buried plastic water pipe from SABESP. It is the beginning on the investigation of this subject in Brazil. Obtaining contributions that are the basis for future research such as:

Data collected from a test rig in São Paulo were used to obtain the bandwidth where the leak affect to the system and the wavespeed. This data has led to new knowledge about the specific vibroacoustic behaviour of such systems in São Paulo.

The study of the distortion due to quantization and clipping for leak signals has led that it is possible to use inexpensive hardware rather than the expensive complex systems generally in use nowadays.

Five indices have been formulated and proposed to quantify the quality and reliability of the time delay estimate. an overall quality index which represents the total effects and features has been quantified in a value. Three levels of reliability for the indices, have been proposed.

A user-friendly software has been developed to detect and locate a leak in buried plastic water pipes, with the following novel characteristics: an automatic selection of bandwidth and an indicator of the quality of the time delay estimate.

Some recommended avenues of work to continue this development are as follow

- To study the soil influence in the filtering characteristics of the sensor-pipe system.
- To study the vibroacoustic characteristics of buried water pipe in Sao Paulo varying the flow of the water, pressure.
- To study the vibroacoustic characteristics of large diameter mains.
- To study the vibroacoustic characteristics of distribution pipes with different materials between two measurement points.
- To study the reflections of the leak in section changes, pipe fittings, valves, etc.
- To improve the correlation software for acquisition with geophones and hydrophones.
- To improve the correlation software for large diameter mains.
- To improve the correlation software for different materials between two measurement points.

REFERENCES

ALMEIDA, F. C. L. **Improved acoustic methods for leak detection in buried plastic water distribution pipes.** 2013. 275 f. Thesis (PhD in Mechanical e Engineer) - University of Southampton, England, 2013.

ALMEIDA, F. C. L.; JOSEPH, P. F.; BRENNAN, M. J.; WHITFIELD, S.; DRAY, S. The dynamic behaviour of a buried water pipe and its effect on leak location using acoustic methods. **Key Engineering Materials**, Pfaffikon, v. 569-570, p. 1194-1201, 2013.

ALMEIDA, F. C. L.; BRENNAN, M. J.; JOSEPH, P. F.; WITHFIELD, S.; DRAY, S.; PASCOALLINI, A. T. On the acoustic filtering of the pipe and sensor in a buried plastic water pipe and its effect on leak detection: an experimental investigation. **Journal Sensors,** Basel, v. 14, p. 5595-5610, 2014.

ALMEIDA, F. C. L.; BRENNAN, M. J.; JOSEPH, P. F.; DRAY, S.; WHITFIELD, S.; PASCOALLINI, A. T. Towards an in-situ measurement of wave velocity in buried plastic water distribution pipes for the purposes of leak location. **Journal of Sound and Vibration**, London, v. 359, p. 40-55, 2015.

ALMEIDA, F. C. L.; BRENNAN, M. J.; PASCOALLINI, A. T.; JOSEPH, P. F.; GAO, Y. On the signum function and its effect on acoustic correlation for leak location in buried plastic water pipes. **Procedia Engineering**, Amsterdam, v. 199, p. 1344-1349, 2017.

BECKER, D. Published by SEWERIN. **Leak detection in water distribution networks by correlation, sound velocity as a possible source of error**. Available in https://www.sewerin.com/cms/en/info-centre/downloads/media/leak-detection-in-drinking-water-distribution-networks-by-correlation.html. Access in: 16 Oct. 2017.

BENNETT, W. Spectra of quantized signals. **Bell System Technical Journal**, Piscataway, v. 27, p. 446-472, 1948.

BRENNAN, M. J.; JOSEPH, P. F.; MUGGLETON, J. M.; GAO, Y. On the use of acoustic methods to detect water leaks in buried water pipes. **Water & Sewerage Journal**, [s.l.], v. 1, p. 11–13, 2006.

BRENNAN, M. J.; GAO, Y.; JOSEPH, P. F. On the relationship between time and frequency domain methods in time delay estimation for leak detection in water distribution pipes, **Journal of Sound and Vibration**, London, v. 304 p. 213-223, 2007.

BRENNAN, M. J.; KROLL DE LIMA, F.; ALMEIDA, F. C. L.; JOSEPH, P. F.; PASCHOALINI, A. T. A virtual pipe rig for testing acoustic leak detection correlators: Proof of concept. **Applied Acoustics**, Oxford, v. 102, p. 137-145, 2016.

BRENNAN, M. J.; KARIMI, M.; MUGGLETON, J. M.; ALMEIDA, F. C. L.; KROLL DE LIMA, F.; AYALA, P. C.; OBATA, D.; PASCHOALINI, A. T. On the effects of soil properties on leak noise propagation in plastic water distribution pipes, **Journal of Sound and Vibration**, London, v. 427, p. 120-133, 2018.

BRENNAN, M. J.; ALMEIDA, F. C. L.; KROLL DE LIMA, F.; AYALA, P. C.; PASCHOALINI, A. T. Measurement of the speed leak noise propagation in buried water pipes: challenges and difficulties. *In*: PROCEEDINGS OF THE INTERNATIONAL SYMPOSIUM ON DYNAMIC PROBLEMS OF MECHANICS, DINAME, 17, 2017, São Sebastião. **Proceedings of the** […]. São Sebastião: ABCM, 2018. p. 511-522. ABCM Series on Mechanical Sciences and Engineering.

CARTER, C. Time Delay Estimation for Passive Sonar Signal Processing. **IEEE Transactions on Acoustics, Speech, and Signal Processing**, Piscataway, v. 29, n. 3, 1981. p. 463-470.

CHAPRA S. C. **Applied numerical methods with MATLAB® for engineers and scientists**. New York: McGraw-Hill Education, 2018. 707 p.

COLE, T. Finite sample correlations of quantized gaussians. **Australian Journal of Physics**, Collingwood, v. 21, p. 273-282, 1968.

COOPER B. F. C. Correlators with two-bit quantization. **Australian Journal of Physics**, Collingwood, v. 23, p. 521-527, 1970.

FUCHS, H. V.; RIEHLE, R. Ten years of experience with leak detection by acoustic signal analysis. **Applied Acoustics**, Oxford, v. 33, p.1-19, 1991.

GAO, Y.; BRENNAN, M. J.; JOSEPH, P. F.; MUGGLETON J. M.; HUNAIDI, H. A model of the correlation function of leak noise in buried plastic pipes. **Journal of Sound and Vibration**, London, v. 227, p. 133-148, 2004.

GAO, Y.; BRENNAN, M. J.; JOSEPH, P.F.; MUGGLETON, J.M.; HUNAIDI, O. On the selection of acoustic/vibration sensors for leak detection in plastic water pipes. **Journal of Sound and Vibration**, London, v. 283, p. 927-941, 2004.

GAO, Y.; BRENNAN, M. J.; JOSEPH, P.F. A comparison of time delay estimators for the detection of leak noise signals in plastic water distribution pipes. **Journal of Sound and Vibration**, London, v. 292, p. 552-570, 2006.

GAO, Y.; BRENNAN, M. J.; JOSEPH, P. F. On the effects of reflections on time delay estimation for leak detection in buried plastic water pipes. **Journal of Sound and Vibration**, London, v. 325, n. 3, p. 649-663, 2009.

GAO, Y.; SUI, F.; MUGGLETON, J. M.; YANG, J. Simplified dispersion relationships for fluid-dominated axisymmetric wave motion in buried fluid-filled pipes. **Journal of Sound and Vibration**, London, v. 375, p. 386-402, 2016.
.
GAO, Y.; LIU Y.; MUGGLETON J. M. Axisymmetric fluid-dominated wave in fluid-filled plastic pipes: loading effects of surrounding elastic medium. **Applied Acoustics**, Oxford, v. 116, p. 43-49, 2017.

GLENN, D.; GARY, J. **The audio dictionary**. 3. ed. Seattle: University of Washington Press, 2005. 516 p.

HAMILTON, S.; CHARALAMBOUS, B. **Leak detection, technology and implementation**. London: IWA publishing, 2013. 106 p.

HUANG, Y.; BENESTY, J. **Audio signal processing for next generation multimedia communication systems**. Boston: Kluwer Academic Publishers, 2004. 369 p.

HUNAIDI, O.; CHU, W. T. Acoustical characteristics of leak signals in plastic water distribution pipes. **Applied Acoustics**, Oxford, v. 58, p. 235–254, 1999.

HUNAIDI, O. **Detecting leaks in water-distribution pipes**. Canada: National Research Council, 2000. 6 p. Construction Technology Update, 40

ISEN, F. **DSP for MATLAB™ and LabVIEW™ I**: fundamentals of discrete signal processing. California: Morgan & Claypool Publishers, 2008. 196 p.

KIHONG, S.; HAMMOND, J. K. **Fundamentals of signal processing**. New York: John Wiley & Sons, 2008. 403 p.

MUGGLETON, J. M.; BRENNAN, M. J.; PINNINGTON, R.J. Wavenumber prediction of waves in buried pipes for water leak detection. **Journal of Sound and Vibration**, London, v. 249, p. 934–954, 2002.

MUGGLETON, J. M.; BRENNAN, M. J.; LINFORD, P. W. Axisymmetric wave propagation in fluid-filled pipes: measurements in *in-vacuo* and buried pipes. **Journal of Sound and Vibration**, London, v. 270, p. 171-190, 2004.

MUGGLETON, J. M.; BRENNAN, M. J. Leak noise propagation and attenuation in submerged plastic water pipes. **Journal of Sound and Vibration**, London, v. 278, p. 527-537, 2004.

MUGGLETON, J. M.; BRENNAN, M. J.; PINNINGTON, R. J.; GAO, Y. A novel sensor for measuring the acoustic pressure in buried plastic water pipes. **Journal of Sound and Vibration**, London, v. 295, p. 1085-1098, 2006.

MUGGLETON, J. M.; BRENNAN, M. J.; GAO, Y. Determining the location of buried plastic water pipes from measurements of ground surface vibration. **Journal of Applied Geophysics**, Amsterdam, v. 75, p. 54-61, 2011.

OBATA, D.; BRENNAN, M. J.; ALMEIDA, F. C. L.; AYALA P. C.; KROLL DE LIMA, F.; PASCHOALINI, A. T. Sincronização de sinais via GPS para sistemas de detecção de vazamentos por correlação cruzada. *In*: CONGRESSO NACIONAL DE ENGENHARIA MECÂNICA, 10, 2018, Salvador. **Anais** [...] Salvador: ABCM, 2018.

OPPENHEIM, A.; SCHAFER, R. **Processamento em tempo discreto de sinais**. 3. ed. São Paulo: Pearson Education, 2012. 665 p.

PELGROM, M. **Analog to digital conversion**. 2. ed. New York: Springer, 2013. 584 p.

PRICE, M. E.; REED, D. W. The influence of mains leakage and urban drainage on groundwater levels beneath conurbations in the UK. **Proceedings of the Institution Civil Engineering**, London, v. 86, p. 31-39, pt. 1, 1989.

COMPANHIA DE SANEAMENTO BASICO DE SÃO PAULO - Sabesp Noticias. **International seminar on loss control**. 2016. Available: http://site.sabesp.com.br/site/imprensa/noticias-detalhe.aspx?secaoId=65&id=7045. Access in: 16 Oct. 2017.

SECRETARIA NACIONAL DE SANEAMENTO AMBIENTAL – SNSA. Sistema Nacional de Informações sobre Saneamento. **Diagnóstico dos serviços de água – 2014**. Brasília: SNSA/MCIDADES, 2016.

SHARMA, A. K. **Text book of index number and time series**. [New Delhi]: Discovery Publishing House, 2005. 240 p.

SRIPAD, A.; SNYDER, D. A necessary and sufficient condition for quantization errors to be uniform and white. **IEEE Transaction Acoustics, Speech and Signal Processing**, Piscataway, v. 25, n. 5, p. 442-448, 1977.

ISHIDO, Y.; TAKAHASHI, S. A new indicator for real-time leak detection in water distribution networks: design and simulation validation. **Procedia Engineering**, Amsterdam, v. 89, 2014, p. 411- 417.

TAN, L.; JIANG, J. **Digital signal processing**: fundamentals and applications. 2. ed. Oxford: Elsevier, 2013. 876 p.

THORNTON J.; STURM R.; KUNKEL, G. **Water loss control**. 2. ed. New York: Mc Graw Hill, 2008. 632 p.

US SAQIB, N.; MYSOREWALA, M. F.; CHEDED, L. A multiscale approach to leak detection and localization in water pipeline network. **Water Resources Management**, Dordrecht, v. 31, n. 12, p. 3829–3842, 2017.

VAN VLECK, J. H. **The spectrum of clipped noise**. Cambridge: Harvard University, 1943. Radio Research Laboratory Research Report, 51.

VAN VLECK, J. H.; MIDDLETON, D. The spectrum of clipped noise. **Proceedings of the IEEE,** Picastaway, v 54, n. 1 p. 2-19, 1966.

WEINREB, S. **A digital spectral analysis technique and its application to radio astronomy**. [Massachusetts: Massachusetts Institute of Technology Technical], 1963. 229 p. Massachusetts Institute of Technology Technical Report, 412. Available in: https://core.ac.uk/download/pdf/4390641.pdf. Access in: 26 ago. 2019.

WIDROW, B.; KOLLAR, I. Statistical Theory of Quantization. **IEEE Transaction On Instrumentation and Measurement**, Piscataway, v. 45, n. 2 p. 353-361, 1996.

WIDROW, B.; KOLLAR, I. **Quantization noise**. Cambridge: Cambridge University Press, 2008. 751 p.

WUU, C. Y.; PEARSON, A. E. On time delay estimation involving received signal. **IEEE Transactions on Acoustics, Speech, and Signal Processing**, Piscataway, v. 32, n. 4, p. 828-835, 1984.

APPENDIX A - WAVENUMBER PREDICTION

This appendix shows how the wavenumber is calculated analytically. The wavenumber in chapter 2 equation 2.5 was mentioned to calculate the wavespeed and the measure of the loss within the pipe wall.

Gao *et al*. (2016) developed for the case of n = 0 mode and with the s = 1 an analytical method for investigating the dispersion characteristics of a buried fluid-filled pipe. Gao *et al*. (2017) extended the analysis to study the loading effects of surrounding elastic medium, acting as a combination of mass, stiffness and radiation damping. In this thesis, soil is the static medium that surrounds the fluid-filled pipe. The wavenumber can be expressed by (BRENNAN *et al*., 2018).

$$k(\omega) = k_{\text{water}}(\omega)\left(1+\frac{K_{\text{water}}}{K_{\text{pipe}}+K_{\text{soil}}}\right)^{\frac{1}{2}}, \tag{A.1}$$

where $k_{\text{water}}(\omega) = \omega/c_{\text{water}}$ is the wavenumber of the water within the pipe, in which $c_{\text{water}} = 1500$ m/s is the speed of sound in water and ω is the angular frequency. The term $K_{\text{water}} = 2B_{\text{water}}/a$ is the stiffness of the water, in which B_{water} is the bulk modulus and a is the mean radius. The term $K_{\text{pipe}} = E_{\text{pipe}}h\Big/\left(a^2\left(1-\nu_{\text{pipe}}^2\right)\right) - \rho_{\text{pipe}}h\omega^2$ is the dynamic stiffness of the pipe-wall, where h is the thickness, E_{pipe}, ρ_{pipe} and ν_{pipe} are the Young's modulus, density and Poisson's ratio of the pipe respectively. The term K_{soil} is the dynamic stiffness of surrounding medium given by (SCUSSEL *et al*, 2018)

$$K_{\text{soil}} = \frac{G_{\text{soil}}}{a}K_{\text{soil}}^{(1)} + \frac{E_{\text{pipe}}h}{a^2\left(1-\nu_{\text{pipe}}^2\right)}K_{\text{soil}}^{(2)}, \tag{A.2}$$

where the terms $K_{\text{soil}}^{(1)}$ and $K_{\text{soil}}^{(2)}$ are given by

$$K_{\text{soil}}^{(1)} = 2 + \frac{k_{\text{r}}^{\text{r}} a k_{\text{r}}^{2} a^{2} \left[\frac{H_0\left(k_{\text{r}}^{\text{r}} a\right)}{H_0^{'}\left(k_{\text{r}}^{\text{r}} a\right)} \right] \left[\frac{H_0\left(k_{\text{d}}^{\text{r}} a\right)}{H_0^{'}\left(k_{\text{d}}^{\text{r}} a\right)} \right]}{k_{\text{r}}^{\text{r}} a k_{\text{d}}^{\text{r}} a \left[\frac{H_0\left(k_{\text{r}}^{\text{r}} a\right)}{H_0^{'}\left(k_{\text{r}}^{\text{r}} a\right)} \right] + k^{2} a^{2} \left[\frac{H_0\left(k_{\text{d}}^{\text{r}} a\right)}{H_0^{'}\left(k_{\text{d}}^{\text{r}} a\right)} \right]} \tag{A.3}$$

and

$$K_{\text{soil}}^{(2)} = -\frac{\nu_{\text{pipe}}^{2}}{\left(1 + \frac{S_1}{k^{2} a^{2}}\right)} + \frac{j 2 \nu_{\text{pipe}} S_2}{ka\left(1 + \frac{S_1}{k^{2} a^{2}}\right)} + \frac{S_2^{2}}{k^{2} a^{2}\left(1 + \frac{S_1}{k^{2} a^{2}}\right)}, \tag{A.4}$$

in which

$$S_1 = -G_{\text{soil}} \frac{\left(1 - \nu_{\text{pipe}}^{2}\right) a}{E_{\text{pipe}} h} \left[\frac{k_{\text{d}}^{\text{r}} a k_{\text{r}}^{2} a^{2}}{k_{\text{r}}^{\text{r}} a^{2} k_{\text{d}}^{\text{r}} \left[\frac{H_0\left(k_{\text{r}}^{\text{r}} a\right)}{H_0^{'}\left(k_{\text{r}}^{\text{r}} a\right)} \right] + k^{2} a^{2} \left[\frac{H_0\left(k_{\text{d}}^{\text{r}} a\right)}{H_0^{'}\left(k_{\text{d}}^{\text{r}} a\right)} \right]} \right] \tag{A.5}$$

and

$$S_2 = \frac{j G_{\text{soil}} \left(1 - \nu_{\text{pipe}}^{2}\right) k a^{2}}{E_{\text{pipe}} h} \left[2 - \frac{k_{\text{r}}^{2} a^{2} \left[\frac{H_0\left(k_{\text{d}}^{\text{r}} a\right)}{H_0^{'}\left(k_{\text{d}}^{\text{r}} a\right)} \right]}{k_{\text{r}}^{\text{r}} a^{2} k_{\text{d}}^{\text{r}} \left[\frac{H_0\left(k_{\text{r}}^{\text{r}} a\right)}{H_0^{'}\left(k_{\text{r}}^{\text{r}} a\right)} \right] + k^{2} a^{2} \left[\frac{H_0\left(k_{\text{d}}^{\text{r}} a\right)}{H_0^{'}\left(k_{\text{d}}^{\text{r}} a\right)} \right]} \right]. \tag{A.6}$$

The terms k_{d}^{r} and k_{r}^{r} are the surrounding soil radial wavenumbers given $k_{\text{d}}^{\text{r}} = \sqrt{k_{\text{d}}^{2} - k^{2}}$ and $k_{\text{r}}^{\text{r}} = \sqrt{k_{\text{r}}^{2} - k^{2}}$, where k_{d} and k_{r} are the compressional and shear wavenumbers in the surrounding soil, respectively, given by $k_{\text{d}}^{2} = \omega^{2} \rho_{\text{soil}} / \left(B_{\text{soil}} - 4 G_{\text{soil}} / 3\right)$ and $k_{\text{r}}^{2} = \omega^{2} \rho_{\text{soil}} / G_{\text{soil}}$, in which ρ_{soil} is the density of the surrounding soil. The term H_0 is the Hankel function of zero order and second kind which describes the outgoing waves in the surrounding soil (SCUSSEL *et al*., 2018), and $'$ denotes the spatial derivative.

APPENDIX B - TOLERANCE ON THE MEASUREMENT OF THE DISTANCE

This appendix shows how the tolerance of the distance is calculated. The distance with the tolerance is placed in the interface of results of the second prototype in chapter 5.

To calculate the estimated location of the leak, it is required accurate estimates of c and T_0 . The estimation of the time delay was investigated widely by Carter (1981), Wuu and Pearson (1984), Huang and Benesty, (2004), Gao *et al*. (2006), Brenan *et al*. (2007) and others. Respect to the estimation of the wavespeed, in the most of the cases, it is estimated from tables which are compiled from simple calculations of from a historical database. An error in the wavespeed estimated will produce a corresponding error in the estimated location of the leak. This error can be determined using the following equation

$$d_{2\mathrm{m}} = \frac{d - c_{\mathrm{m}} T_0}{2}, \tag{B.1}$$

where $d_{2\mathrm{m}}$ and c_{m} are the estimated measured distance and estimated wavespeed. Combining this equation with equation 1.1 is obtained

$$\frac{\Delta d_2}{d} = \left(\frac{1}{2} - \frac{d_2}{d}\right)\frac{\Delta c}{c}, \tag{B.2}$$

where $\Delta c = c - c_m$ and $\Delta d_2 = d_2 - d_{2\mathrm{m}}$ Equation B.2 shows that if the leak is exactly in the middle of the measurement positions, the time delay is zero and there is no error in the leak location due the error of the wavespeed estimate. However, when the leak is close to the measurement points the error increases. As an example d =100 and 10% of error in the wavespeed estimate, with the leak in one of the measurement positions. The resultant error in the location of the leak in this case is 5% of the length of the pipe.

APPENDIX C - MEASUREMENTS OF LEAK SIGNALS OF THE EXPERIMENTS CARRIED OUT IN THE SABESP TEST RIG

Figure 50 - Measurement of leak signals, accelerometers are placed at points P1 and P2 with the leak simulated in valve 1 (See Table 2, case P1P2-v1; Date 13/03/16) (a) and (b) Power Spectral Density (PSD) for the access point 1 and 2. (c) Modulus of cross-spectral density (CSD) for signals recorder from the access point 1-2; (d) Coherence; (e) Phase of the cross-spectral density (CSD) and (f) Cross-correlation Coefficient (CCC) evaluated over the bandwidth selected. (Values in dB ref. V^2).

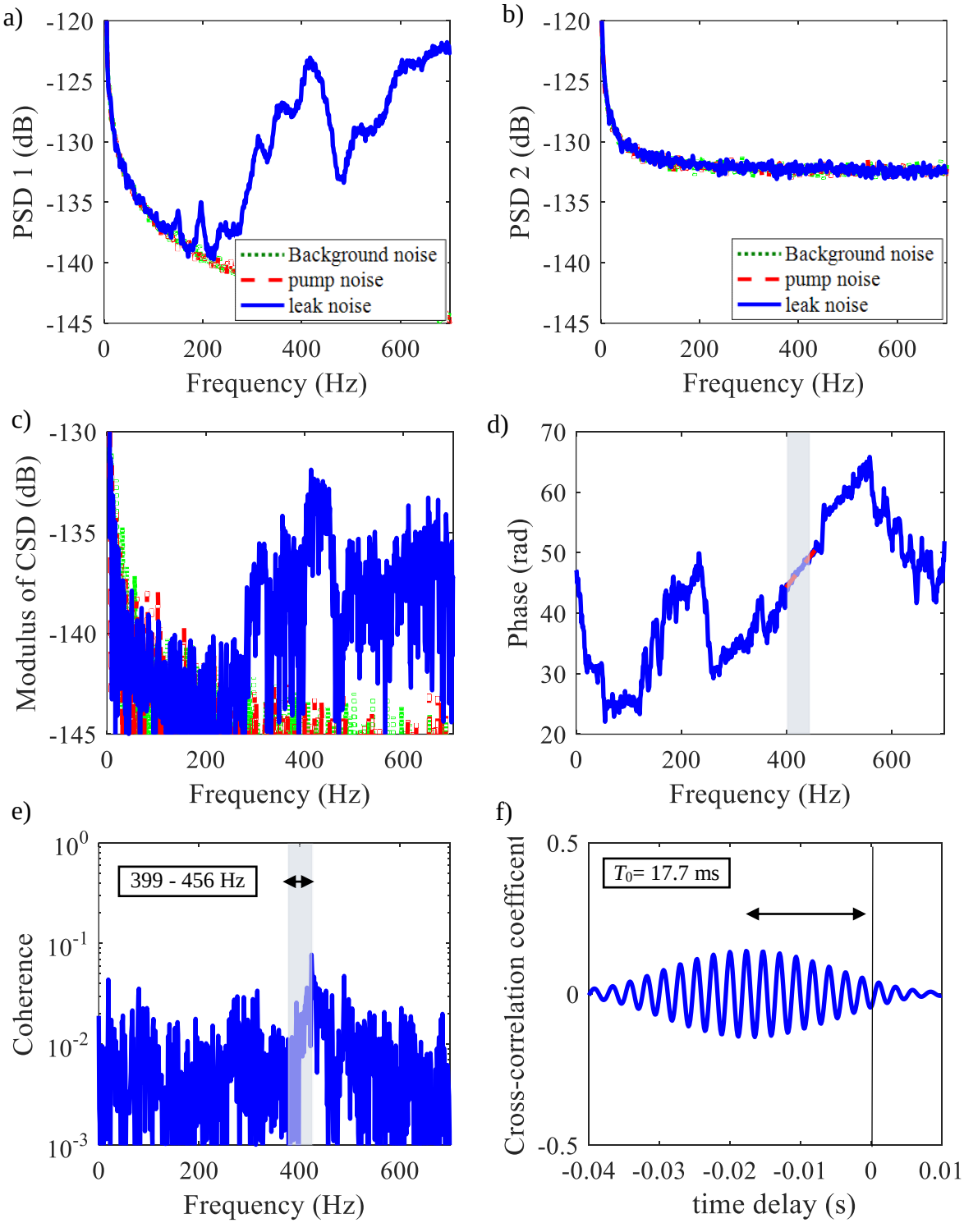

Figure 51 - Measurement of leak signals, accelerometers are placed at points P1 and P2 with the leak simulated in valve 1 (See Table 2, case P1P2-v1; Date 18/04/16) (a) and (b) Power Spectral Density (PSD) for the access point 1 and 2. (c) Modulus of cross-spectral density (CSD) for signals recorder from the access point 1-2; (d) Coherence; (e) Phase of the cross-spectral density (CSD) and (f) Cross-correlation Coefficient (CCC) evaluated over the bandwidth selected. (Values in dB ref. V^2).

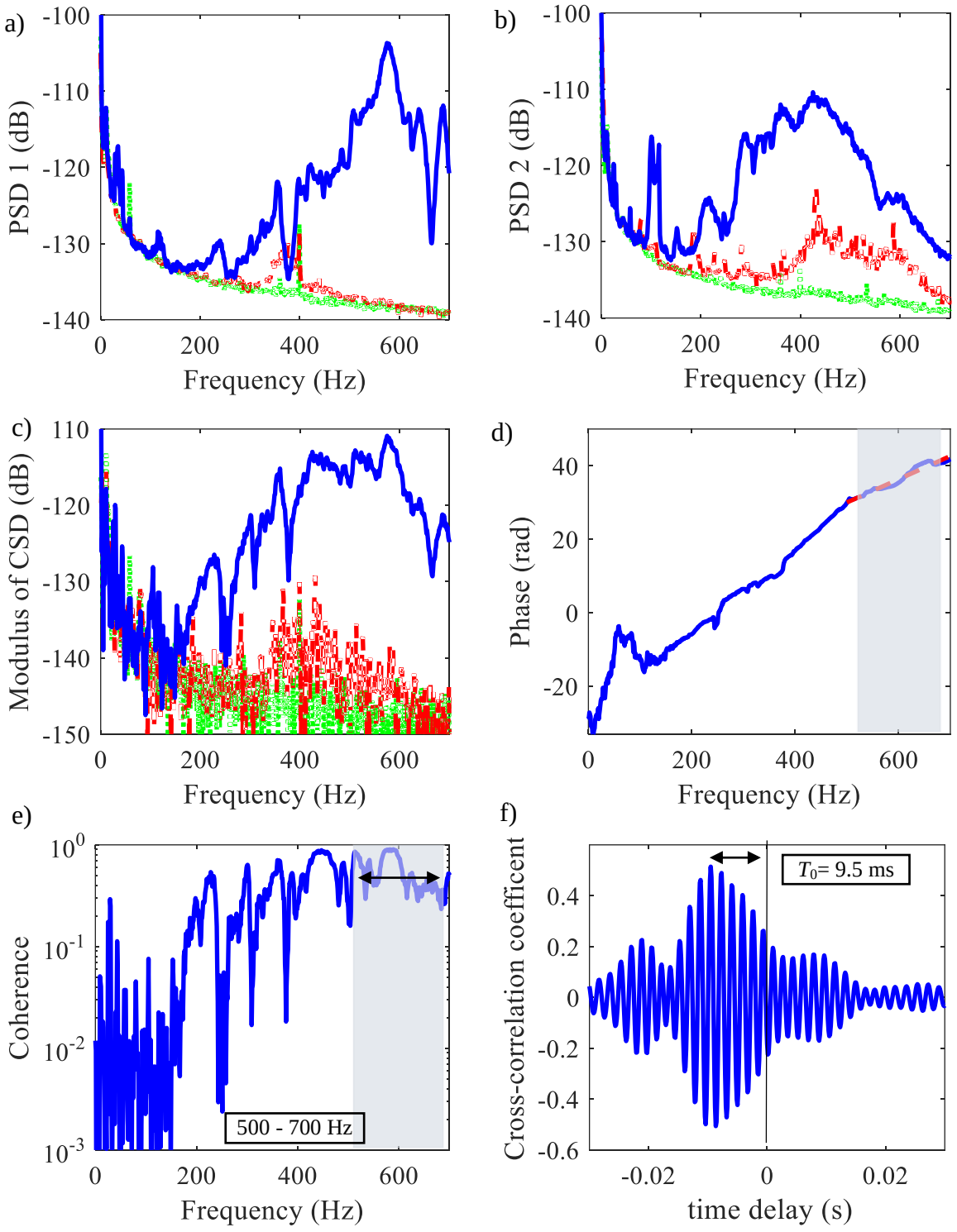

Figure 52 - Measurement of leak signals, accelerometers are placed at points P3 and P4 with the leak simulated in valve 2 (See Table 2, case P3P4-v2; Date 18/04/16) (a) and (b) Power Spectral Density (PSD) for the access point 3 and 4. (c) Modulus of cross-spectral density (CSD) for signals recorder from the access point 3-4; (d) Coherence; (e) Phase of the cross-spectral density (CSD) and (f) Cross-correlation Coefficient (CCC) evaluated over the bandwidth selected. (Values in dB ref. V^2).

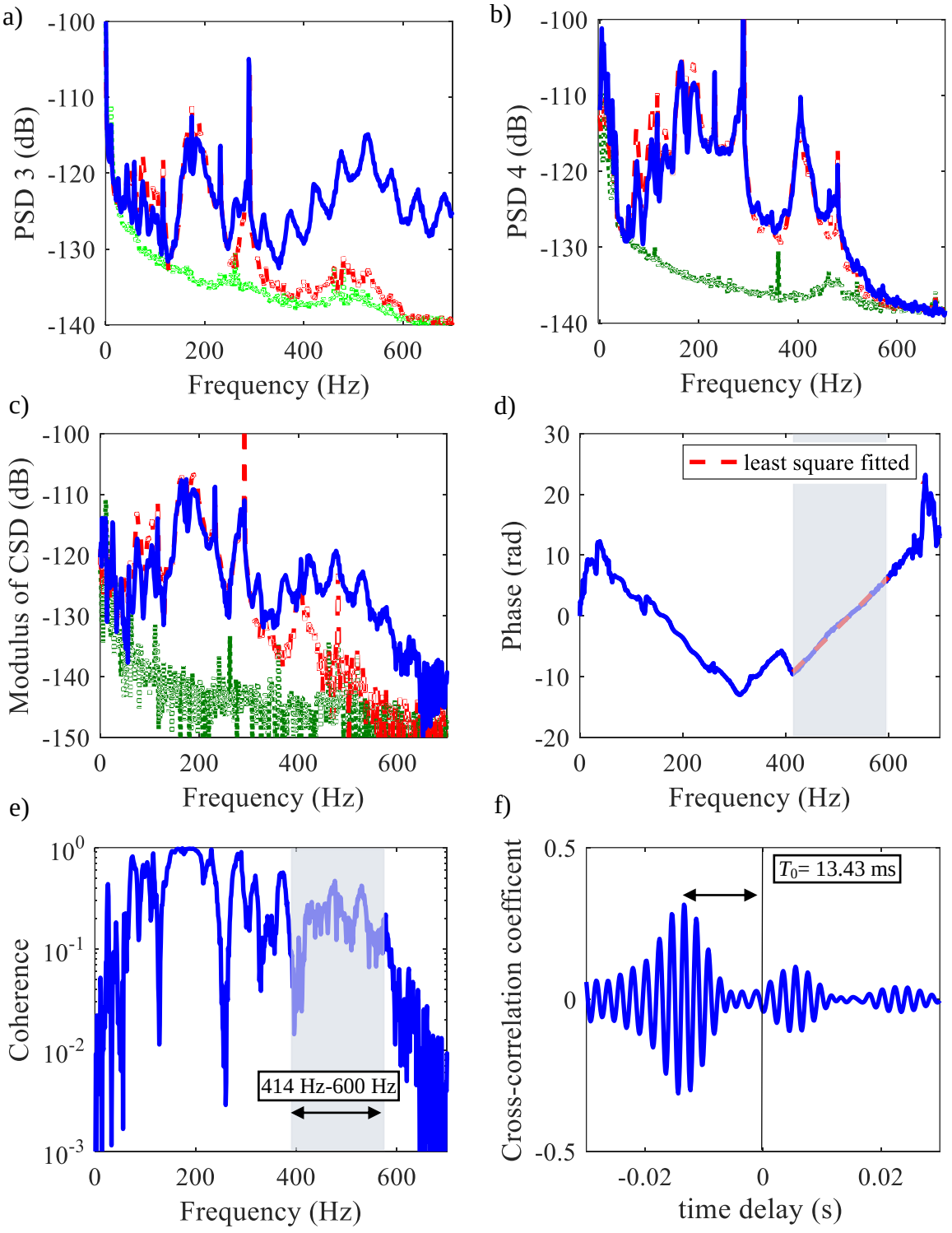

Figure 53 - Measurement of leak signals, accelerometers are placed at points P3 and P4 with the leak simulated in valve 3 (See Table 2, case P3P4-v3; Date 18/04/16) (a) and (b) Power Spectral Density (PSD) for the access point 3 and 4. (c) Modulus of cross-spectral density (CSD) for signals recorder from the access point 3-4; (d) Coherence; (e) Phase of the cross-spectral density (CSD) and (f) Cross-correlation Coefficient (CCC) evaluated over the bandwidth selected. (Values in dB ref. V^2).

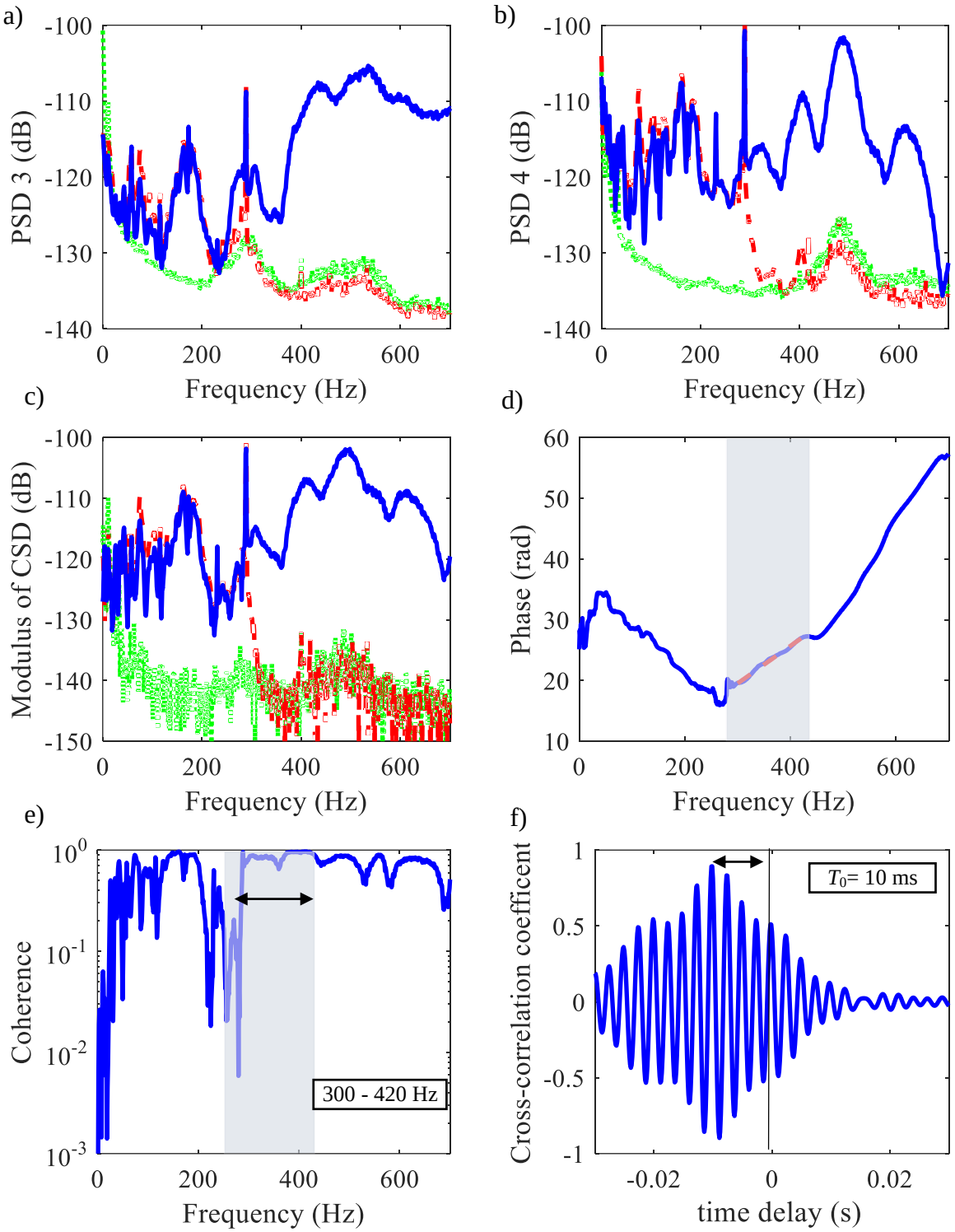

Figure 54 - Measurement of leak signals, accelerometers are placed at points P3 and P4 with the leak simulated in valve 4 (See Table 2, case P3P4-v4; Date 18/04/16) (a) and (b) Power Spectral Density (PSD) for the access point 3 and 4. (c) Modulus of cross-spectral density (CSD) for signals recorder from the access point 3-4; (d) Coherence; (e) Phase of the cross-spectral density (CSD) and (f) Cross-correlation Coefficient (CCC) evaluated over the bandwidth selected. (Values in dB ref. V^2).

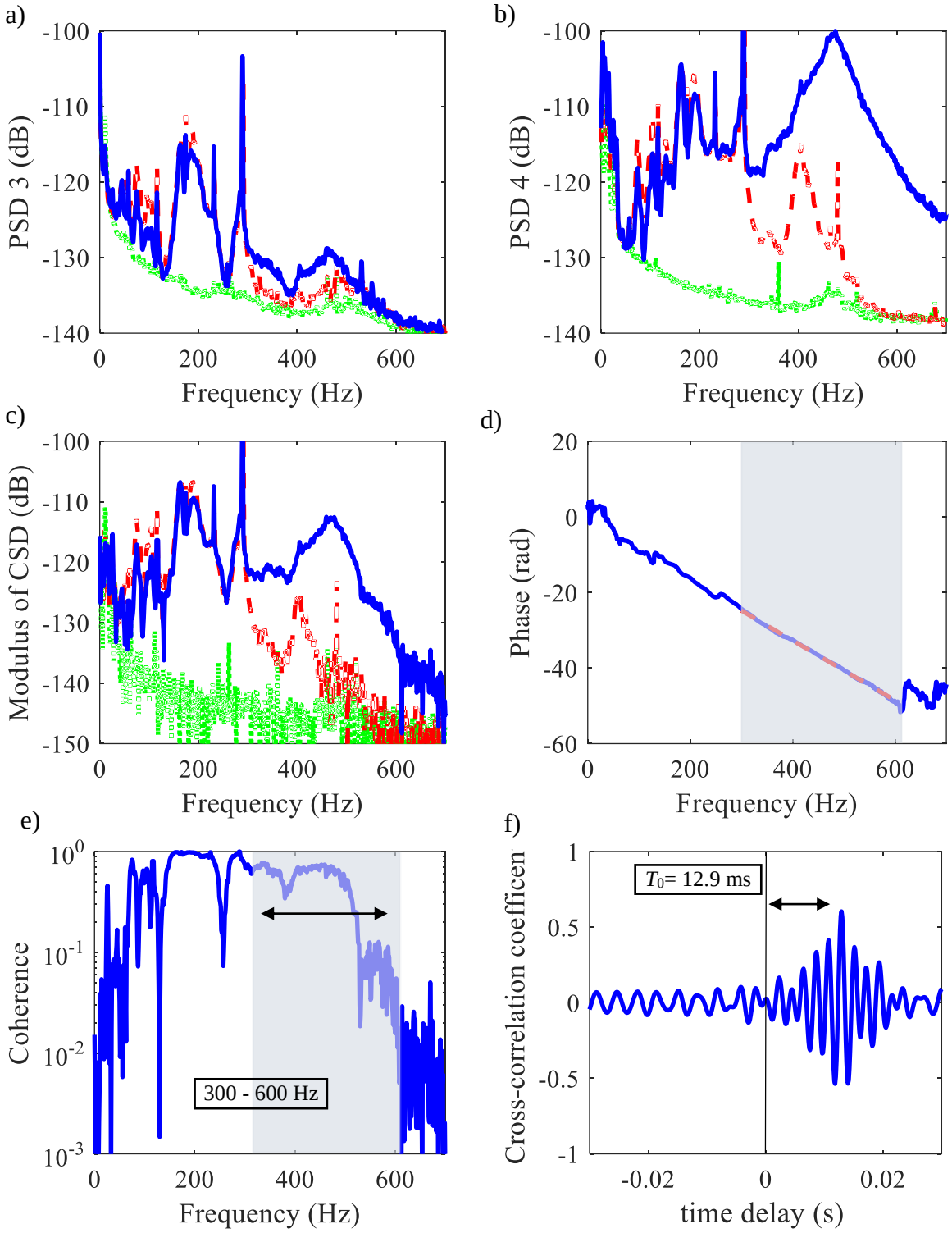

Figure 55 - Measurement of leak signals, accelerometers are placed at points P5 and P6 with the leak simulated in valve 4 (See Table 2, case P5P6-v4; Date 18/04/16) (a) and (b) Power Spectral Density (PSD) for the access point 5 and 6. (c) Modulus of cross-spectral density (CSD) for signals recorder from the access point 5-6; (d) Coherence; (e) Phase of the cross-spectral density (CSD) and (f) Cross-correlation Coefficient (CCC) evaluated over the bandwidth selected. (Values in dB ref. V^2).

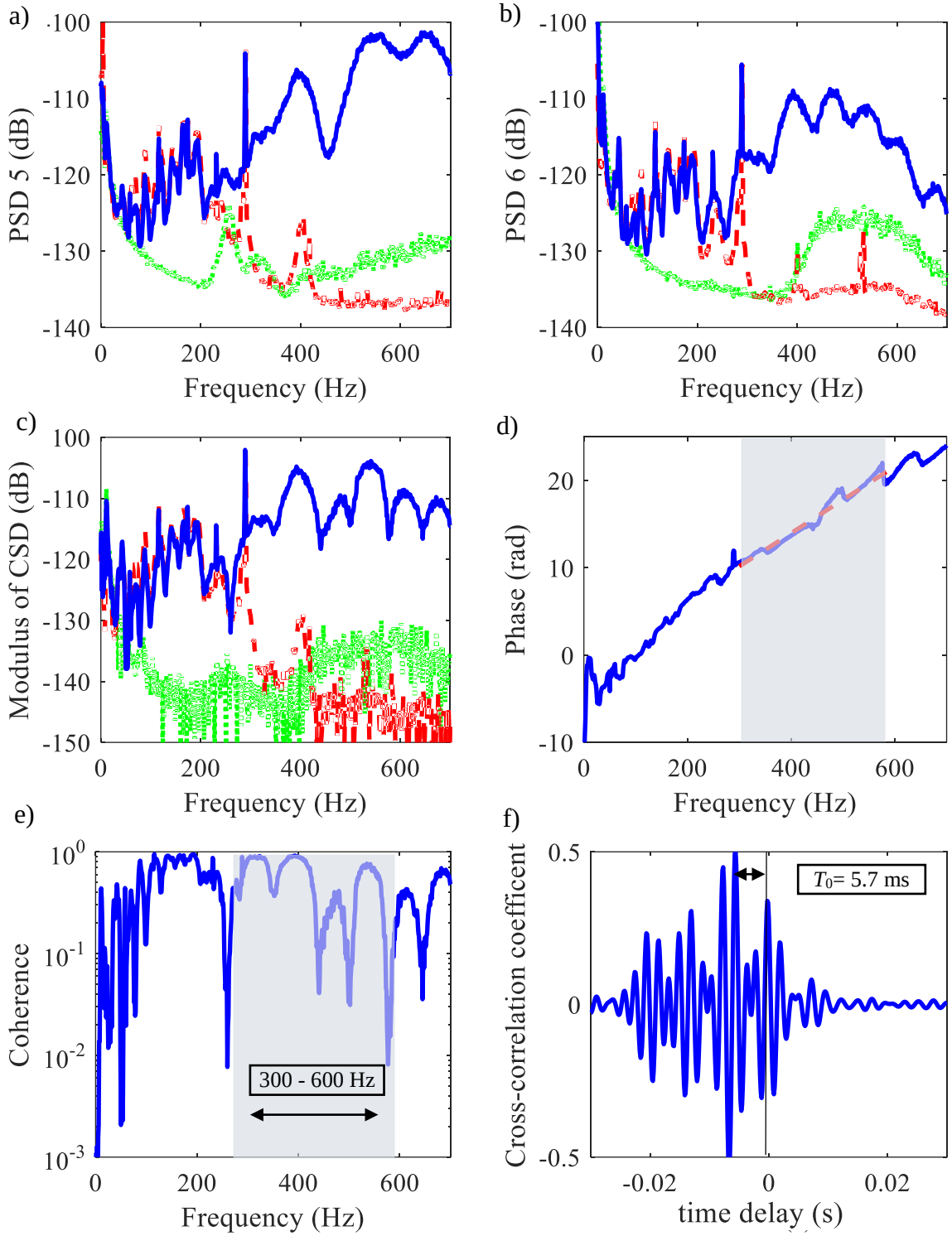

Figure 56 - Measurement of leak signals, accelerometers are placed at points P1 and P2 with the leak simulated in valve 1 (See Table 2, case P1P2-v1; Date 17/03/17) (a) and (b) Power Spectral Density (PSD) for the access point 1 and 2. (c) Modulus of cross-spectral density (CSD) for signals recorder from the access point 1-2; (d) Coherence; (e) Phase of the cross-spectral density (CSD) and (f) Cross-correlation Coefficient (CCC) evaluated over the bandwidth selected. (Values in dB ref. V^2).

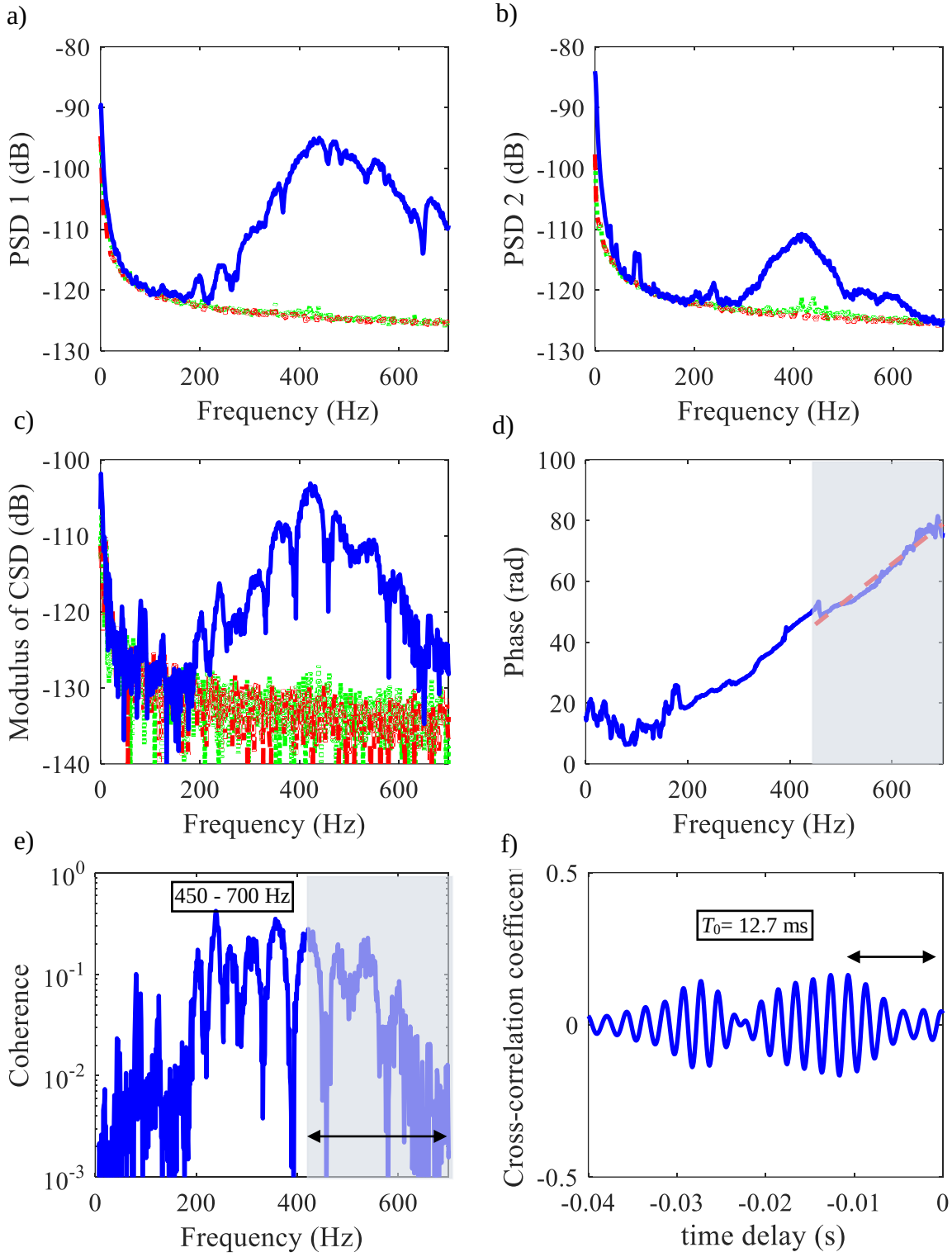

Figure 57 - Measurement of leak signals, accelerometers are placed at points P1 and P2 with the leak simulated in valve 2 (See Table 2, case P1P2-v2; Date 17/03/17) (a) and (b) Power Spectral Density (PSD) for the access point 1 and 2. (c) Modulus of cross-spectral density (CSD) for signals recorder from the access point 1-2; (d) Coherence; (e) Phase of the cross-spectral density (CSD) and (f) Cross-correlation Coefficient (CCC) evaluated over the bandwidth selected. (Values in dB ref. V^2).

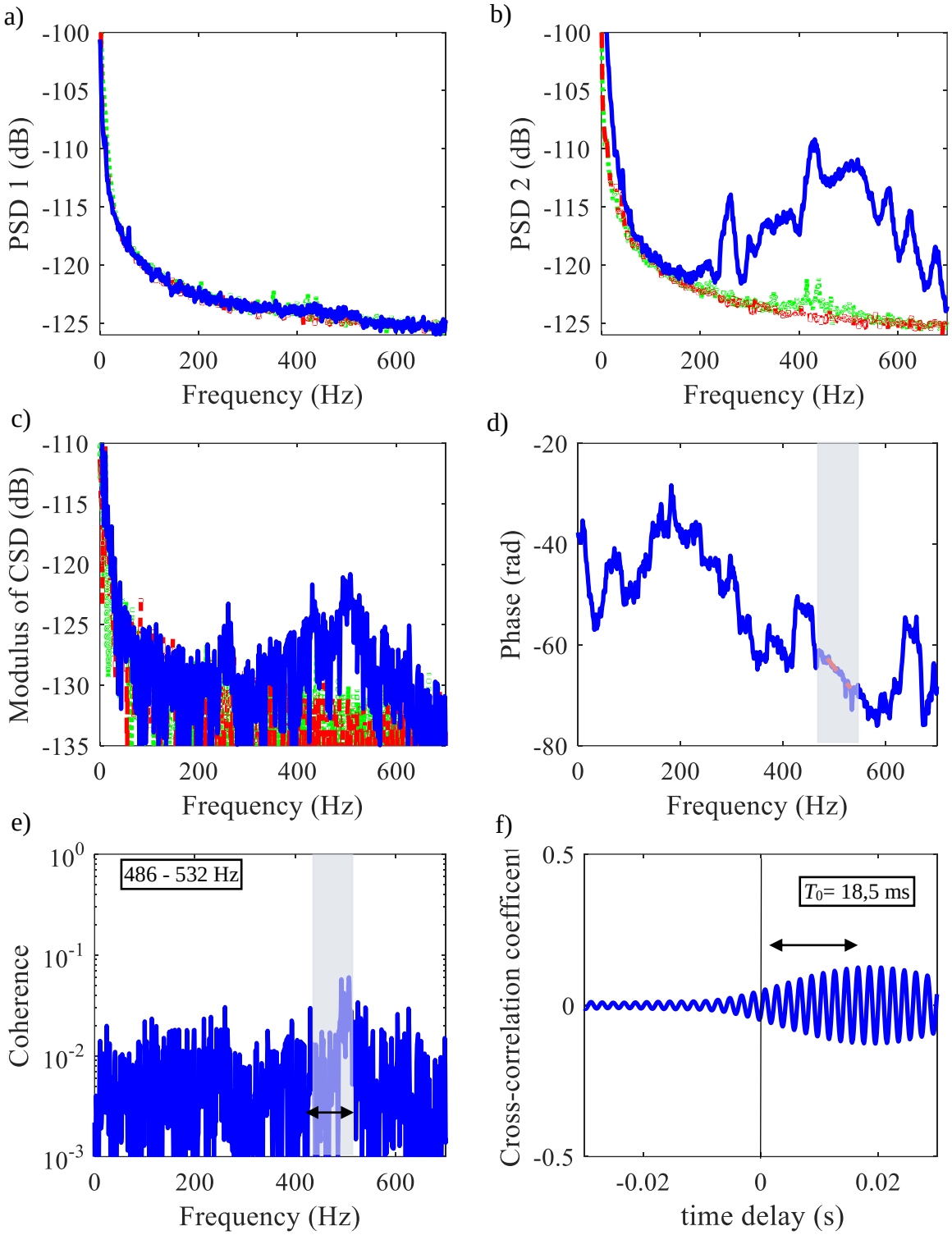

Figure 58 - Measurement of leak signals, accelerometers are placed at points P3 and P4 with the leak simulated in valve 3 (See Table 2, case P3P4-v3; Date 17/03/17) (a) and (b) Power Spectral Density (PSD) for the access point 3 and 4. (c) Modulus of cross-spectral density (CSD) for signals recorder from the access point 3-4; (d) Coherence; (e) Phase of the cross-spectral density (CSD) and (f) Cross-correlation Coefficient (CCC) evaluated over the bandwidth selected. (Values in dB ref. V^2).

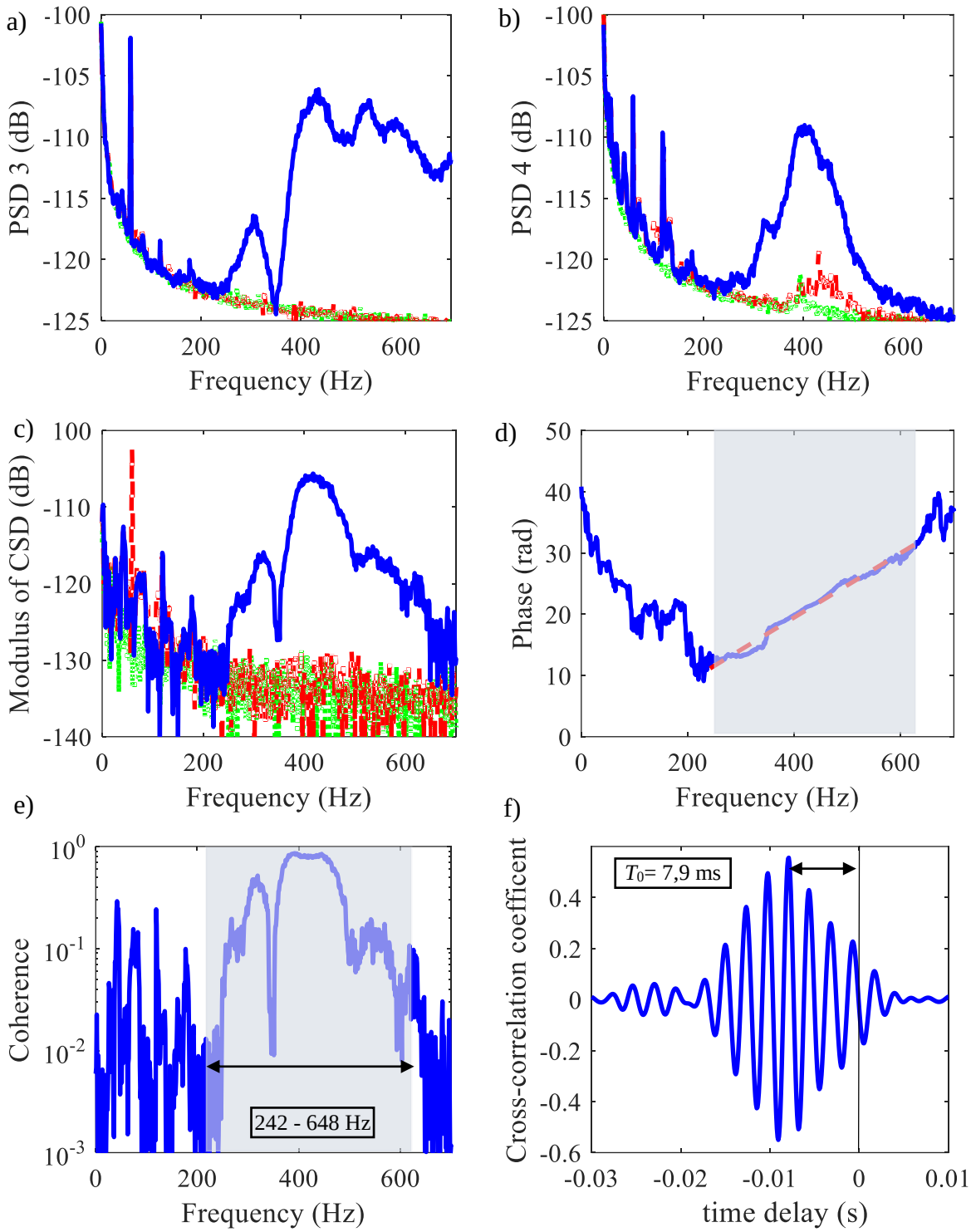

Figure 59 - Measurement of leak signals, accelerometers are placed at points P3 and P4 with the leak simulated in valve 4 (See Table 2, case P3P4-v4; Date 17/03/17) (a) and (b) Power Spectral Density (PSD) for the access point 3 and 4. (c) Modulus of cross-spectral density (CSD) for signals recorder from the access point 3-4; (d) Coherence; (e) Phase of the cross-spectral density (CSD) and (f) Cross-correlation Coefficient (CCC) evaluated over the bandwidth selected. (Values in dB ref. V^2).

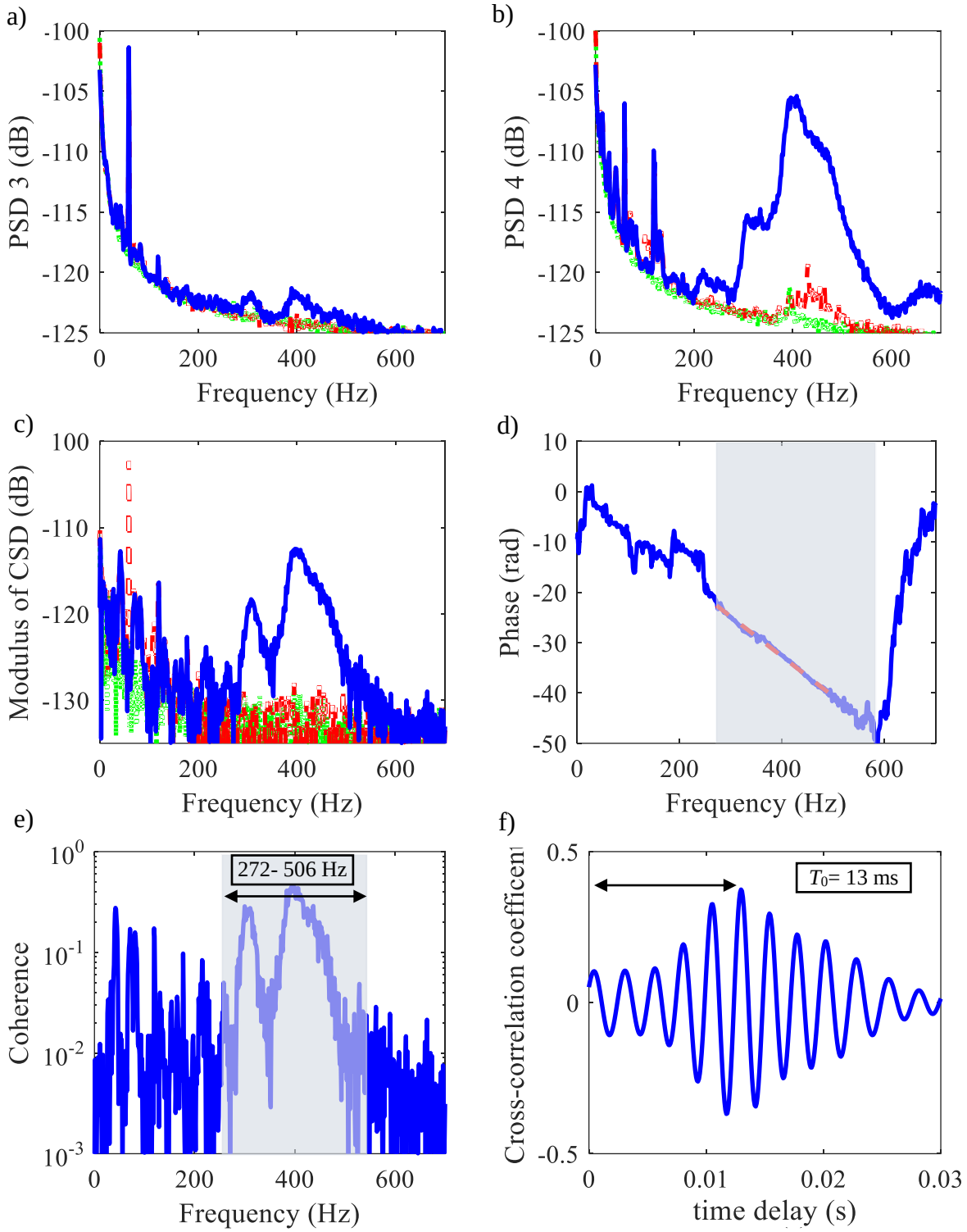

Figure 60 - Measurement of leak signals, accelerometers are placed at points P5 and P6 with the leak simulated in valve 4 (See Table 2, case P5P6-v4; Date 17/03/17) (a) and (b) Power Spectral Density (PSD) for the access point 5 and 6. (c) Modulus of cross-spectral density (CSD) for signals recorder from the access point 5-6; (d) Coherence; (e) Phase of the cross-spectral density (CSD) and (f) Cross-correlation Coefficient (CCC) evaluated over the bandwidth selected. (Values in dB ref. V^2)

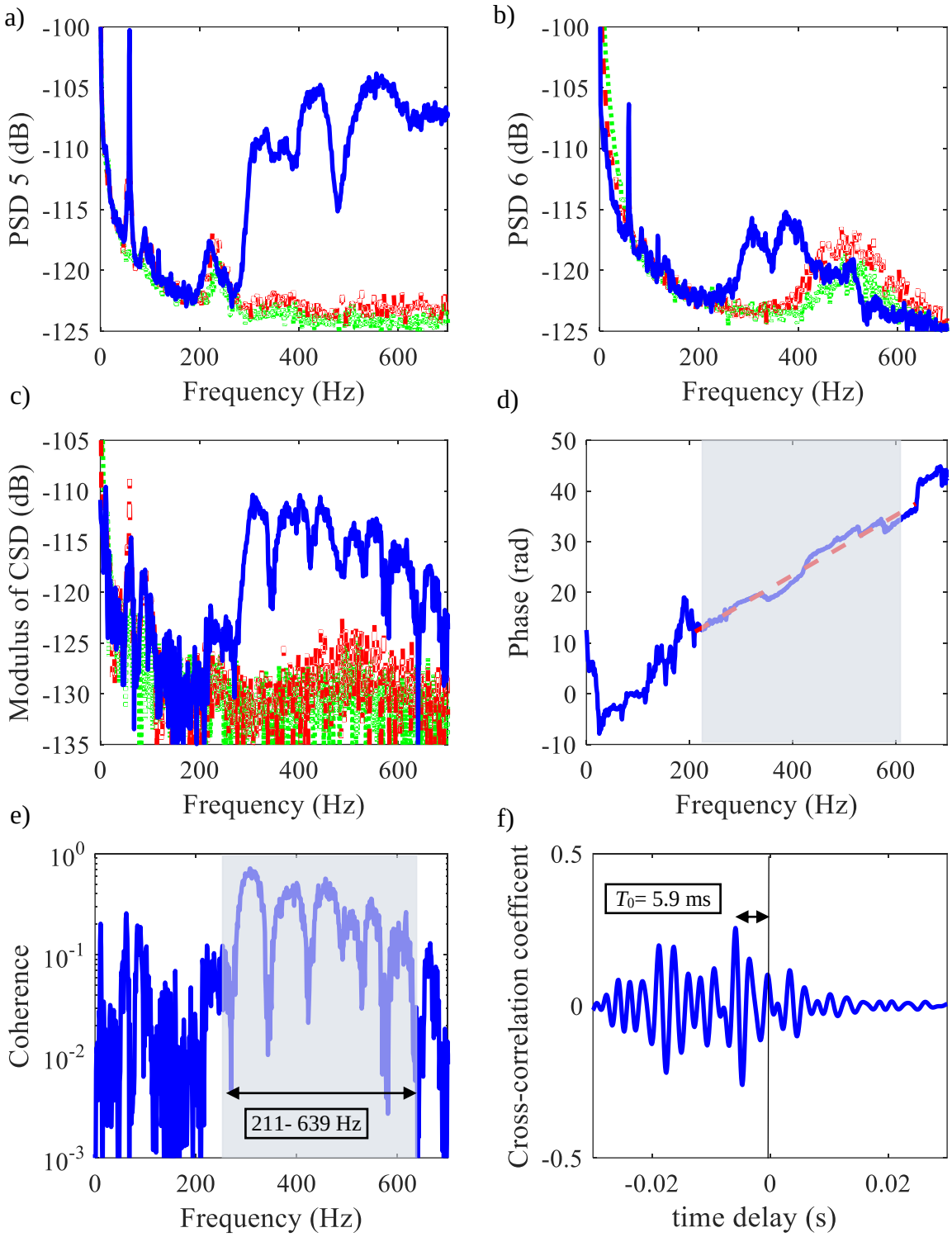

Figure 61 - Measurement of leak signals, accelerometers are placed at points P5 and P6 with the leak simulated in valve 5 (See Table 2, case P5P6-v5; Date 17/03/17) (a) and (b) Power Spectral Density (PSD) for the access point 5 and 6. (c) Modulus of cross-spectral density (CSD) for signals recorder from the access point 5-6; (d) Coherence; (e) Phase of the cross-spectral density (CSD) and (f) Cross-correlation Coefficient (CCC) evaluated over the bandwidth selected. (Values in dB ref. V^2)

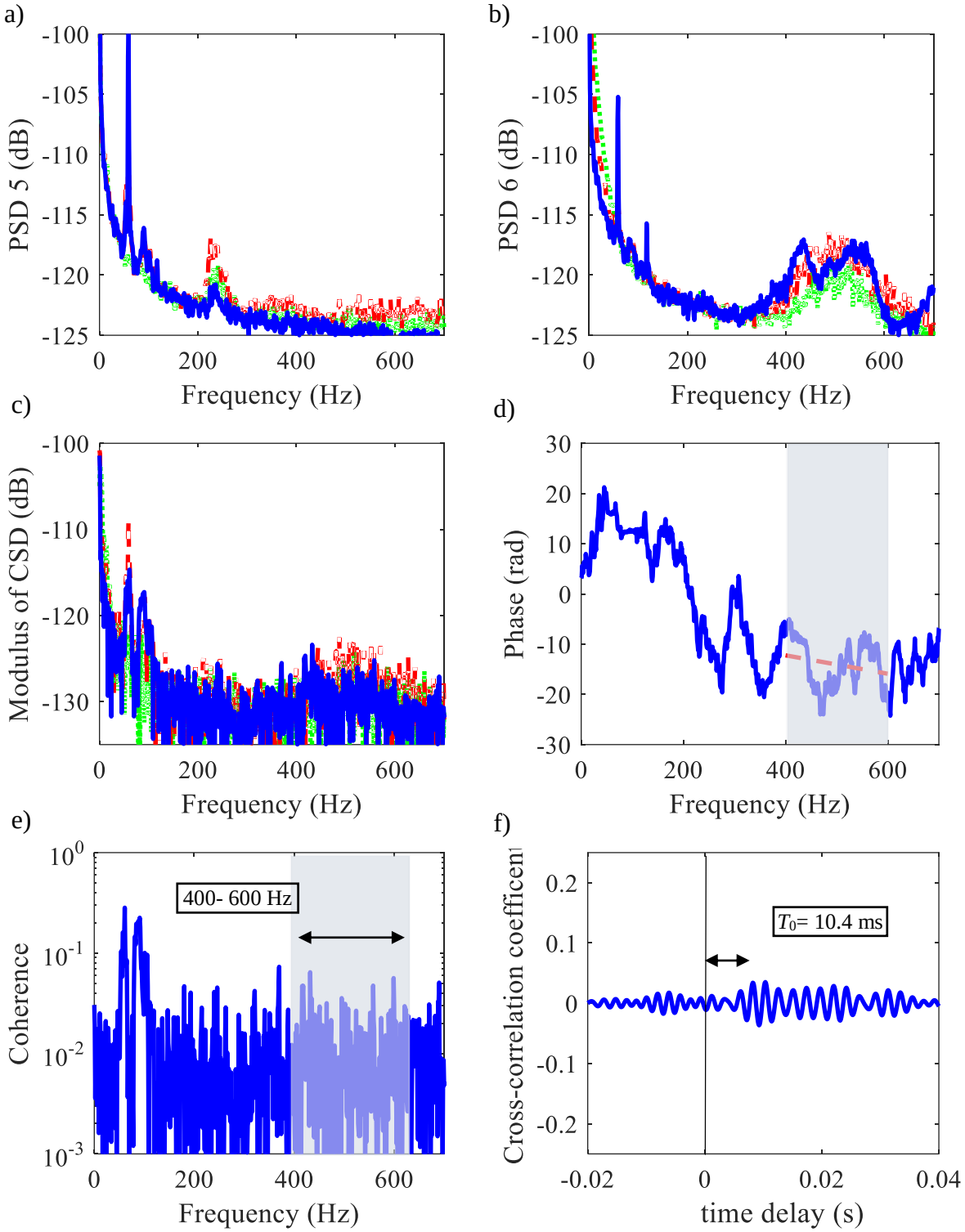

Figure 62 - Measurement of leak signals, accelerometers are placed at points P1 and P2 with the leak simulated in valve 1 (See Table 2, case P1P2-v1; Date 28/06/17) (a) and (b) Power Spectral Density (PSD) for the access point 5 and 6. (c) Modulus of cross-spectral density (CSD) for signals recorder from the access point 1-2; (d) Coherence; (e) Phase of the cross-spectral density (CSD) and (f) Cross-correlation Coefficient (CCC) evaluated over the bandwidth selected. (Values in dB ref. V^2).

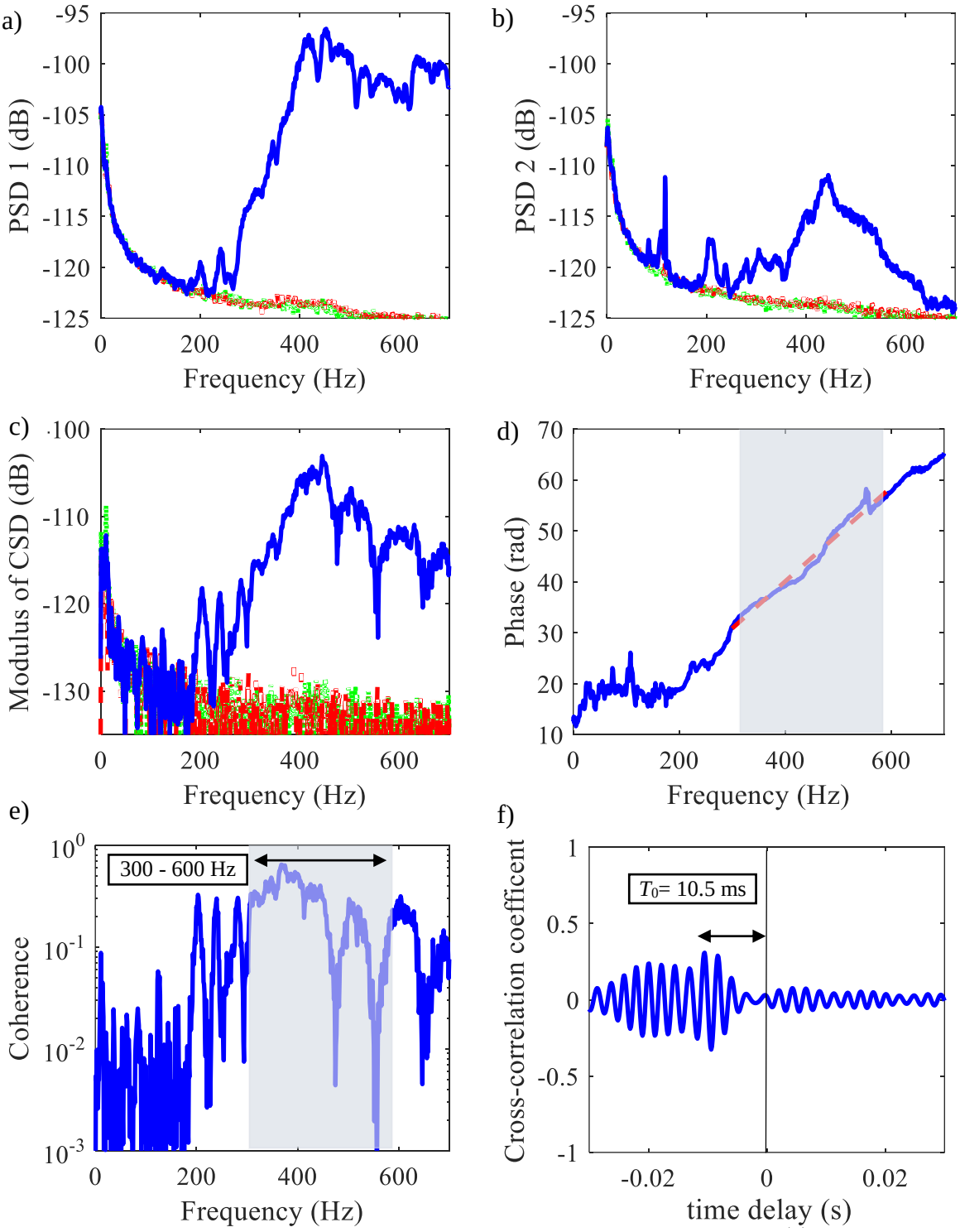

Figure 63 - Measurement of leak signals, accelerometers are placed at points P1 and P2 with the leak simulated in valve 2 (See Table 2, case P1P2-v2; Date 28/06/17) (a) and (b) Power Spectral Density (PSD) for the access point 1 and 2. (c) Modulus of cross-spectral density (CSD) for signals recorder from the access point 1-2; (d) Coherence; (e) Phase of the cross-spectral density (CSD) and (f) Cross-correlation Coefficient (CCC) evaluated over the bandwidth selected. (Values in dB ref. V^2).

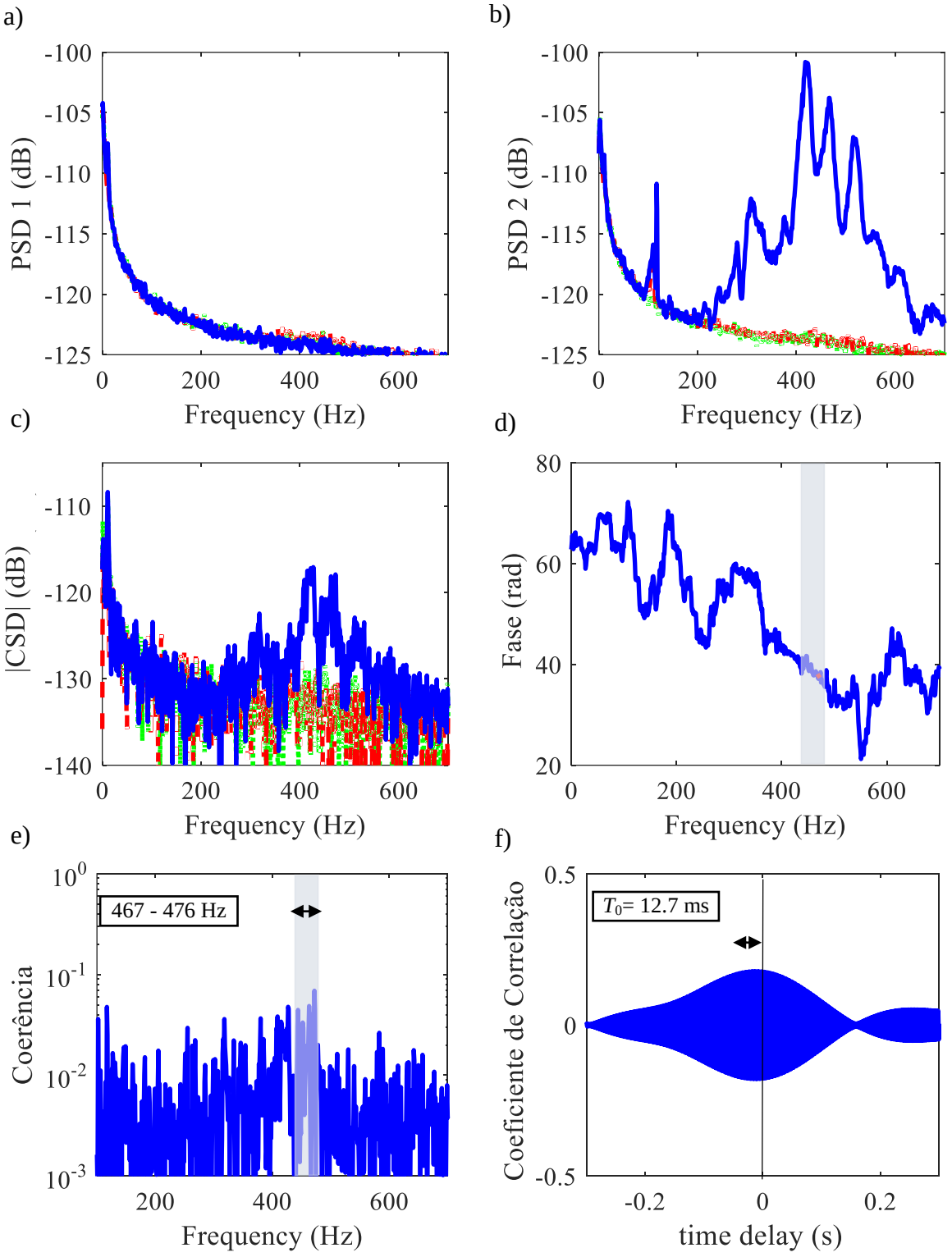

Figure 64 - Measurement of leak signals, accelerometers are placed at points P3 and P4 with the leak simulated in valve 2 (See Table 2, case P3P4-v2; Date 28/06/17) (a) and (b) Power Spectral Density (PSD) for the access point 3 and 4. (c) Modulus of cross-spectral density (CSD) for signals recorder from the access point 3-4; (d) Coherence; (e) Phase of the cross-spectral density (CSD) and (f) Cross-correlation Coefficient (CCC) evaluated over the bandwidth selected. (Values in dB ref. V^2).

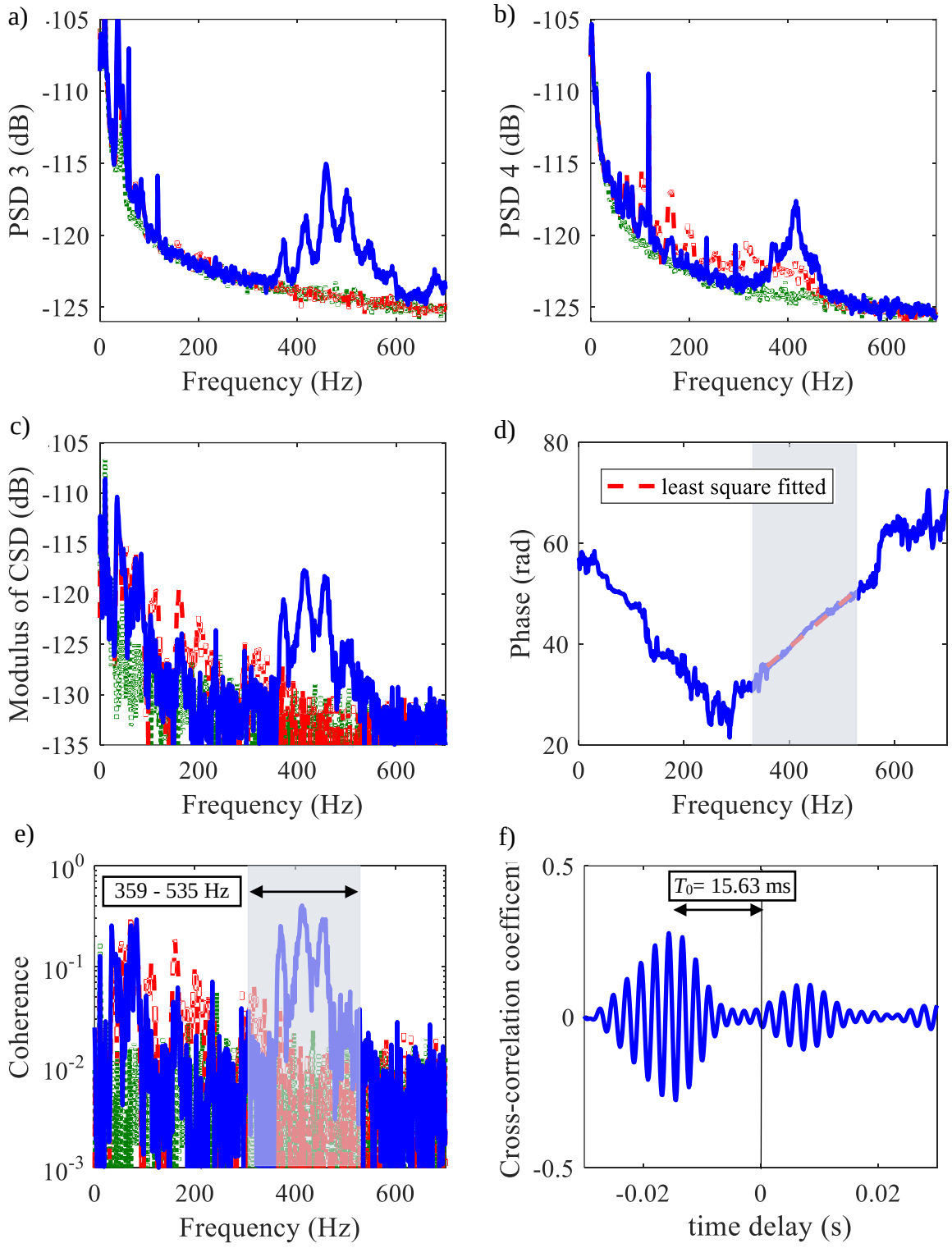

Figure 65 - Measurement of leak signals, accelerometers are placed at points P3 and P4 with the leak simulated in valve 3 (See Table 2, case P3P4-v3; Date 28/06/17) (a) and (b) Power Spectral Density (PSD) for the access point 3 and 4. (c) Modulus of cross-spectral density (CSD) for signals recorder from the access point 3-4; (d) Coherence; (e) Phase of the cross-spectral density (CSD) and (f) Cross-correlation Coefficient (CCC) evaluated over the bandwidth selected. (Values in dB ref. V^2).

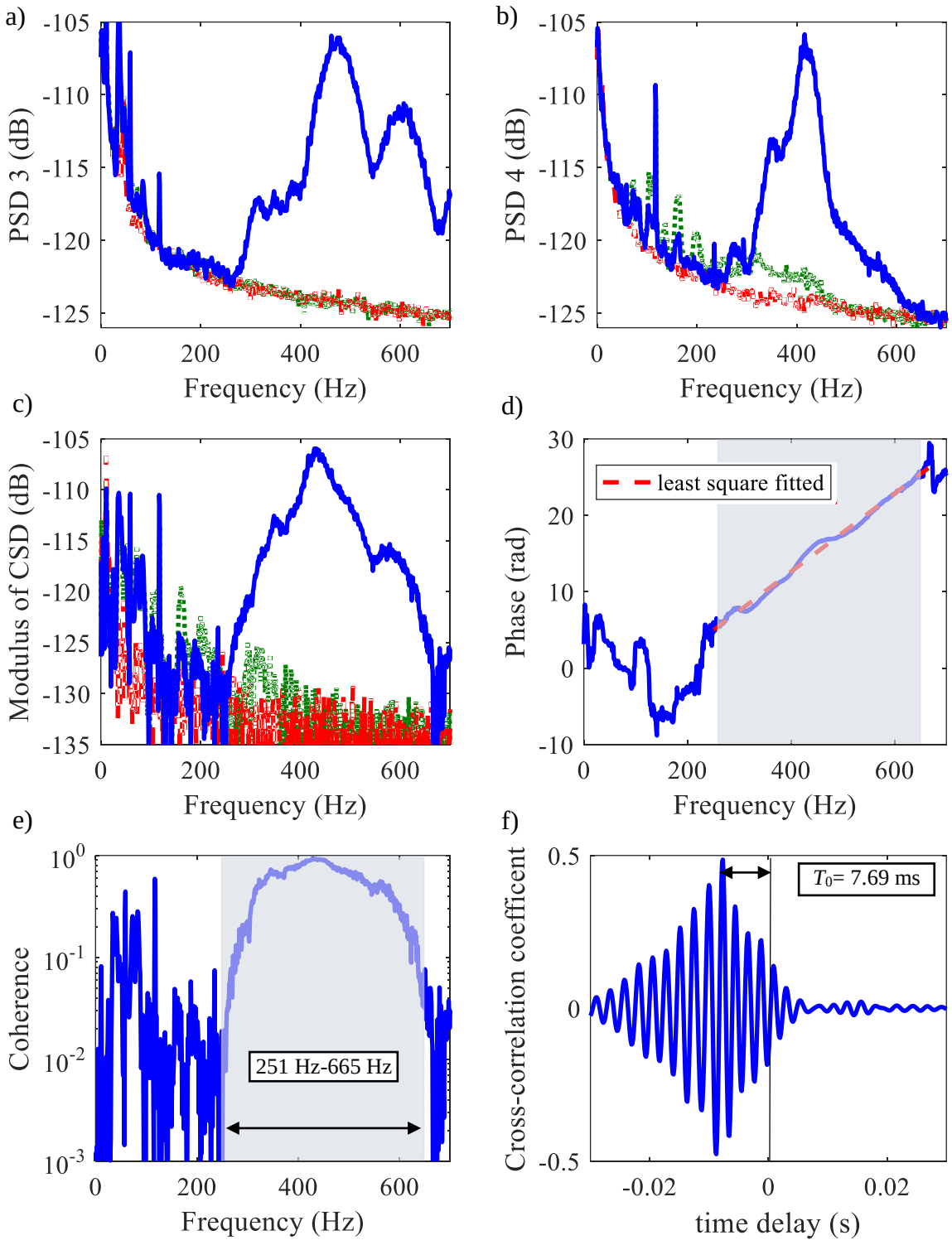

Figure 66 - Measurement of leak signals, accelerometers are placed at points P3 and P4 with the leak simulated in valve 4 (See Table 2, case P3P4-v4; Date 28/06/17) (a) and (b) Power Spectral Density (PSD) for the access point 3 and 4. (c) Modulus of cross-spectral density (CSD) for signals recorder from the access point 3-4; (d) Coherence; (e) Phase of the cross-spectral density (CSD) and (f) Cross-correlation Coefficient (CCC) evaluated over the bandwidth selected. (Values in dB ref. V^2).

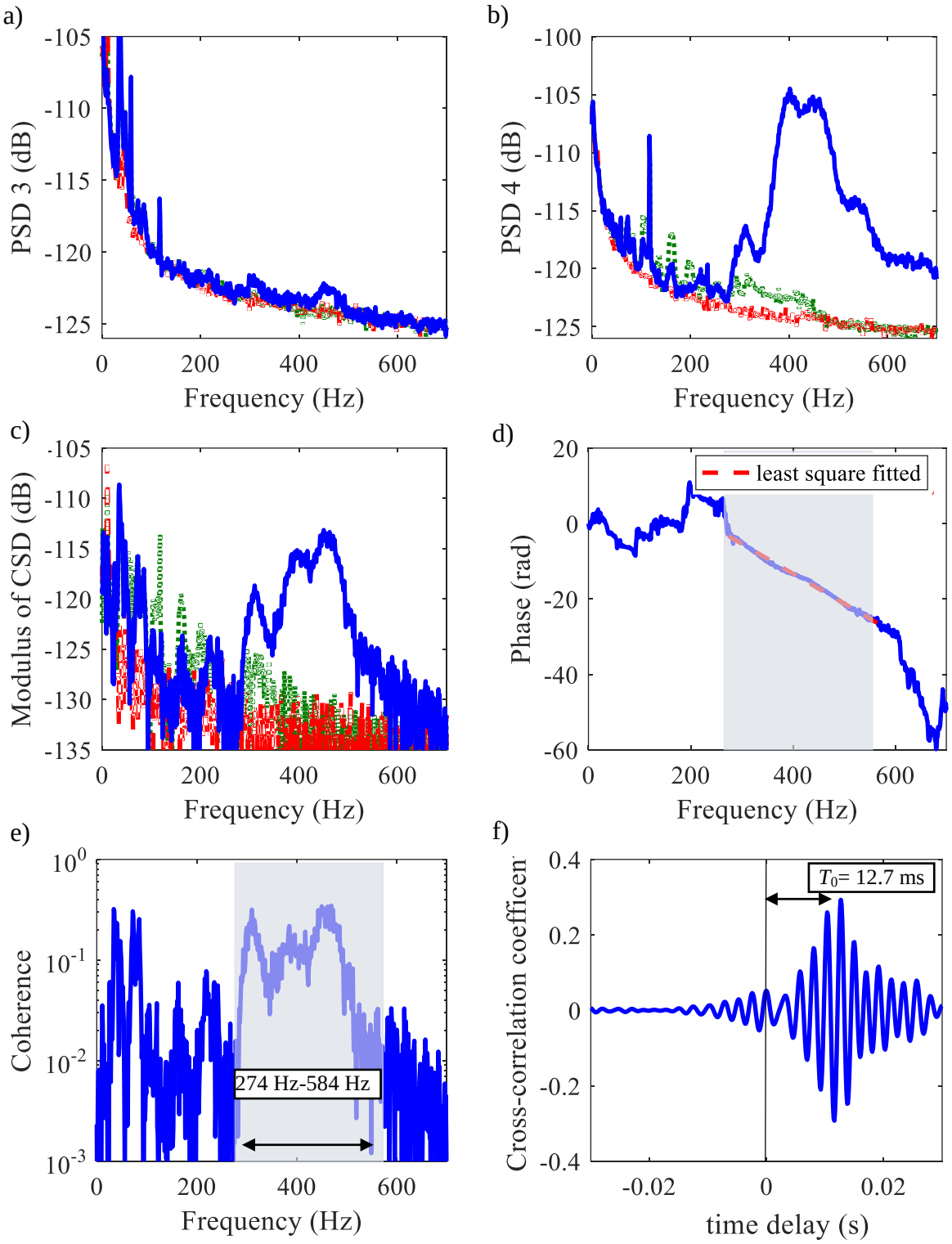

Figure 67 - Measurement of leak signals, accelerometers are placed at points P5 and P6 with the leak simulated in valve 4 (See Table 2, case P5P6-v4; Date 28/06/17) (a) and (b) Power Spectral Density (PSD) for the access point 5 and 6. (c) Modulus of cross-spectral density (CSD) for signals recorder from the access point 5-6; (d) Coherence; (e) Phase of the cross-spectral density (CSD) and (f) Cross-correlation Coefficient (CCC) evaluated over the bandwidth selected. (Values in dB ref. V^2).

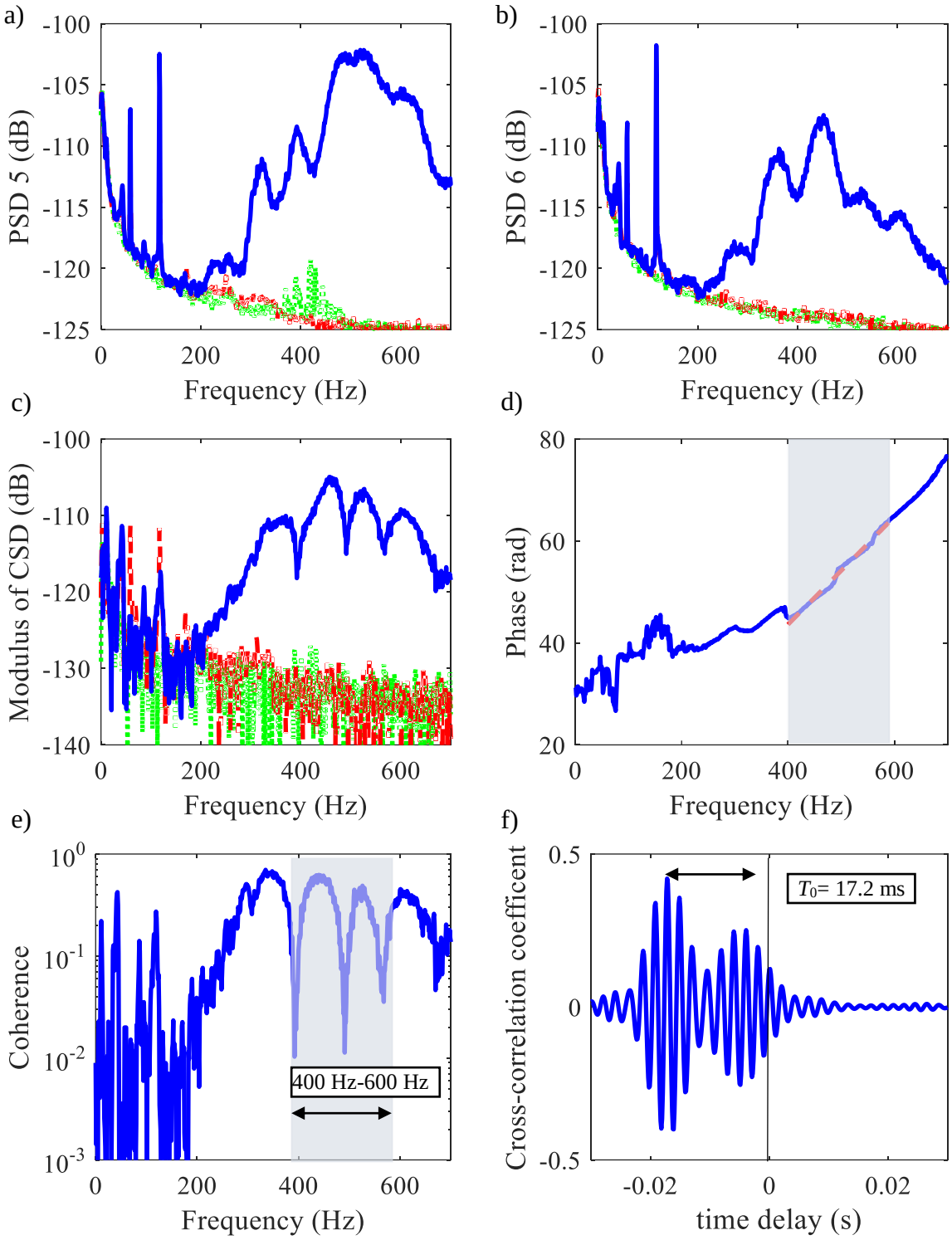

Figure 68 - Measurement of leak signals, accelerometers are placed at points P5 and P6 with the leak simulated in valve 3 (See Table 2, case P5P6-v3; Date 28/06/17) (a) and (b) Power Spectral Density (PSD) for the access point 5 and 6. (c) Modulus of cross-spectral density (CSD) for signals recorder from the access point 5-6; (d) Coherence; (e) Phase of the cross-spectral density (CSD) and (f) Cross-correlation Coefficient (CCC) evaluated over the bandwidth selected. (Values in dB ref. V^2).

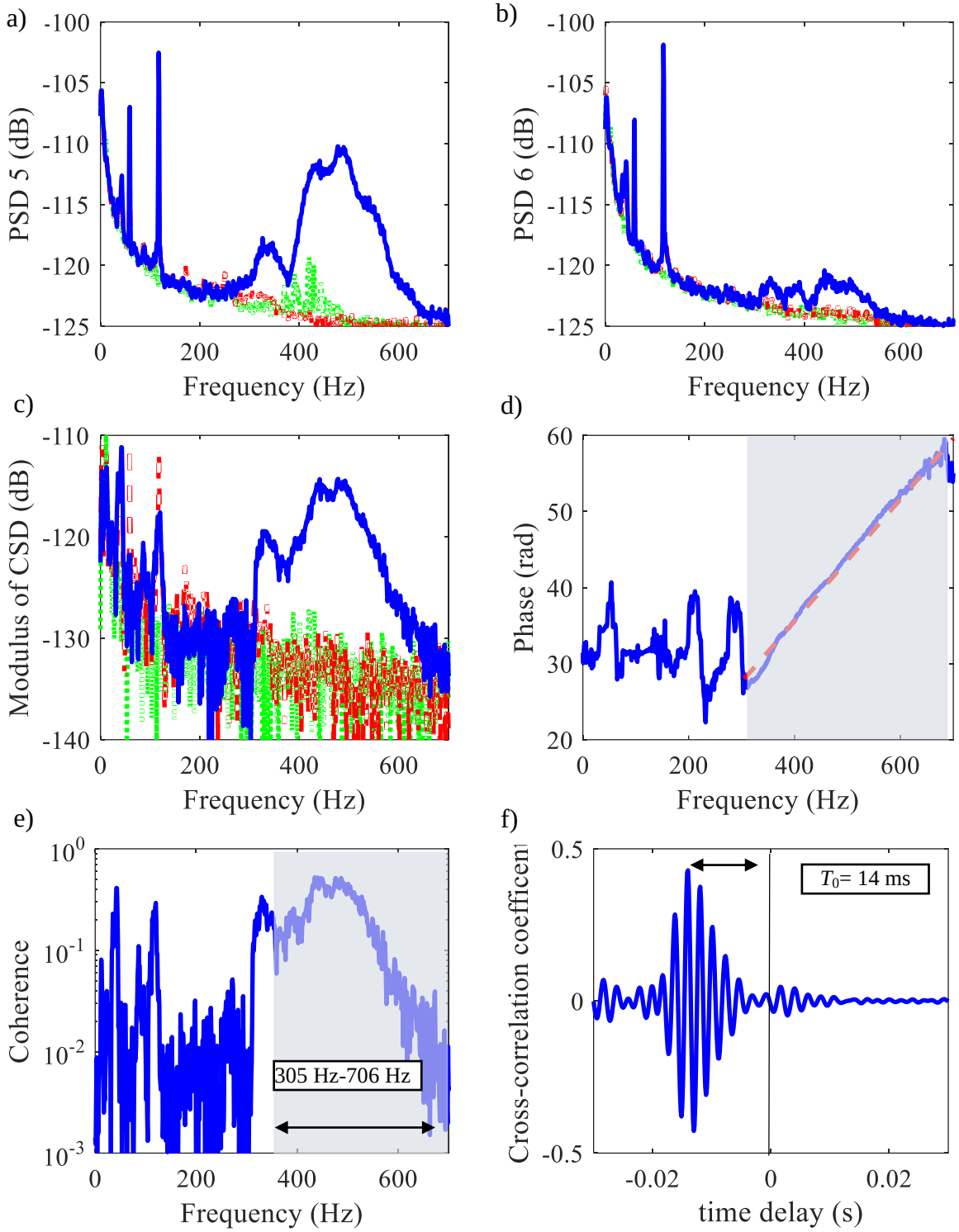

Figure 69 - Measurement of leak signals, accelerometers are placed at points P5 and P6 with the leak simulated in valve 5 (See Table 2, case P5P6-v5; Date 28/06/17) (a) and (b) Power Spectral Density (PSD) for the access point 5 and 6. (c) Modulus of cross-spectral density (CSD) for signals recorder from the access point 5-6; (d) Coherence; (e) Phase of the cross-spectral density (CSD) and (f) Cross-correlation Coefficient (CCC) evaluated over the bandwidth selected. (Values in dB ref. V^2).

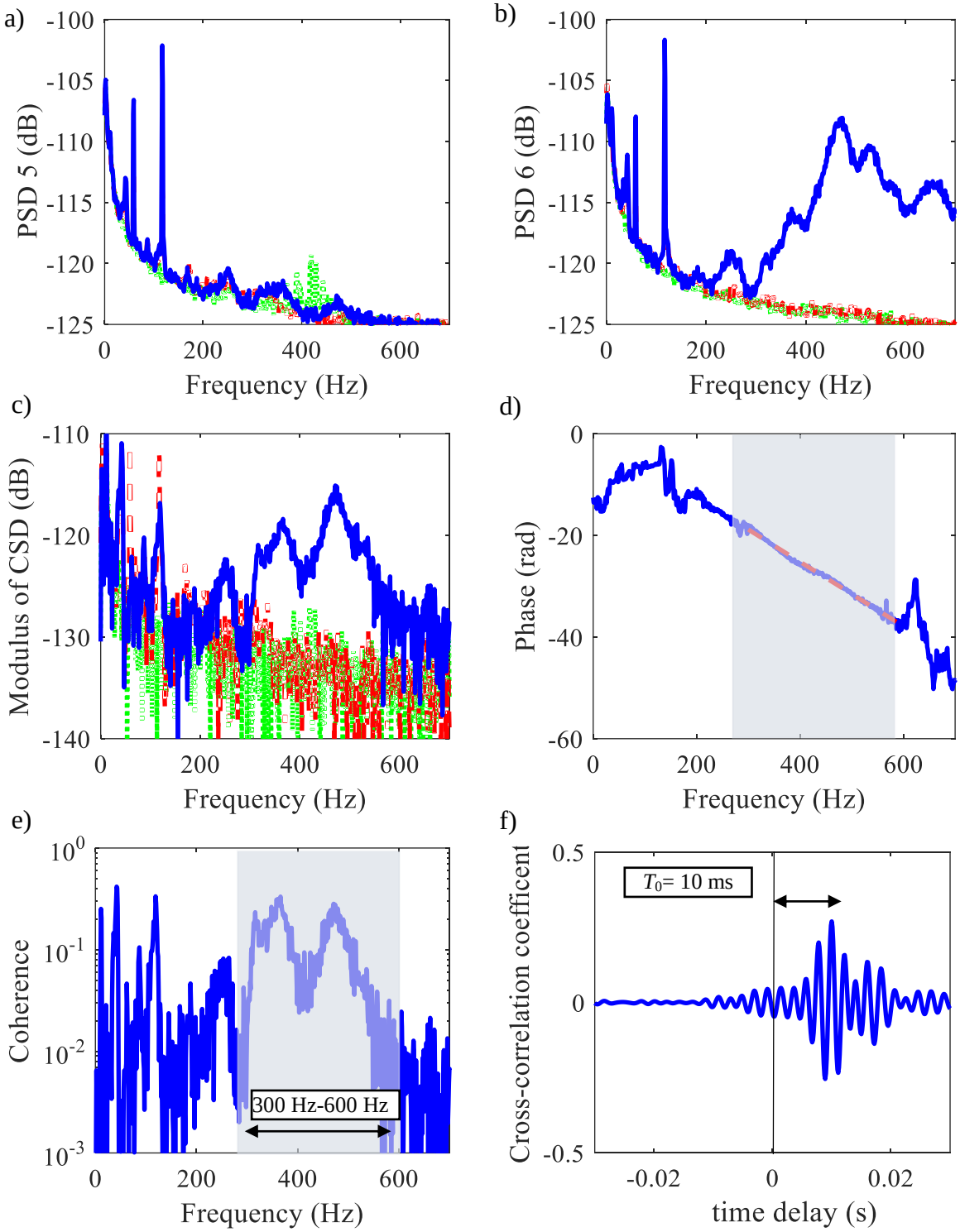

APPENDIX D - PRINCIPAL CODE OF THE CORRELATION PROGRAM

This Appendix shows the principal code of the correlator program developed in GUIDE (Graphical User Interface Development Environment) which is an application from Matlab®.

```
%%%%%%%%%%%%%%
%% PARAMETER MODULE
%%%%%%%%%%%%%%

%%Pipe dimensions

di = str2double(get(handles.diametro,'String'));          % internal diameter
h = str2double(get(handles.espessura,'String'));          % thickness
d = str2double(get(handles.distancia,'String'));          % distance between access points

%% selection of the pipe material
a = get(handles.listamaterial,'value');
if a ==1
    modyoung = 2.4*10^9;%2
   setappdata(0,'modyoung',modyoung)              % Young modulus of PVC
elseif a ==2
    modyoung = 1.8*10^9;
   setappdata(0,'modyoung',modyoung)              % Young modulus of  Polypropylene
   elseif a ==3
    modyoung = 3.5*10^9;%1.2
   setappdata(0,'modyoung',modyoung)              % Young modulus of Polyethylene
   elseif a ==4
    modyoung = 180*10^9;
   setappdata(0,'modyoung',modyoung)              % Young modulus of Fe ductile
   elseif a ==5
    modyoung = 200*10^9;
   setappdata(0,'modyoung',modyoung)              % Young modulus of Ac. Galvanized
   elseif a ==6
    modyoung = 190*10^9;
   setappdata(0,'modyoung',modyoung)              % Young modulus of Ac. stainless
   elseif a ==7
    modyoung = 69*10^9;
   setappdata(0,'modyoung',modyoung)              % Young modulus of Aluminium
   elseif a ==8
    modyoung = 105*10^9;
   setappdata(0,'modyoung',modyoung)              % Young modulus of Brass
   elseif a ==9
    modyoung = 110*10^9;
   setappdata(0,'modyoung',modyoung)              % Young modulus of Cu
end
b = get(handles.listasolo,'value');
if b ==1
```

```
    modcis = 1*10^7;%2                                  % shear modulus of sand

   setappdata(0,'modcis',modcis)
elseif b ==2
    modcis = .8*10^8;%2.41                              % shear modulus of clay

   setappdata(0,'modcis',modcis)
end

G=modcis;                                               % Shear modulus
E=modyoung;                                             % Young modulus
rt = di/2;                                              % pipe radius
aa = (rt)-(h/2);                                        % diameter medius
cw = 1500;                                              % wavespeed of the sound in the
water ter
Bw = 2.25*10^9;                                         % bulk modulus of water
aux1 = (E*h)/(2*Bw*aa);
aux2 = G/Bw;
c = cw*(1/(1+(1/(aux1+aux2))))^0.5
c= round(c)                                             % Wavespeed

%%%%%%%%%%%%%%%%
%% CALCULATION MODULE
%%%%%%%%%%%%%%%%

fs=handles.sampling_frequency;                          % Sampling frequency
s1 = handles.data_orig(:,1);                            % Leak signal data position 1
s2 = handles.data_orig(:,2);                            % Leak signal data position 2
s1 = s1-mean(s1);
s2 = s2-mean(s2);

%% Coherence, CSD, PSD and Phase settings
n = 0.5;
np = 1;
nfft = fix(np*fs);
over_lap = fix(nfft*n);
[Ss1s1] = cpsd(s1,s1,hanning(nfft),over_lap,nfft,fs,'twosided');          %  PSD1
[Ss2s2] = cpsd(s2,s2,hanning(nfft),over_lap,nfft,fs,'twosided');          %  PSD2
[Ss1s2_2,Fc] = cpsd(s1,s2,hanning(nfft),over_lap,nfft,fs,'onesided');     %  CPSD
[Ss1s2_t, Fc_t] = cpsd(s1,s2,hanning(nfft),over_lap,nfft,fs,'twosided');  %
Cs1s2_2 = mscohere(s1,s2,hanning(nfft),over_lap,nfft,fs);                 %  Coherence
ks1s2 = unwrap(angle(Ss1s2_2));                                           %  Phase
df = Fc(2);


%% selecting automatic bandwidth with the limit of coherence 10^-3
    ffreq=10;
    ff=round(((ffreq)/df)+1);
    lim = 10^-3;
    [~,sp] = max(Cs1s2_2(ff:round((fs/2)/df)));
```

```
    for high1 = sp:1:length(Cs1s2_2)
        if Cs1s2_2(high1) < lim
            break
        end
    end
    for low1 = sp:-1:1
        if Cs1s2_2(low1) < lim
            break
        end
    end
    low1 = low1+1;
    high1 = high1-1;
    low_final1=Fc(low1);
    high_final1=Fc(high1);

%% Butter Filter
f1=low_final1;
f2=high_final1;
[B,A] = butter(4,[f1/(fs/2) f2/(fs/2) ],'bandpass');        % Butterworth filter
s1_f = filtfilt(B,A,s1);                                    % filter the signal 1
s2_f = filtfilt(B,A,s2);                                     % filter the signal 2
s1=s1_f;
s2=s2_f;
%% Correlação Cruzada
[Rxy,tau]=xcorr(s1,s2);                                     % cross correlation
[Rxx,tau]=xcorr(s1,s1);                                      % auto correlation
[Ryy,tau]=xcorr(s2,s2);                                      % auto correlation
a1 = max(Rxx);
a2 = max(Ryy);
CR = Rxy/sqrt(a1*a2);
tau = tau./fs;
valormax = max(CR);
posicao = find(CR==valormax);
Var01 = tau(posicao);
Tf = Var01

%% defining the new phase shift
%evaluation of the straight line coefficients
low_final = round(((f1)/df)+1);
high_final = round(((f2)/df)+1);
y = ks1s2(low_final:high_final); % phase CPSD
x = Fc(low_final:high_final); % freq
W = abs(Ss1s2_2(low_final:high_final)); % CPSD
c11 = sum(W);
c12=sum(W.*x);
c21=c12;
c22=sum(W.*x.*x);
b1=sum(W.*y);
b2=sum(W.*x.*y);
C=[c11 c12; c21 c22];
```

```
b=[b1 b2]';
a=C\b;
ks1s2_2 =-( ks1s2-(round(a(1)/(2*pi))*2*pi));
kk=ks1s2_2(low_final:high_final);
P=polyfit(ff,kk,1);
y4 = polyval(P,Fc(low_final:high_final));

%% Plotting Phase
axes(handles.csd_phase)
plot(Fc,ks1s2_2,'b',ff,y4,'r--','linewidth',2)

if 0> y4 (length(y4))*1.3
    aa= y4 (length(y4));
else
   aa=0;
end
if y4 (length(y4))*1.3>0
   bb=ks1s2_2(high1);
else
   bb=0;
end
xlim([0 Fc(high1)*1.3])
ylim([aa*1.3 bb*1.3])
xlabel('Frequência (Hz)')
ylabel('Fase (rad)')
set(gca,'fontsize',14,'Fontname','MS Sans Serif');

%% Plotting Cross-Correlation
axes(handles.correlation_coefficent)
cla
% scaling cross-correlation coefficient
xx=((d-(c*tau))/2);
% obs
if dm1<=0
   xx=((d-(c*tau))/2)-dm1-var;
else
end
plot(xx,CR/max(CR),'b','linewidth',2)
ylabel('Função de correlação')
xlabel('distância (m)')
xlim([0 d])
ylim([0 1])
set(gca,'fontsize',14,'Fontname','Arial');
```

```
%%%%%%%%%%%
%% QUALITY INDEX
%%%%%%%%%%%

%% 1. bandwidth Index
dw = high_final1-low_final1;
wc = (high_final1+low_final1)/2;
shape=dw/wc;
alpha=shape/2;
m=sin(2*pi*alpha);
kbd_t=1-sin(2*pi*alpha)/(2*pi*alpha);          %%rescaling
 if kbd_t>=1
    kbd_t=1;
 end

%%%%%%%%%%%%%%%%%%%%%%%%%%%%%%%%%%%
%% 2. Coherence Index
Q = trapz(Fc(low_final:high_final),Cs1s2_2(low_final:high_final));
Q1= (Fc(high_final)-Fc(low_final));
p_area=Q1\Q;
kco=p_area

%%%%%%%%%%%%%%%%%%%%%%%%%%%%%%%%%%%
%% 3. phase
Rr=ks1s2(low_final:high_final); %phase bandwidth
Ra=y4; %from polyfit
p_nor=Rr./Ra;
kk1=std(p_nor)
kph1=1-std(p_nor)
 kk=std(abs(p_nor-1));
kph=1-kk

%%%%%%%%%%%%%%%%%%%%%%%%%%%%%%%%%%%
%% 4. Cross-correlation coefficient
kpk=valormax

%%%%%%%%%%%%%%%%%%%%%%%%%%%%%%%%%%%
%% 5. shape pract
CR=CR/max(CR);
[value,pos]=findpeaks(CR);
[~,loc]=sort(CR(pos),'descend');
locff=loc(2);
ksh=1-CR(pos(locff))

%%%%%%%%%%%%%%%%%%%%%%%%%%%%%%%%%%%
%% Integrating with geometric mean the quality indices
result= 10*((kbd*kco*kph*kpk*ksh)^(1/5));
```

```
%% Showing levels of Quality Index

   if result>=0 && result<=2

set(handles.quadro_texto_qualidade,'string',sprintf('%0.1f',result),'BackgroundColor',[1 0.8
0.8])
        set(handles.correlation_coefficent,'Fontname','Arial','FontSize',14,'Color',[1 0.8 .8]);
   elseif result>=1 && result<7

set(handles.quadro_texto_qualidade,'string',sprintf('%0.1f',result),'BackgroundColor',[1 1 .8])
        set(handles.correlation_coefficent,'Fontname','Arial','FontSize',14,'Color',[1 1 .8]);
   elseif  result>=7 && result<=10

set(handles.quadro_texto_qualidade,'string',sprintf('%0.1f',result),'BackgroundColor',[.76 .87
.78])
        set(handles.correlation_coefficent,'Fontname','Arial','FontSize',14,'Color',[.76 .87
.78]);
    end
```